Supported copper oxide catalysts for octanal hydrogenation:

The influence of water

By

Alisa Govender

Submitted in fulfillment of the academic requirements for the degree of Master of Science at the

School of Chemistry

University of KwaZulu-Natal

Durban

South Africa

June 2010

As the candidates supervisor I have approved this thesis for submission

_____	_____	_____
Name	Signature	Date

Disclaimer: Small parts of the text relating to the aims and objectives of this project were deleted at the request of the sponsoring company to achieve "IP clearance"

Abstract

Copper oxide supported on alumina (CuO/Al_2O_3), silica (CuO/SiO_2) and chromia (CuO/Cr_2O_3) have been synthesized and characterized. These catalysts were characterized using XRD, SEM, TEM, ICP, BET surface area and pore volume, TPR, TPD, TGA-DSC and IR. The hydrogenation of octanal using these catalysts was investigated; however, the primary focus of the project was the influence of water on the reaction and the catalysts.

The initial study using CuO/Al_2O_3 showed that the optimum operating conditions for subsequent catalytic testing was 160 °C and a hydrogen to aldehyde ratio of two. Under these conditions, a conversion of 99 % and selectivity to octanol of 97 % was achieved.

Further catalytic testing, using CuO/Al_2O_3 and CuO/Cr_2O_3, was carried out by introducing water-spiked feed into the reaction system after steady state was reached using fresh feed. Based on literature, it was initially expected that the presence of water would cause catalyst poisoning and subsequently catalyst deactivation. However, contrary to the expectation, the presence of water did not influence the activity of these two catalysts. Furthermore, the selectivity to octanol increased to 98.5 % when CuO/Al_2O_3 was used for the reaction, whilst a minor change in the selectivity to octanol (0.5 %) was obtained when CuO/Cr_2O_3 was used. The interaction of the water with the surface hydroxyls on alumina is most likely the reason for the increase in the selectivity to octanol when using CuO/Al_2O_3.

In contrast to the other two catalysts, the reaction over CuO/SiO_2 showed a steady decrease in both the conversion of octanal and the selectivity to octanol with time-on-stream when using fresh feed. After 55 hours on stream, the conversion reached 22 %, (from an initial 95 %) whilst the selectivity to octanol reached 89 % (from an initial 98 %). This decline in the conversion and selectivity to octanol was possibly due in part, to the low isoelectric point of silica, with mechanical failure being the major contributing factor to the catalyst's deactivation. The decrease in the BET surface area and the presence of smaller particles in the SEM image, confirmed that mechanical failure occurred.

Since steady state was not reached and deactivation occurred, the reaction over CuO/SiO_2 was also carried out using water-spiked feed. The conversion of octanal was seen to gradually decrease to 73 % after 55 hours on stream, whilst the selectivity to octanol remained unchanged at 98 % for the duration of the reaction. This showed the beneficial effect of the presence of water by slowing down the decline in catalytic activity and maintaining the selectivity to octanol. The improved selectivity obtained in the presence of water was attributed to its interaction with the silica surface hydroxyls. Since octanal conversion continued to decrease, it indicated that mechanical failure was the primary cause in the loss of catalytic activity.

The used catalysts were characterized using XRD, SEM, EDS composition scanning, TEM, BET surface area and pore volume, TGA-DSC and IR. The catalysts used for the reaction with the fresh feed and the water-spiked feed were characterized and compared. Except for the deactivation of CuO/SiO_2, the characterization of these catalysts showed that the presence of water did not negatively impact the make-up of the catalyst.

Preface

The experimental work described in this thesis was carried out in the School of Chemistry, University of KwaZulu-Natal, from January 2008 to March 2010, under the supervision of Professor Holger B. Friedrich.

These studies represent the original work by the author and have not otherwise been submitted in any form for any degree or diploma to any tertiary institution. Where use has been made of the work of others it is duly acknowledged in the text.

Declaration 1

Plagiarism

I, Alisa Govender, declare that

1. The research reported in this thesis, except where otherwise indicated, is my original work.
2. This thesis has not been submitted for any degree or examination at any other university.
3. This thesis does not contain other person's data, pictures, graphs or other information, unless specifically acknowledged as being sourced from other persons.
4. This thesis does not contain other person's writing unless specifically acknowledged as being sourced from other researchers. Where other written sources have been quoted, then:
    a. Their words have been re-written but the general information attributed to them has been referenced
    b. Where the exact words have been used, then their writing has been placed in italics and inside quotation marks, and referenced.
5. This thesis does not contain text, graphics or tables copied and pasted from the internet, unless specifically acknowledged, and the source being detailed in the thesis and in the References sections.

_____

Signed

Declaration 2

Conference Contributions and Publications

Parts of this thesis have been presented at conferences or publications as listed below.

(A) Conference contributions:

1. Oral presentation

   CATSA 2009, Worster and MSSA 2009, Durban

   Deactivation of supported copper oxide catalysts for aldehyde hydrogenation reactions

(B) Publications:

1. *The influence of water on the hydrogenation of octanal using supported CuO catalysts*

   Currently in preparation

2. *Deactivation of CuO/SiO_2 during the hydrogenation of octanal and the influence of water*

   Currently in preparation

_____

Signed

Table of Contents

List of Abbreviations

ATR-IR	Attenuated Total Reflectance-Infrared
BET	Brunauer Emmet Teller
CrO_x	Chromium oxides
EDS	Energy Dispersive Spectroscopy
EXAFS	Extended X-Ray Absorption Fine Structure
FID	Flame Ionization Detector
FT-IR	Fourier Transform-Infrared
FWHM	Full Width at Half Maximum
GC	Gas Chromatography
GC-MS	Gas Chromatography-Mass Spectrometry
GHSV	Gas Hourly Space Velocity
ICP-OES	Inductively Coupled Plasma-Optical Emission Spectroscopy
IR	Infrared
JCPDS	Joint Committee on Powder Diffraction Standards
LEED	Low Energy Electron Diffraction
LHSV	Liquid Hourly Space Velocity
M^0	Metal in the zero oxidation state
mL	Millilitre
MS	Mass Spectrometry
NH3-TPD	Ammonia Temperature Programmed Desorption
PIXE	Proton Induced X-Ray Emission
RRF	Relative Response Factor
s	Second
SADP	Selected Area Electron Diffraction Pattern
SAED	Selected Area Electron Diffraction
SASOL	South African Coal, Oil and Gas Corporation
SEM	Scanning Electron Microscopy
SEM-EDX	Scanning Electron Microscopy-Energy Dispersive X-Ray
SIMS	Secondary Ion Mass Spectroscopy
TEM	Transmission Electron Microscopy
TG/DTA	Thermogravimetric Analysis-Differential Thermal Analysis
TGA-DSC	Thermogravimetric Analysis-Differential Scanning Calorimetry

TPH	Temperature Programmed Hydrogenation
TPO	Temperature Programmed Oxidation
XPS	X-Ray Photoelectron Spectroscopy
XRD	X-Ray Diffraction
XRE	X-Ray Emission

List of Figures

List of Schemes

List of Tables

Acknowledgements

First and foremost, all glory, honor and praise goes to my Lord and Savior Jesus Christ. He has brought me to the place that I am at and all that I have is only because of Him. I love you Jesus with all of who I am.

To my parents, thank you for your love, support and motivation. My daddy always took me where ever I needed to and go and waited rather patiently for me all the time. And my mum made sure that I never gave up and pushed me to do what I didn't want to but it was worth all the effort in the end. I love you both!

Many thanks to Professor Holger Friedrich for his help and insight into the work and for always being ready to help and for making sure that I was always fine. I thank Dr James Wesley-Smith, Ms Sharon Eggers and Mrs Priscilla Martins (EM Unit at UKZN) for their help with and teaching me TEM and SEM. Thank you to Dr Sam Mahomed of SASOL R & D for initiating this project and for all the assistance during my studies. I thank Mr Francois Human and Mr Enrico Caricato of SASOL R & D; I really appreciate the assistance with the reactor setup. A special thank you goes out to Mrs Esti van Ryneveld of SASOL R & D for her constant readiness to help with all the reactor issues and for helping me know and learn all that I have in the last year.

Thank you to my friends for all the fun and laughter and being there for me. We made it through some tough times but we are still standing strong as The Dream Team! I thank the 'oldies' of the catalysis research group who were always ready to help and answer every question. Especially, Thirusha, I really appreciate everything that you have done for me and for imparting all your knowledge. And to all other members of group, thank you for anything that you have done.

And finally, to Calvin, thank you for being a support and always making sure that my work was done and being there to listen to my boring science. I love you!!!

Chapter 1

Introduction

Hydrogenation reactions catalyzed by supported metal catalysts are often used in the chemical industry. Such reactions find application in the preparation of pharmaceuticals and fine chemicals. Oxygenated compounds such as aldehydes are an example of the starting material utilized in catalytic hydrogenation in the fine chemicals sector. Hydrogenation is often used in industry to convert products obtained from other processes that have little commercial importance to products with an increased demand and need in the chemicals industry.[1, 2]

One example of the above-mentioned is the hydrogenation of aldehydes, produced from the oxo process (hydroformylation). This reaction leads to the production of oxo alcohols which are important chemical commodities.[3-7] It is possible, however, for impurities and by-products (formed upstream) to be present in the feedstock to the hydrogenation reaction. Water is an example of a possible contaminant in the feed to the hydrogenation reactor but this could negatively impact the reaction by causing catalyst poisoning. This can lead to the deactivation of the catalyst, since it has been shown that water, in both the liquid and vapor form, can cause catalyst deactivation[8-11] (discussed further in Chapter 3).

Since hydrogenation of oxo aldehydes leads to the production of important organic chemicals,[7] it is essential for catalyst deactivation, if any, to be avoided or delayed. For this study, octanal has been used as a model aldehyde to investigate the influence of water during the hydrogenation reaction. The results of this study will help ascertain the effects of water on the hydrogenation catalysts studied and consequently on the conversion of octanal and selectivity to octanol. Supported metal catalysts that are often utilized for commercial hydrogenation processes include copper supported on silica (Cu/SiO_2), copper supported on chromia (Cu/Cr_2O_3) and copper supported on alumina (Cu/Al_2O_3). These catalysts are therefore attractive for use in this study.

In order to understand the results of this study, knowledge of catalysis and the concepts associated with it is required. This information is provided in Sections 1.1 – 1.5.

1.1. Catalysis

Catalysis refers to "the phenomenon occurring when a catalyst acts".[12] Two types of catalytic systems exist, namely homogeneous catalysis and heterogeneous catalysis. The definitions of these two types of catalysis are based upon the phase in which the chemical reaction takes place. Homogeneous catalysis refers to a single phase chemical reaction without the existence of a phase boundary, whilst heterogeneous catalysis is when the chemical reaction occurs at an interface of two phases (the phase boundary separates the catalyst from the reactant molecules).[13] The phases in which catalytic reactions can occur are in solution, within solution-like confines of micelles and the molecular-scale solution pockets of large enzyme molecules, within polymer gels, within molecular-scale cages of crystalline solids and on the surface of solids.[14]

1.1.1. Fundamental principles of catalysis

Chemical thermodynamics and chemical kinetics are areas that are central to the understanding of catalysis. Chemical kinetics forms the quantitative framework of catalysis, whilst the qualitative framework is provided by reaction mechanisms.[14] Catalytic reaction kinetics forms the basis for the definitions of activity, selectivity and stability. The activity of a catalyst is given by the reaction rate, or reaction rate constant for the conversion of reactants and products. The selectivity of a catalyst is a measure of the catalyst's ability to direct the conversion to the desired product.[14] Since a catalyst accelerates the rate of a chemical reaction; it indicates that the reaction must be able to occur without a catalyst. It is also important that the chemical equilibrium reached remains unchanged with the use of a catalyst.[13]

The potential energy diagram shown in Figure 1.1 can be used to explain the steps that occur in a catalyzed reaction. Initially, the reactants are transported to the catalyst and are then adsorbed onto the surface of the catalyst. These adsorbed reactants interact with each other to form the product. This product is then desorbed from the catalyst surface and transported away from the catalyst.[13] In order for these steps to occur, the activation

energy for the catalyzed reaction must be lower than for the uncatalyzed reaction. This is graphically illustrated in Figure 1.1 in which it is shown that the potential energy for a catalyzed reaction is much lower than for the corresponding reaction without a catalyst.[12]

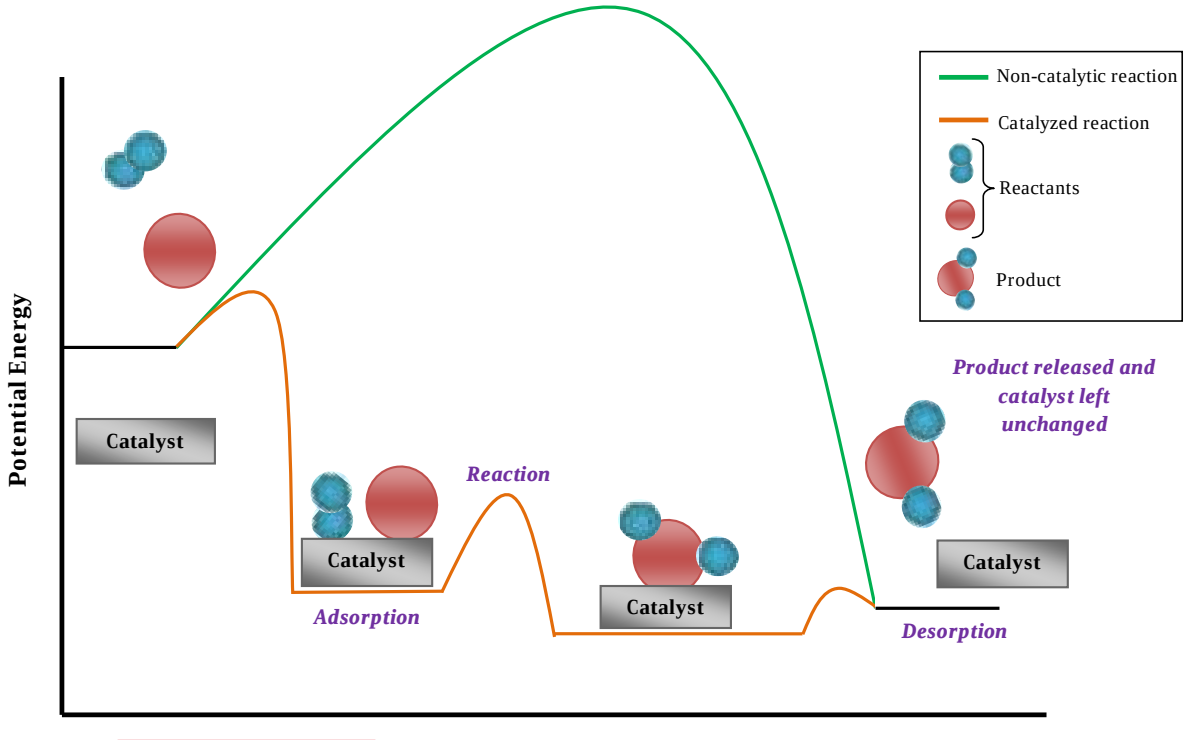

Figure 1.1: Potential Energy diagram (adapted from reference 7)[15]

1.2. Heterogeneous Catalysis

This project was based on heterogeneous catalysis occurring on the solid surface of metals. Section 1.1 highlighted the definition of heterogeneous catalysis. Using heterogeneous catalysis for this study is advantageous since there is simple separation and recovery of the catalyst.[16] This will allow for spent catalyst characterization which is a necessity for a deactivation study. In addition, heterogeneous catalysis is best suited for the investigation since this type of catalysis is used for gas- and liquid-phase operations and continuous-reactor operations.[16] In the subsections to follow, aspects specific to heterogeneous catalysis are highlighted.

1.2.1. The catalytic cycle

Figure 1.2 shows a graphical representation of molecular and atomic level processes involved in a catalytic reaction. The process outlined in Figure 1.2 uses carbon monoxide (CO) oxidation as an example.

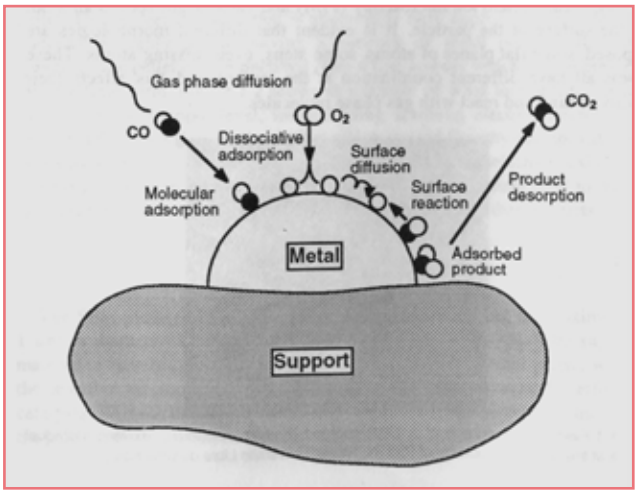

Figure 1.2: The heterogeneous catalytic cycle for the oxidation of carbon monoxide[17]

With reference to Figure 1.2, gas phase diffusion is the first step of the catalytic process. The molecule diffuses through the gas phase to the metal surfaces and adsorbs to it in a molecular form. It is then followed by surface diffusion, when the dissociation of a molecule into atoms may occur depending on the internal bond strength of the molecule. The surface reaction then occurs, where the O_2 atoms react with the CO to form the adsorbed product, CO_2. This step is often the rate determining step of the catalytic reaction. The final step of the cycle is product desorption, where the product to surface bond is broken, CO_2 enters the gas phase, diffuses down the catalyst pores to emerge at the end of the reactor.[17]

1.2.2. Surface adsorption

The adsorption of the reactant gas molecule onto the catalyst surface is the first step of the catalyst cycle.[17] Two types of adsorption exist, these being chemisorption and physisorption. Chemisorption involves the molecules and surface making contact by

means of the formation of a chemical bond. When the contact between the molecule and surface is made possible through a physical process involving weak Van der Waals forces, the adsorption is termed physisorption.[14] The advantage of the adsorption of the gas phase molecule onto a solid surface is that the intermediate is stabilized. The absence of the interaction or contact between the gas phase reactant molecule and the catalyst surface would result in the intermediate having unsatisfied valences and a relatively unstable configuration.[17]

1.3. Catalysts

Catalysts are the key 'ingredient' to an efficient chemical process and the occurrence of the processes of life and are responsible for making possible the fundamental principle of catalysis that was highlighted in Section 1.1.1. It is necessary to remember that in creating this new and easier pathway for reactant molecules to be converted into product molecules, catalysts do not get consumed in the reaction, instead, they are regenerated during the rearrangement to product molecules.[12]

1.3.1. Types of catalytic material

Various types of catalytic material exist ranging from solid materials to biological enzymes, from gas phase molecules to liquid coatings on surfaces. Metals and many types of metal oxides are used. Metals are attractive as catalysts due to their high surface energy making them highly active, however selectivity to the desired product must also be considered. Many metal catalysts are placed on a support, such as alumina or silica, since these metal catalysts are thermally unstable in the high surface area form that they must be used in.[17] The shape of the catalyst is also important to allow for efficient functioning of the catalytic process and reactor. Catalysts can be in a powder form, or as pellets with various pore sizes. The shape or physical form of the catalyst used depends on the process it is to be used for and on the reactor system which it will be used in.[17]

Catalysts can be made in a variety of ways. The most common methods are impregnation, slurry precipitation, co-precipitation, fusion, physical mixing, wash coating and pelleting. Pelleting is used to make the macroscopic form of the catalyst which is used in the

industrial plant. The method chosen to make the catalyst depends on the individual synthesizing it and the properties desired in the catalyst.[17]

1.3.2. Supported metal catalysts

The most commonly used catalyst in industry is the supported metal and metal oxide catalyst, making it an important component of heterogeneous catalysis.[18] Such catalysts play a major role in society and the economy.[19] The commercial applications that utilize these catalysts include oil refining, chemicals manufacture and environmental catalysis. These applications encompass reactions such as oxidation, (de)-hydrogenation and isomerization.[19, 20] Synthesizing supported catalysts must produce a catalyst with high activity, selectivity and stability.[21] To achieve such features, the active metal phase must be highly dispersed throughout the support, resulting in a large specific surface area and maximum specific activity. The catalyst support can disperse the metal and increase its thermal stability and hence the catalyst life.[21] Supported metal catalysts are discussed in more detail in the subsections to follow.

1.3.2.1. Reasons for supporting catalysts

A catalyst is supported because the support can:

(a) Act as a thermal stabilizer, where the support stabilizes the catalyst against agglomeration and coalescing;

(b) Act as a component enhancing selectivity (the support causes resistance to by-product formation) or poison resistance;

(c) Decrease the density of the catalyst and allow for the diluting of costly ingredients with less costly ingredients and

(d) Resist breakage and minimize pressure drop (achieved using supports such as saddles, rings, etc.).[22, 23]

1.3.2.2. Effects of supporting a metal catalyst

The attachment of the support can have the following beneficial effects:

(a) The support can not only be an inert backbone but also promote selectivity by leading to the preferred orientations of the substrate at the catalytic site;

(b) The supported metal catalyst can have different chemical properties to the non-supported metal catalyst;

(c) Using a multidentate ligand as a support for a metal catalyst can alter the stereochemistry around the metal ion;

(d) The position of the equilibrium between metal ions and their surrounding ligands may be altered by supporting the metal catalyst and

(e) Catalytically active structures that are normally unstable can be stabilized with the use of a support.[23]

It is clearly seen that the attachment of the support to the metal catalyst produces a united catalyst that can possess the advantage of being highly selective.[23] This further supports the use of supported catalysts for this study.

1.3.2.3. Types of supports

There are two main classes of supports that exist. These are organic polymers and inorganic supports. Polymers that function as supports include polystyrene, polypropylene, polyacrylates and polyvinyl chlorides. Such supports possess advantages such as easy functionalization, chemical inertness and a wide range of physical properties; however, these polymers have poor mechanical properties and heat transfer abilities. Inorganic supports, on the other hand, possess this quality that organic polymers lack. Silica, alumina, glasses, clays and zeolites are among the inorganic supports that have been used. Other supports include titania, zirconia, chromia and other metal oxides. Inorganic supports tend to be mainly metal oxides and contain hydroxyl groups which affect attachment.[23] Table 1.1 lists some supports and the catalytically active phase and selected reactions that they have been used for.

Table 1.1: Some examples of supports used for the active phase in selected catalytic reactions[24]

Support	Catalytically Active Phase	Application
γ-Alumina, Al_2O_3	Cu-ZnO	Methanol synthesis
	Pd, Pt, Ru, Rh	Hydrogenation
Silica, SiO_2	CrO_x	Polymerization
	V_2O_5	Oxidation
Carbon	Pd, Pt	Hydrogenation

1.3.2.4. Preparation of supported metal catalysts

Three methods are commonly used to prepare supported metal catalysts. These methods are:

(i) Impregnation or ion-exchange of the metal catalysts on the support;

(ii) Co-precipitation;

(iii) Deposition precipitation;

(iv) Drying and calcination and

(v) Reduction.[21]

1.3.2.4.1. Impregnation methods

Impregnation preparation methods can be subdivided into two categories: (a) incipient or dry wetness and (b) wet or soaking impregnation. These categories are classified based on the amount of solution used. Generally, impregnation methods involve contact between the support and a certain quantity of the metal precursor (often a salt) followed by aging, drying and calcination.[21]

(a) Incipient wetness

In this technique, the evacuated support is stirred while the impregnating solution is sprayed on the support. A primary requirement for successful synthesis of a supported metal catalyst is that the metal precursor is distributed evenly throughout the support. This is easily achieved in this technique by the evacuation of the air trapped in the inner pores. The advantages associated with this technique are that it is a simple and economical preparation method yielding reproducible metal loadings.[21] A disadvantage, however, is that the reproducible metal loading is dependent on the solubility of the metal precursor.[21]

(b) Wet impregnation

In contrast to incipient impregnation, wet impregnation is distinguished by the use of an excess of solution with respect to the pore volume of the support. The procedure is similar to dry impregnation, involving aging, stirring, filtering and drying. Since precursor-support interaction is encountered, the concentration of the metal precursors on the support is dependent on the concentration of the solution, the pore volume of the support and the type and/or concentration of adsorbing sites existing at the surface.[21]

1.3.2.4.2. Co-precipitation

This procedure involves the addition of a precipitating agent to prepared solutions of the metal salt of the catalytically active material and the support. This produces hydroxides and/or carbonates, which, after washing, can be transformed to oxides by heating.[21, 24] The method of co-precipitation yields a porous material with high surface area and a uniform distribution on a molecular scale of the different active species in the final catalyst.[21, 24] The following variables must be carefully controlled during the synthesis:

(a) Mixing (must be efficient);

(b) The procedure and order in which solutions are added;

(c) Temperature;

(d) Aging time of precipitate;

(e) Filtering;

(f) Washing procedure and

(g) pH.[21]

The co-precipitation method for synthesizing supported metal catalysts has evolved into the most preferred synthetic route since it can produce catalysts with a metal loading greater than 10 – 15 %.[21]

1.3.2.4.3. Deposition precipitation

This method involves the precipitation of a metal hydroxide or carbonate on the particles of a powder support by the reaction of a base with the metal precursor.[21] The rate of nucleation and growth of the particles inside the pores of the support affects the distribution of the particles on the support. Ideally, rapid nucleation and growth is unwanted since it produces large crystallites and inhomogeneous distribution.[21] Thus, an essential requirement for this preparation method becomes an efficient mixing in conjunction with a slow addition of the alkali solution. Following this step are filtration, washing, drying and heating. The disadvantage of this preparation method is that catalysts contain a low concentration of metal.[21]

1.3.2.4.4. Drying

Once the supported catalyst is prepared, it becomes necessary to remove the solvents used in the previous steps. The drying treatment is usually performed at temperatures between 80 ℃ and 200 ℃.[21]

1.3.2.4.5. Calcination

The process of calcination causes the decomposition of the metal precursor which produces an oxide and generates gaseous products such as H_2O and CO_2. This heat treatment allows for the removal of these gases as well as anions and cations introduced in the previous preparation steps. The temperature chosen to calcine the catalyst is one that is higher than the temperature of the reaction. In addition, the heat treatment

process is carried out in an oxidizing atmosphere. Not only can the process of calcination decompose the catalyst, it can also cause sintering of the precursor or the formed oxide and the possibility of a reaction between the formed oxide and the support occuring.[21]

1.3.2.4.6. Reduction

Thermal treatment of the metal oxide or metal precursor in hydrogen flow, reducing it to a metal is termed reduction. Variables such as rate of heating, final temperature and time of reduction, hydrogen concentration and flow must be carefully selected based upon the type of metal, catalytic system and reaction to be performed. Essential requirements for this treatment are:

(a) A low water vapor concentration to prevent detrimental effects with dispersion of the metal;

(b) High enough hydrogen flows so that the water can be removed from the support during reduction and

(c) Direct reductions of some metal precursors should be avoided. For example, metal chlorides should not be directly reduced since this produces corrosive hydrochloric acid in the presence of water vapor.[21]

1.4. Catalytic Reactors

Chemical reactions that utilize catalysts are termed catalytic reactions and those vessels that are specifically designed to host these types of reactions are termed catalytic reactors. A number of reactor types exist and some examples include:

(a) Fixed-bed reactors;

(b) Fluidized-bed reactors;

(c) Batch reactors;

(d) Bubble column reactors;

(e) Continuous stirred-tank reactors and

(f) Trickle column reactors.[12]

A fixed-bed reactor contains a tube that is packed with 'coarse' catalyst particles through which the reactants flow. This obstacle to gas flow by the catalyst particles creates a pressure drop across the bed, thus demanding the application of positive pressure at the inlet to ensure a optimum flow rate.[12] Fluidized bed reactors are similar to fixed-bed reactors in that they are also used for gaseous reactants. However, in the fluidized bed reactor, the catalyst is made up of fine particles, causing the gas to attain a critical velocity upon flowing upwards through the catalyst bed. As a result, the catalyst bed expands to a great extent, which influences the movement of the particles, hence the term fluidized bed.[12] Batch reactors are used when the reactant is a gas as well as a liquid and has the catalyst as a fine powder suspended in the liquid reactant or solution which is kept under stirring. The continuous stirred-tank reactor and the trickle-column reactor may also be used for gaseous and liquid reactants. A 'coarse' catalyst is used for both these reactors, however for the trickle column, the catalyst is packed into a column, whilst in the continuous stirred-tank reactor, it is held in a wire-mesh basket which is rotated in the liquid as gas is bubbled below it.[12]

1.5. Fundamental Terminology

In catalytic reactor work and catalysis in general, there are a number of terms that need to be known. This is necessary since much of the quantitative data is determined by these concepts. These terms include contact time, space velocity, activity, selectivity, conversion and yield.

Contact time refers to the average time spent by a reactant molecule on the catalyst bed. It is determined by the free volume in the bed (inclusive of the pore volume) divided by the flow rate of the gas.[12] Contact time can be determined using the formula given by Equation 1.1.

$$\textit{Contact time} = \frac{\text{Volume of catalyst (ml)}}{\text{Flow rate of gas (ml/s)}} \quad \textbf{Equation 1.1}$$

Space velocity is the reciprocal of the contact time and is the number of volumes of gas flowing through the free volume of the catalyst in unit time.[12] The space velocity is frequently expressed in h^{-1} provided that the quantities of the catalyst and the reactants are expressed in the same units. Depending on the phase in which the reactant is, the space velocity may be termed gas hourly space velocity (GHSV) or liquid hourly space velocity (LHSV).[25] Equation 1.2 is the mathematical representation of space velocity and can be used to determine this value.

$$\textbf{\textit{Space velocity}} = \frac{1}{\text{Contact time}} \quad \textbf{Equation 1.2}$$

The yield of a product may be described as the amount, in mass or moles, of the product obtained from the quantity of reactant used. The yield of any particular product can be determine from Equation 1.3.[25]

$$\textbf{\textit{Yield of product}} = \frac{\text{Amount of reactant converted into product}}{\text{Amount of reactant introduced}} \quad \textbf{Equation 1.3}$$

The conversion of a reactant (X) may be described as the amount of X that has reacted from the quantity of X introduced into the reaction system. The conversion of reactant X can be determined from Equation 1.4.[25]

$$\textbf{\textit{Conversion}} = \frac{\text{Amount of reactant X reacted}}{\text{Amount of reactant X introduced}} \quad \textbf{Equation 1.4}$$

The selectivity of a catalyst, as defined in Section 1.1.1, is dependent on the reaction system as well as the duration of the reaction. In addition, a catalyst's selectivity is a function of conversion.[25] Using Equation 3 and 4, the formula for the determination of selectivity is given by Equation 1.5.

$$\textbf{\textit{Selectivity}} = \frac{\text{Yield}}{\text{Conversion}} \quad \textbf{Equation 1.5}$$

The activity of a catalyst refers to the rate of chemical change occurring in the catalytic system or how fast the chemical reaction reaches equilibrium in the presence of a catalyst.[14, 26, 27] The more complex route to the determination of the activity of a catalyst is by calculating kinetic activities derived from fundamental rate laws. A simpler route exists in which the activity of a catalyst can be determined from a more practical viewpoint.[26] The activity of a catalyst may be determined from the reaction rate, which is given by the conversion of the reactant per unit time per volume or mass of catalyst. However, for comparative measurements and particularly for deactivation studies, there are four activity measures that may be used. These activity measures are:

(a) Conversion when the reaction conditions are kept constant;
(b) Space velocity when there is a known constant conversion;
(c) Space-time yield (amount of product formed per volume of catalyst per unit time) and
(d) Temperature that is needed for a particular conversion.[26]

Of these four activity measures, the most suitable route for the determination of the activity of the catalysts in this study is by comparing the conversion when the reaction conditions are kept constant.

1.6. Catalyst Characterization

The information discussed in the preceding sections lays the foundation required to understand catalytic testing and the quantitative aspects of it. However, explaining the observed trends from the catalytic testing requires catalyst characterization. [28] In addition, the information obtained from various characterization techniques provides useful information that can explain the catalytic functionalities of the catalysts being used and the observed trends for a particular reaction under investigation.[28] Some methods for characterization are spectroscopy, microscopy, diffraction and methods based on adsorption and desorption or bulk reactions.[24] The basis of the properties of a heterogeneous catalyst surface is its composition and structure on the atomic scale, thus making the primary focus of catalyst characterization the examination of the surface atom by atom under the reaction conditions in which the catalyst functions. However, various factors such as the presence of metal oxide, or sulfide particles, can make catalyst characterization complex. Thus, a simplified model catalyst in its operating system is

created to characterize the catalyst.[24] There are a number of characterization techniques that are available; however only a few are utilized for any particular study. Techniques such as Low Energy Electron Diffraction (LEED), Secondary-Ion Mass Spectroscopy (SIMS) and X-Ray Photoelectron Spectroscopy (XPS) form a more sophisticated class of methods and are generally used for specialized model systems. Other techniques such as X-Ray Diffraction (XRD), Extended X-Ray Absorption Fine Structure (EXAFS), X-Ray Emission (XRE) and Proton Induced X-Ray Emission (PIXE) are more universally applicable.[22] Some of the characterization techniques utilized in this study are discussed below.

1.6.1. X-Ray diffraction

X-Ray Diffraction (XRD) is a commonly used characterization technique and has existed for a long time. This method yields information that allows for the identification of the crystalline phases inside the catalysts. The information is obtained by means of lattice structural parameters. An insight into the particle size is also obtained from the XRD data. This technique is attractive for catalyst characterization since the information obtained from the analysis is clear and can sometimes be obtained under reaction conditions. However, such information is obtained for large crystalline particles only, hence either too small or amorphous particles will not be detected.[24]

1.6.2. X-Ray photoelectron spectroscopy

The use of X-ray Photoelectron Spectroscopy (XPS) as a catalyst characterization technique yields information pertaining to the elemental composition, the oxidation state of the elements and sometimes the dispersion of one phase over another.[24] The physical phenomenon occurring in this technique is the photoelectric effect where a photo emission or auger process may occur. In this technique, the intensity of photoelectrons as a function of their kinetic energy is measured. Also, the photoelectron peaks are labeled according to the quantum numbers of the level from which the electron originates.[24] The assignment of each peak in an XPS spectrum to a particular element is obtained by looking at the binding energy tables. XPS is also useful for surface morphology determination in that it can recognize how well particles are dispersed over a support.[24] Since XPS measures the intensity from particles and the intensity of the support, it

becomes ideal to utilize when techniques such as electron microscopy, particle size determination and hydrogen chemisorption cannot distinguish between support and active phase.[24]

1.6.3. Electron microscopy

Electron microscopy is used to determine the size and shape as well as the surface morphology of supported particles. Due to the interaction between the primary electron beam and the sample, a number of detectable signals arise. Each type of detectable signal forms the basis of the various types of electron microscopy techniques that exist. The illustration in Figure 1.3 shows, in short, what happens when a primary electron beam strikes the sample.[24]

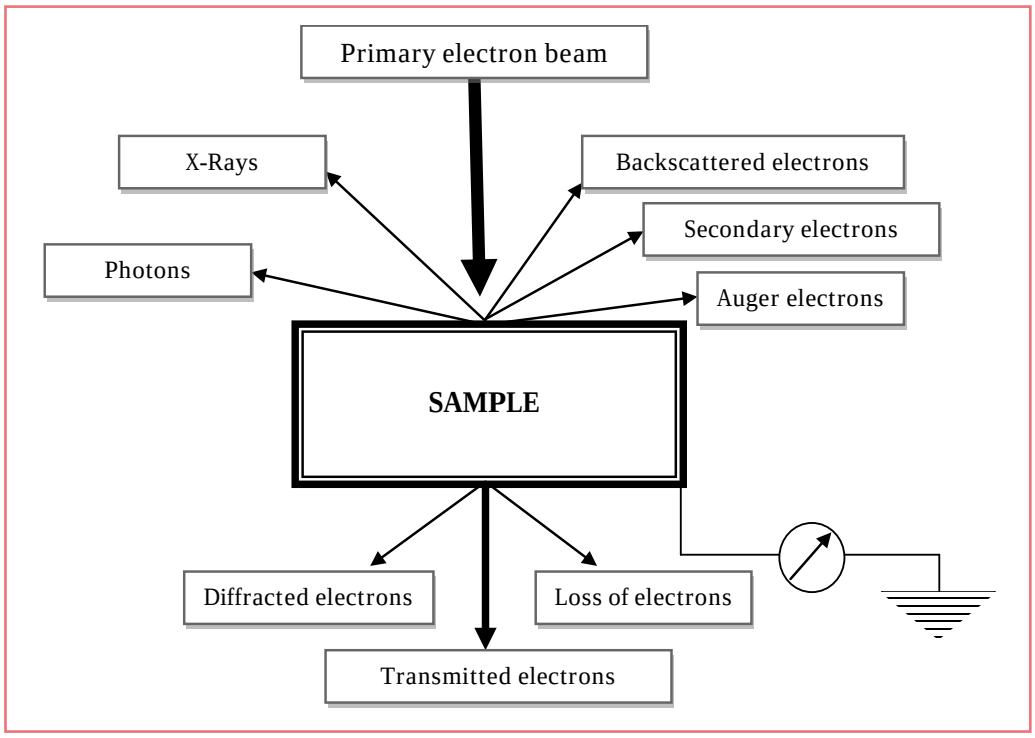

Figure 1.3: An illustration showing the detectable signals that arise when the primary electron beam interacts with the sample[24]

As discussed by *Chorkendorff and Niemantsverdriet* [24], once the primary electron beam strikes the sample, the following phenomenon occurs resulting in the respective signals:

- Electrons are diffracted by particles yielding crystallographic information provided that these particles are favorably oriented towards the beam.[24] Such information is obtained by performing selected area electron diffraction using the Transmission Electron Microscope (TEM). The diffraction patterns obtained may be used to determine information about the crystal structure of the particles.

- Electrons can collide with atoms in the sample and be scattered back.[24] Such events may be investigated using Scanning Electron Microscopy (SEM) with a backscattered electron detector. The use of a backscattered electron detector allows for atomic number contrast to be investigated. This is because the ability of an element to back scatter electrons is dependent on how heavy the atom is. Thus, heavier atoms will appear brighter in a backscattered image since these atoms will produce more backscattered electrons.[29]

- Auger electrons and X-Rays are formed in the relaxation of core-ionized atoms. The X-Rays emitted allow for the determination of the elemental composition of a material since characteristic X-Rays are emitted for each element.[24]

- In addition to these processes, electrons may be lost or cause the excitation of characteristic transitions in the sample and photons are emitted causing cathodoluminescence.[24]

These detectable signals have formed the basis of the microscopy techniques that exist today, namely, TEM and SEM. Scanning electron microscopy is based on the interaction of the primary electron beam with the sample and the detection of the secondary electrons and can determine contrast due to the topology and composition of a surface. Transmission electron microscopy is based on the interaction of the primary electron beam with the sample and the detection of the transmitted electrons. The electron beam in TEM projects all the information of the sample being analyzed in a two dimensional image of sub-nanometer resolution. This image produced is the bright field image. A dark field image may also be obtained (using the diffracted electrons) in which the regions of the sample that produce a selected reflection (a spot) in the diffraction pattern will appear bright in the dark field image.[24, 30] This characterization technique is useful for particle size determination or particle distribution determinations as well as for obtaining crystallographic information of the sample.[24]

1.6.4. Temperature-programmed reactions

Temperature-programmed reactions involve monitoring a chemical reaction while the temperature increases linearly with time. The reactions that may be monitored are reduction, oxidation and/or sulfidation, as well as ammonia desorption. Temperature-Programmed Reduction (TPR) gives information on the temperature required for the complete reduction of a catalyst and the degree to which it is reduced. Temperature–Programmed Oxidation (TPO) and Temperature-Programmed Sulfidation (TPS) analyses are useful for studying the oxidation and sulfidation processes, respectively, as well as the catalysts used for these processes.[24] Ammonia–Temperature Programmed Desorption (NH_3-TPD) is often used for the determination of surface acidity. The NH_3-TPD profile obtained allows for the determination of the acidity of the catalyst and the strength of the acid sites.[31, 32] Due to the small size of the ammonia molecule, it has the ability to enter the pores of the catalysts and to react with the Brønsted and Lewis acid sites.[32] Acidity measurements are useful since their determination allows for the prediction of catalytic activity and in addition, the results obtained from catalytic reactions may be correlated to the acidity of the catalyst used.[31]

1.6.5. Brunauer-Emmett-Teller Method

The Brunauer-Emmett-Teller (BET) method is a gas adsorption method used for the determination of the surface area of finely divided and porous materials. This technique also allows for the determination of pore size distribution. The most applicable adsorptive for surface area determinations is generally nitrogen.[33]

1.6.6. Inductively coupled plasma-optical emission spectroscopy

Inductively Coupled Plasma–Optical Emission Spectroscopy (ICP-OES) is used for the determination of the elemental composition of the catalyst. The catalyst is digested prior to analysis and thus the elemental composition of the entire sample is determined. This technique is preferred since it is faster than other available spectroscopic techniques such atomic emission spectroscopy and there is a good detection limit and a high linear range.[34]

1.6.7. Thermogravimetric analysis and differential scanning calorimetry

Thermogravimetric Analysis (TGA) is used to determine the changes in weight with changes in temperature. The peaks obtained in a TGA curve correspond to the loss of molecules from the sample. Differential Scanning Calorimetry (DSC) is a technique that is used to determine endothermic or exothermic processes. The peak area under a DSC curve is equal to the enthalpy change. The use of DSC will indicate whether the weight loss observed in the TGA analysis is an exothermic or endothermic process.

1.6.8. Infra-red spectroscopy

Infra-Red (IR) is a diagnostic tool utilized for the determination of functional groups present in the catalyst. Molecules vibrate or rotate at specific frequencies. These frequencies correspond to discrete energy levels and it is on this that IR spectroscopy is based. When a sample is analyzed using this technique, it is subjected to infrared light. This light passes through the sample and is absorbed. The amount of this light that is not absorbed is transmitted and is detected by the instrument. This information can be related to wavelengths at which the energy is absorbed. These absorption wavelengths correspond to specific functionalities that make-up a compound. Attenuated Total Reflectance (ATR) is used together with IR spectroscopy however it allows for direct analysis of solids and liquids. This technique is based on total internal reflection and uses an ATR crystal that is in contact with the sample.

1.7. References

1. R. N. Landau, U. Singh, F. Gortsema, Y. Sun, S. C. Gomolka, T. Lam, M. Futran and D. G. Blackmond, *J. Catal.*, 1995, **157**, 201.
2. R. M. Rioux and M. A. Vannice, *J. Catal.*, 2003, **216**, 362.
3. X. Wang, G. Li and U. S. Ozkan, *J. Mol. Catal. A: Chem*, 2004, **217**, 219.
4. X. Wang and U. S. Ozkan, *J. Mol. Catal. A: Chem*, 2005, **232**, 101.
5. X. Wang, R. Y. Saleh and U. S. Ozkan, *J. Catal.*, 2005, **231**, 20.
6. X. Wang and U. S. Ozkan, *J. Catal.*, 2004, **227**, 492.
7. J. J. McKetta, *Encyclopedia of Chemical Processing and Design*, Marcel Dekker Inc., New York, 1990.
8. W. B. Burford and J. C. W. Frazer, *J. Am. Chem. Soc.*, 1945, **67**, 331.
9. J. Chang, T. Lin and C. Cheng, *Ind. Eng. Chem. Res.*, 1997, **36**, 5096.
10. Z. Ma, R. Jia and C. Liu, *J. Mol. Catal. A: Chem*, 2004, **210**, 157.
11. W. Wang, M. Qiao, H. Li, W. Dai and J. Deng, *Appl. Catal. A: Gen.*, 1998, **168**, 151.
12. G. C. Bond, *Heterogeneous Catalysis: Principles and applications*, Oxford University Press, Oxford, 1974.
13. G. C. Bond, *Principles of Catalysis*, The Chemical Society, London, 1972.
14. B. C. Bates, *Catalytic Chemistry*, John Wiley & Sons Inc., New York, 1992.
15. *ESA - Impress Catalysts or making it happen*, http://www.sapceflight.esa.int/impress/text/education/Images/Catalysis/Image_002.png, Accessed 24/11/2009.
16. R. A. Sheldon and R. S. Downing, *Appl. Catal. A: Gen.*, 1999, **189**, 163.
17. M. Bowker, *The basis and applications of Heterogeneous Catalysis*, Oxford University Press, Oxford, 1998.
18. A. J. v. Dillen, R. J. A. M. Terörde, D. J. Lensveld, J. W. Geus and K. P. d. Jong, *J. Catal.*, 2003, **216**, 257.
19. K. P. d. Jong, *Curr. Opin. Solid State Mater. Sci.*, 1999, **4**, 55.
20. B. L. Mojet, J. T. Miller, D. E. Ramaker and D. C. Koningsberger, *J. Catal.*, 1999, **186**, 373.
21. F. Pinna, *Catal. Today*, 1998, **41**, 129.
22. F. R. Hartley, *Supported Metal Complexes: A new generation of catalysis*, D. Riedel Publishing Company, Holland, 1985.
23. A. B. Stiles, *Catalyst Supports and supported metal catalysts: Theoretical and applied concepts*, Butterworths Publishers, Stoneham, 1987.

24. I. Chorkendorff and J. W. Niemantsverdriet, *Concpets of modern catalysis and kinetics*, Wiley -VCH Verlag GmBH & Co. KGaA, Weinham, 2003.
25. J. Haber, *Pure & Appl. Chem.*, 1991, **63**, 1227.
26. J. Hagen, *Industrial Catalysis A Practical Approach*, Wiley-VCH, Weinham, 1999.
27. C. N. Satterfield, *Heterogenous catalysis in industrial practice*, Second edn., Krieger Publishing Company, Malabar Florida, 1996.
28. G. V. Sagar, P. V. R. Rao, C. S. Srikanth and K. V. R. Chary, *J. Phys. Chem. B*, 2006, **110**, 13881.
29. J. J. Bozzola and L. D. Russell, *Electron Microscopy: Principles and techniques for biologists*, Jones and Bartlett Publishers, Boston, 1992.
30. D. H. Kay, *Techniques for electron microscopy*, Blackwell Scientific Publishers, Oxford, 1965.
31. D. R. Brown and C. N. Rhodes, *Thermo. Acta*, 1997, **294**, 33.
32. A. M. Venezia, V. L. Parola, B. Pawelec and J. L. G. Fierro, *Appl. Catal. A: Gen.*, 2004, **264**, 43.
33. K. S. W. Sing, D. H. Everett, R. A. W. Haul, L. Mascou, R. A. Pierotti, J. Rouquérol and T. Siemieniewska, *Pure & Appl. Chem.*, 1985, **57**, 603.
34. D. A. Skoog, D. M. West, F. J. Holler and S. R. Crouch, *Fundamentals of Analytical Chemistry*, Eighth edn., Thomson Brooks/Cole, Belmont, 2004.

Chapter 2

Aldehydes, Alcohols and Hydrogenation: A Brief Introduction

Chapter 1 discussed the concepts used to describe catalytic data. By using the characterization techniques outlined in Section 1.6, an understanding of the make-up of the catalyst will be provided. This will aid in explaining the catalytic data obtained. However, a comprehensive reasoning of the observed catalytic results such as selectivity and conversion requires knowledge of the reaction under investigation and the structure of the reactants. Thus, since this study investigates the hydrogenation of octanal to octanol, a brief introduction to these compounds and the hydrogenation of octanal is provided in this chapter.

2.1. Aldehydes

An aldehyde is a type of organic compound belonging to the Class II carbonyl compound since it does not possess a functionality that can be replaced by a nucleophile.[1] The general structure of an aldehyde is given in Figure 2.1, which shows that an aldehyde is comprised of a carbonyl group (C=O), a hydrogen and an alkyl or aryl group (-R) that is bonded to the carbonyl carbon. Aldehydes often possess a characteristic pleasant odor and are generally in a liquid form and have a high boiling point.[1, 2]

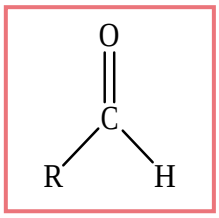

Figure 2.1: General structure of an aldehyde

There are a number of routes *via* which aldehydes may be prepared by. Industrially, however, aldehydes are typically synthesized by the oxidation of the related alcohol.[3] Another commercially known process that yields an aldehyde as a product is the hydroformylation of an olefin to produce an aldehyde having one additional carbon to that of the olefin reactant. The synthetic routes for the synthesis of aldehydes include:

(a) Hydroboration – oxidation of a terminal alkyne;
(b) Primary alcohol oxidation by e.g. pyridinium chlorochromate;
(c) Swern oxidation of a primary alcohol and
(d) Rosenmund reduction, amongst others.[1]

Due to the properties that an aldehyde possesses (namely the polarity of the C=O group and the acidity of the α-hydrogen), these compounds have become attractive for uses in many other organic reactions. The reactions that exist for aldehydes as a starting material include:

(a) Reduction of the aldehyde to a primary alcohol;
(b) Oxidation of aldehydes to carboxylic acids;
(c) Cannizzaro reaction;
(d) Nucleophilic addition reactions and
(e) Displacement at the α-carbon.[2]

Aldehydes are widely used for small scale reactions. In industry, formaldehyde is the most commonly used aldehyde. Some common uses for aldehydes are as solvents, in perfumes, as flavoring agents, as well as intermediates in the plastics, dyes and pharmaceutical industries.[2, 3]

2.1.1. Octanal

Octanal is an organic compound that belongs to the aldehyde group of organic compounds and may also be known as capryl aldehyde, caprylic aldehyde or octyl aldehyde.[4] As can be seen from the structure in Figure 2.2, octanal is an eight carbon aldehyde. This aldehyde exists as a colorless liquid and the non-synthetic route to obtaining octanal is via an isolation process of orange oil.[5] Due to the fruit-like citrus odor that this compound exhibits; octanal finds application as a flavoring or for perfumery purposes.[6]

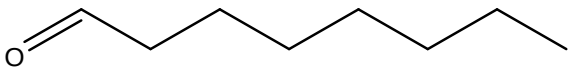

octanal

Chemical Formula: $C_8H_{16}O$
Exact Mass: 128.12
Molecular Weight: 128.21
m/z: 128.12 (100.0%), 129.12 (8.7%)
Elemental Analysis: C, 74.94; H, 12.58; O, 12.48

Figure 2.2: Structure of octanal

2.2. Alcohols

Alcohols, like aldehydes, are a class of organic compounds and may be described as alkanes that possess a hydroxyl (OH) group in place of one hydrogen atom. The general structure of an alcohol is shown in Figure 2.3.[1, 3] Due to the presence of the hydroxyl group alcohols have the ability to form hydrogen bonds which directly influences their physical and chemical properties.[3] The physical characteristics of an alcohol range from liquids for the low molecular weight alcohols to solids for the higher molecular weight alcohols.

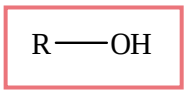

Figure 2.3: General structure of an alcohol

There are a number of synthetic routes that may be utilized for the synthesis of an alcohol. Industrially, alcohols are produced from petroleum, coal, or other natural products.[7] The synthetic production of alcohols may be achieved by:

(a) The hydration of an alkene in an acid-catalyzed medium;
(b) The reaction of an alkyl halide with hydroxide and
(c) Reduction of an aldehyde, ketone, acyl chloride, ester or carboxylic acid, amongst other organic compounds.[1]

Alcohols can also be obtained *via* a non-synthetic route from various sources (often a natural resource); some from the isolation of volatile oils and others may be obtained by extraction from a number of sources.[8]

Some uses of alcohols may be as sweeteners and in the manufacture of perfumes, as valuable intermediates in the synthesis of other compounds and as alcohol fuel. The reactions for which alcohols may be used are:

(a) Oxidation (both chemical and biological);
(b) Dehydration of the alcohol to alkenes or ethers;
(c) Substitution to form alkyl halides;
(d) Esterification and
(e) In the formation of alkoxides.[8]

It is important to note that alcohols are one of the most commonly produced industrial organic chemicals, with some of the more important alcohols being methanol, ethanol, isopropanol, ethylene glycol and glycerol.[8]

2.2.1. Octanol

Octanol belongs to the alcohol group of organic compounds and is comprised of an eight carbon atom chain and the hydroxyl group (1-octanol is shown in Figure 2.4). The synonyms for octanol are caprylic alcohol, n-octyl alcohol and octan-1-ol.[9] The isomers that exist for this alcohol are 2-octanol, 3-octanol and 4-octanol. Octanol has a penetratingly sweet odor and is in the form of a colourless liquid.[9]

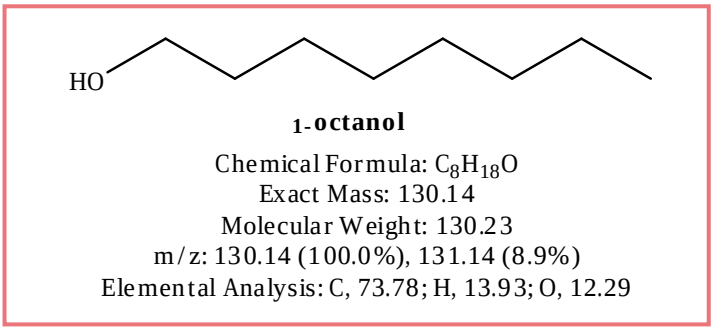

Figure 2.4.: Structure of octanol

There are a wide variety of uses that exist for octanol. These uses include:

(a) In the manufacture of perfumes and other chemicals;
(b) To mask industrial odors;
(c) For formulating wetting and foam control agents;
(d) For flavoring foods;
(e) In resistant coatings and linings;
(f) As a component in pesticide formulations and
(g) In the plastics industry.[10]

Octanol is produced world-wide with the leading regions for the production of octanol being Asia, Western Europe and the United States. It has been found that the world production of octanol is on the increase, indicating that this chemical is leaning toward becoming an important, valued and sort-after product in the chemical industry.[11]

2.3. Hydrogenation

Hydrogenation is a chemical reaction involving the reduction of organic compounds by hydrogen. These compounds include ketones, aldehydes, alkenes, alkynes and imines. When a catalyst is present in the reaction, it is termed catalytic hydrogenation. During this process, finely divided metals or supported metal catalysts induce the reaction to take place on its surface.[12] The general process of catalytic hydrogenation is the attack of a reducible function or ring system of compounds by hydrogen, under a certain pressure at room temperature or elevated temperature in the presence of a catalyst.[12] Some important factors to consider in hydrogenation are:

(a) The catalyst must be able to adsorb and activate the compounds and hydrogen;
(b) The molecule must have an optimal spatial arrangement;
(c) The final product of the reaction must be removed from the catalyst surface;
(d) Good contact between the portion of the molecule being reduced and the catalyst surface must be maintained;
(e) The solvents used;
(f) Promoters for speeding up the reaction and
(g) The effect of acids and bases on the reduction process.[12]

Hydrogenation reactions are used in industry, however, of the variety of hydrogenation reactions that are carried out, only a few are applied on a considerable scale. Petroleum refineries, the pharmaceutical and fine chemical industry are some of the industries that make uses of hydrogenation reactions.[13]

2.3.1. Hydrogenation catalysts

The process of hydrogenation can be catalyzed by either a heterogeneous or homogeneous catalyst. Heterogeneous catalysts for hydrogenation reactions have been widely studied. Initially, these catalysts were the only known catalyst types for catalytic hydrogenation. However, the discovery of Wilkinson's catalyst began the journey into homogeneous catalysis for hydrogenation reactions. These homogeneous catalysts can be placed on supports making them heterogeneous-type catalysts.

Catalytic hydrogenation with heterogeneous catalysts began in 1897 when Sabatier discovered that nickel in the presence of hydrogen led to reduction.[12, 14] Since then many discoveries have been made introducing various metal based compounds as catalysts for hydrogenation reactions. Such catalysts are Raney nickel, Adam's platinum oxide, Adkin's copper chromite catalyst and a number of other catalysts containing noble and transition metals placed on different supports.[14] Catalytic low pressure hydrogenation reactions have colloidal palladium and platinum catalysts, Adam's platinum oxide, Hartung's palladium on carbon and supported rhodium catalysts as their foundation.[12] The introduction of high-pressure hydrogenation reactions was made by Ipatieff in 1904 when he used nickel as the catalyst.[12] High-pressure hydrogenation reactions under less harsh conditions have been established by the discovery of Raney nickel, nickel on kieselguhr, copper chromite and ruthenium on a support or as the dioxide.[12] Commonly used hydrogenation catalysts include copper chromite, nickel, cobalt and the noble metals. Of these former mentioned hydrogenation catalysts, nickel is often used due to its ability to readily adsorb hydrogen into the spaces that exist between the metal atoms.[13]

The discovery of the various hydrogenation catalysts has made it possible for catalytic hydrogenation to become a commercial process. In early years, catalytic hydrogenation was commercially applied to the reduction of unsaturated fats and oils for the production of solid, stable edible fats, and fats and oils used for soap manufacture.[14] Since then,

commercial catalytic hydrogenation processes are used in the production of organic compounds as well as in the petroleum and petrochemical industries (incorporating hydroprocessing, hydrocracking, hydrorefining, hydroisomerization, hydrodealkylation and hydrogenation).[14]

2.3.2. Hydrogenation of aldehydes

From the discussion on hydrogenation in Section 2.3 above, it becomes evident that the hydrogenation of aldehydes involves the addition of hydrogen to the aldehyde which is subsequently reduced to the corresponding alcohol. For linear aldehydes (those aldehydes comprised of an alkyl group without unsaturated bonds), the carbonyl group is subjected to hydrogenation. However, for those aldehydes which contain unsaturated groups, hydrogenation becomes possible for the unsaturated groups and the carbonyl group as well; thus, selective hydrogenation is used to obtain the desired hydrogenated product. The general reaction for the hydrogenation of an aldehyde and α, β-unsaturated aldehyde is given in Schemes 2.1 and 2.2 respectively.

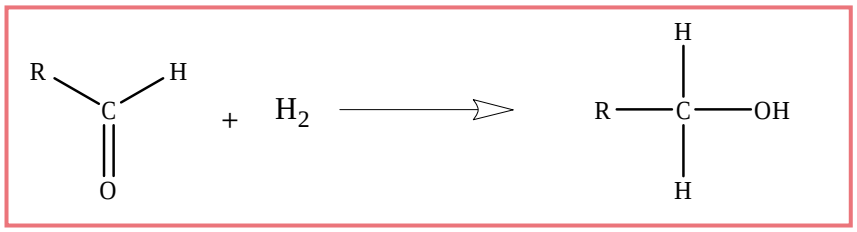

Scheme 2.1: General reaction for the hydrogenation of an aldehyde

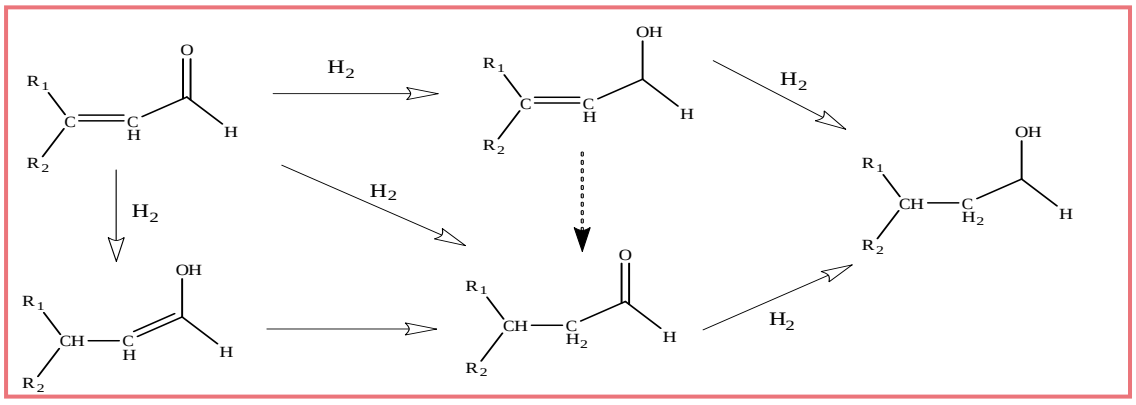

Scheme 2.2: Reaction pathways in the hydrogenation of α, β-unsaturated aldehydes[15]

A number of aldehyde hydrogenation catalysts exist, the most prominent examples being those based on copper (Cu), nickel (Ni), cobalt (Co), rhodium (Rh) and platinum (Pt).[16, 17] However, only those catalysts that are based on Cu, Ni or Pt have the ability to preferentially hydrogenate the carbonyl group.[18] Due to the large costs attached with the use of Pt-based catalysts, Cu- and Ni-based catalysts have been widely used on a commercial scale for the hydrogenation of aldehdyes.[17] Typical operating conditions for the heterogeneously catalyzed hydrogenation of aldehydes are 100 – 150 °C and a pressure of up to 30 bar.[16] The importance of the hydrogenation of aldehydes is linked to its use in converting the aldehydes produced in the oxo process (i.e. hydroformylation) to the major class of organic chemicals, the oxo process alcohols.[19]

2.3.2.1. Hydrogenation of octanal

From the discussions above, it is evident that the hydrogenation of octanal involves the reduction of the carbonyl group (C=O) to the hydroxyl group (-OH) which will yield the corresponding alcohol, octanol. The chemical reaction for this process is given in Scheme 2.3 below.

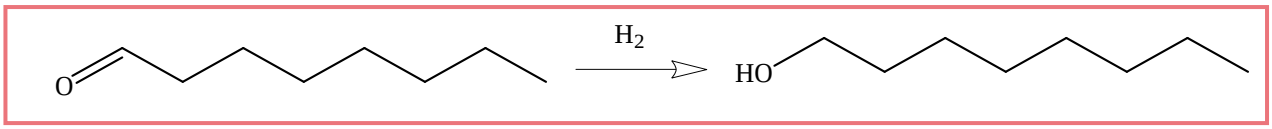

Scheme 2.3: Reaction for the hydrogenation of octanal to octanol

However, as with most chemical reactions, the reaction network and product distribution/composition is not as simple as described in Scheme 2.3. In fact, a far more diverse reaction network exists, with a number of different products being obtained due to the additional reactions that occur in the reaction system. There are two reactions in the octanal hydrogenation system that will be of particular interest:

(a) The desired reaction which forms octanol from the hydrogenation of octanal and
(b) The undesired reactions or side reactions that yield heavy products.[19]

It is expected that the major heavy products would be dimers and trimers formed from aldol condensation of the aldehyde.[19] This hypothesis is based on the work done by *Wang*

et al.[20] on the hydrogenation of the linear aldehydes hexanal and propanal where propanal were used as a model aldehyde to determine the reaction intermediates, products and side reactions. *Wang et al.*[20] showed that propanal is a representative model compound for the study of the hydrogenation reaction of linear aldehydes. This implies that the results of their work can be used as an indication of the expected results during the hydrogenation of octanal.

2.4. References

1. P. Y. Bruice, *Organic Chemistry*, Fourth edn., Pearson Education International, Upper Saddle River New Jersey, 2004.
2. J. March and W. H. Brown, *Aldehyde*, *Chemical compound*, http://www.britannica.com/EBchecked/topic/13527/aldehyde/277613/Uses-of-aldehydes, Accessed 31 March, 2010.
3. J. McMurry and R. C. Fay, *Chemistry*, Second edn., Prentice Hall Inc., Upper Saddle River, New Jersey, 1998.
4. *Octanal*, http://www.chemblink.com/products/124-13-0.htm, Accessed 15 March, 2010.
5. *International Flavors & Ingredients*, *Octanal 35 % (Nat)*, http://www.iff.com/Ingrediants.nsf, Accessed 15 March, 2010.
6. *ChemSynthesis chemical database*, *Octanal*, http://www.chemsynthesis.com, Accessed 15 March, 2010.
7. N. Industries, *Alcohol - History, Names, Properties and Uses, Production, Reactions*, http://www.science.jrank.org/pages/190/Alcohol.html, Accessed 01 April, 2009.
8. L. G. Wade, *Encyclopedia Britannica*, *Alcohol Chemical compound*,http://www.britannica.com, Accessed 31 March, 2010.
9. *Safety data for octyl alcohol*, http://www.msds.chem.ox.ac.uk/oc/octyl_alcohol.html, Accessed 15 March, 2010.
10. *Cheminfo Chemical profiles created by CCOHS*, http://www.intox.org/databank/documents/chemical/chem581/ae581.htm, Accessed 15 March, 2010.
11. *Annual production of two hundred and ninety thousand tons of butanol production*, http://www.au.fjfdi.com/en/cn/project.asp?job=showen&id=8291&yuyan=en, Accessed 15 March, 2010.
12. M. Freifelder, *Practical catalytic hydrogenation*, Wiley-Interscience, Canada, 1971.
13. C. N. Satterfield, *Heterogeneous Catalysis in Industrial Practice*, Second edn., Krieger Publishing Company, Malabar, Florida, 1996.
14. R. J. Peterson, *Hydrogenation catalysts*, Noyes Data Corporation, Parkridge, New Jersey, USA, 1977.
15. P. Gallezot and D. Richards, *Catal. Rev. - Sci. Eng.*, 1998, **40**, 81.
16. J. Hagen, *Industrial Catalysis A Practical Approach*, Wiley-VCH, Weinham, 1999.
17. J. Jeon, J. Yim and Y. Park, *Chem. Eng. J.*, 2008, **140**, 555.

18. A. Saadi, R. Merabti, Z. Rassoul and M. M. Bettahar, *J. Mol. Catal. A: Chem.*, 2006, **253**, 79.
19. X. Wang and U. Ozkan, *J. Mol. Catal. A: Chem.*, 2005, **232**, 101.
20. X. Wang, R. Saleh and U. Ozkan, *J. Catal.*, 2005, **231**, 20.

Chapter 3

Catalyst Deactivation: A Short Overview and Case Study

As discussed in Section 1.3, a number of industrial chemical processes cannot occur without a key component, a catalyst. There is no doubt that the effectiveness of the catalyst is based on a high activity however selectivity to the desired products is of a vital importance. Unfortunately catalysts cannot maintain their initial effectiveness. A chief contributor to the decline of the catalysts efficacy is catalyst deactivation. *Forzatti* and *Lietta*[1] has defined catalyst deactivation as the loss or decline of the activity and/or selectivity of a catalyst with time due to physical or chemical processes that occur during the main reaction. *Bartholomew*[2] has stated that the deactivation of a catalyst is inevitable, but most of its consequences can be slowed down, prevented, avoided or reversed thus making the research into catalyst deactivation issues of significant importance.

Discoveries in the latter mentioned areas result in a groundbreaking impact on commercial catalytic processes. Deactivation mechanisms that exist are poisoning, coking, sintering, attrition/crushing and leaching. *Bartholomew*[2] provides a wide review into the mechanisms of catalyst deactivation. Other descriptions of catalyst deactivation mechanisms are provided by *Forzatti* and *Lietta*[1] and *Moulijn et al.*[3] with more focused reviews given by *Twigg* and *Spencer*[4] and *Besson* and *Gallezot*[5]

As mentioned in Chapter 1, the presence of water in the octanal feed could lead to catalyst deactivation. Hence, it is necessary to understand the concept of deactivation and to know the research that has been done in this area. This will allow for a proper understanding and reasoning of the results obtained from the study. In the following, a brief overview and some case studies specific to hydrogenation (or otherwise stated) systems will be covered for the five deactivation mechanisms above mentioned.

3.1. Poisoning

Poisoning refers to the blocking of catalytically active sites of a catalyst by reactants, products or impurities *via* strong chemisorption of these components. *Bartholomew*[2] highlights the multifold mechanisms of poisoning of a metal surface by sulphur atoms during ethylene hydrogenation. The mechanism is briefly summed up as the physical adsorption of the poison thus blocking active sites, the alteration of adsorptivity of other species due to electronic changes and the modification of the chemical nature of the active sites bringing about reconstruction.[1, 2] An important fact regarding catalyst deactivation by poisoning is that the amount of poison adsorbed forms a thin layer on the surface and therefore does not add to the solid volume of the catalyst in significant proportions, also it does not affect the catalyst/support pore volume.[6]

Poisons may be selective, non-selective or anti-selective; as well as reversible or irreversible. Based on the activity of a catalyst with respect to poison concentration, selective and anti-selective poisoning yields a non-linear relationship. For selective poisoning the more active sites are blocked and for anti-selective poisoning the less active site is blocked first. Non selective poisoning displays a linear relationship between activity and poison concentration, indicating a proportional loss of activity with the concentration of added poison.[1, 2] A reversible poison displays adsorption that is strong but 'weak' enough to allow for its removal from the catalyst surface (catalyst regeneration). An irreversible poison displays very strong adsorption and causes permanent damage to the catalyst.

Forzatti and *Lietta*[1] lists examples of poisons of industrial catalysts and states that typical poisons for metals of groups VIII B (such as Ni, Pd, Pt) and I B (such as Cu, Ag, Au) are molecules containing elements of group V A (e.g. S).[1] In addition compounds that have unoccupied orbital's or unpaired electrons are considered potential poisons. More examples of poisons are provided by *Moulijn et al.*[3] and *Bartholomew*[2]. Investigations into catalyst deactivation caused by the presence of poisons that have unoccupied orbital's or unpaired electrons, have shown similar influence on the catalytic reaction, whilst their regeneration procedures are entirely different.[1, 5] Poisons that are classified by the two former mentioned poison categories, have been shown to have the ability to poison nickel catalysts used for used hydrogenation reactions and cause their deactivation.[7-9]

Organic impurities present in the feedstock or as by-products of a reaction are also capable of causing catalyst deactivation *via* the poisoning mechanism.[4] An example of this type of poison is carboxylic acid, which is a by-product of a number of different hydrogenation reactions. Since carboxylic acids possess the ability to strongly adsorb to the active metal, they can block the active sites present in the catalyst, which subsequently leads to the deactivation of the catalyst.[10] This was demonstrated by *Abdullah et al.*[11] using IR spectroscopy. In their study, different carboxylic acids were adsorbed on the reduced catalyst. The IR study showed that the M^0 active site was no longer available for C=O adsorption, hence poisoning the carbonyl group hydrogenation reaction. Surface poisoning can also be deduced by a decrease in the BET surface area. A regeneration method for carboxylic acid poisoned catalysts was presented by *Hoffer et al.*[10] which involved hydrogen treatment at 120 °C, whilst *Besson* and *Gallezot*[5] state that the washing of the spent catalyst in a basic medium will remove the strongly adsorbed acidic species. Another regeneration technique called 'flashing' was shown to be useful for removing adsorbed carboxylate groups from the catalyst surface, however, effectiveness of this regeneration technique is temperature dependent.[11]

A common side reaction in all aldehyde hydrogenation reactions is the decarbonylation of the aldehyde. The carbon monoxide (CO) produced has been shown to cause catalyst deactivation, by strongly adsorbing to the surface of the active metal.[12, 13] The use of ATR-IR spectroscopy has proven to be useful for determining the poisoning of a catalyst by CO.[12] Whilst *Burgerner et al.*[12] showed that the regeneration of CO poisoned catalysts by oxidative treatment was not successful, *Englisch et al.*[13, 14] showed that the initial activity of the spent catalyst can be regained by the removal of CO *via* evacuation or hydrogenation at 400 °C for gas phase reactions and by purging the spent catalyst with air for the liquid phase reactions.[12, 13] Alumina- and silica-supported Pt-Sn catalysts used for crotonaldehyde hydrogenation were investigated by *Coloma et al.*[15]. An *in-situ* DRIFTS study was used and indicated that these catalysts deactivated due to the irreversible adsorption of CO formed from the decarbonylation of crotonaldehyde. These results are in accordance with other studies on the crotonaldehyde hydrogenation system using various supported metal catalysts.[13, 14, 16, 17]

Water, in both the liquid and vapor form, has been shown to cause catalyst deactivation.[18-21] Nickel hydrogenation catalysts have been found to deactivate in the presence of water

vapor with pressures as low as 3 x 10^{-4} mm, however, the influence of the water on the 'make-up' of the catalyst causing deactivation was not shown.[18] In the study carried out by *Chang et al.*[19], it was shown that the Pd/δ-Al_2O_3, used for the selective hydrogenation of isoprene, deactivated rapidly after the water-containing feed was introduced to the system. Using FT-IR and CO chemisorptions, the deactivation of the catalyst was found to be due to the adsorption of the water molecules on the Pd (active metal) clusters.[19] The regeneration studies by both *Chang et al.*[19] and *Burford* and *Frazer*[18] showed that hydrogen reactivation with heating can renew the activity of the spent catalyst,[18, 19] however, the temperature of the hydrogen regeneration procedure can influence the efficiency of the reactivation[19]. In those reactions that do not involve hydrogenation, it has been shown using XPS that water reacts with the active metal oxide to produce an inactive metal hydroxide, which leads to the poisoning of the catalyst.[20] However, *Wang et al.*[21] have also shown that the water promoted deactivation of amorphous NiB/SiO_2 during the selective hydrogenation of cyclopentadiene to cyclopentene, is due to the surface oxidation of elemental Ni to $Ni(OH)_2$ (as determined by XPS). This result was also obtained by *Zhang et al.*[22] in their study on the selective hydrogenation of reformate oils over amorphous NiB/SiO_2 catalysts, whilst *Wu et al.*[23], in their study on the deactivation of amorphous NiB/MgO hydrogenation catalysts, concluded that water leads to an activity decrease, but does not influence catalyst deactivation significantly.[23] Similarly, *Wang et al.*[24, 25] showed that the conversion of hexanal (in the gas phase hydrogenation) decreased when water was introduced into the reactor system. Although there was some loss of catalytic activity, the selectivity to the hexanol was maintained and may be due to the water inhibiting heavy product formation.[24, 25] However, in the liquid phase hydrogenation of hexanal, no change in conversion was observed when water was added to the reaction system. Only a slight increase in the selectivity to hexanol was observed.[25]

Studies have shown the deactivation effects of sulphur-containing compounds.[23, 26-34] Some of these studies are discussed in this section. *Wu et al.*[23] investigated the deactivation of the amorphous NiB/MgO catalyst in the hydrogenation of sulfolene and found that the catalyst deactivated primarily due to the poisoning by sulphur-containing compounds. This deduction was made from the TEM images and XPS and IR spectra of the spent catalyst.[23] Compounds such as phosphorus can also cause the poisoning of the catalyst leading to loss of activity.[27] *Chang et al.*[33] showed that the sulphur-poisoned

catalyst can be regenerated by hydrogen reactivation; however, the initial activity cannot be regained.

Rodríguez et al.[35] studied the deactivation of spinel-type Ni catalysts and is an example of how catalyst deactivation influences the selectivity of the catalyst.[35] The $NiAl_2O_4$ and $NiZnAl_2O_4$ catalysts were subjected to poisoning by pre-treating the catalyst with H_2S, as well as poisoning during the main reaction. It was found that both catalysts investigated showed a fast increment in the coking rate and ethane selectivity when the H_2S was introduced during the reaction. Poisoning of these catalysts by pretreating with H_2S yielded different results for each catalyst. In the $NiAl_2O_4$ catalyst, the active metallic sites responsible for structure-sensitive reactions, such as coke formation, are preferentially deactivated by the sulphur forming amorphous carbon. This indicates selective poisoning. However, the zinc modified catalyst showed a lower hydrogenation yield and a greater coke formation of different morphology (amorphous and filamentous carbon were present). This indicates that the dominant sites were poisoned. These results display the effect of charge transfer on catalyst deactivation. The presence of electron-donating (e.g. nitrogen-containing compounds) or electron-attracting compounds (e.g. sulphur- or chlorine-containing compounds) on the catalyst surface influences the reactions or side reactions occurring on the catalyst surface, thus often enhancing the deactivation of the catalyst *via* a particular mechanism. Hence, the presence of the electron-attracting H_2S on the catalyst surface enhances the side reactions such as coke formation, due to an effect of charge transfer to sulphur which increases the strength of adsorption of ethyne molecules, thus favoring their degradation towards coke.[35]

Waghray and *Blackmond*[31] have also shown that the poisoning of the catalyst can improve the selectivity to the desired product. Their work involved the hydrogenation of 3-methyl-2-butenal over promoted and unpromoted Ru/SiO_2 catalysts. Using *in-situ* IR, the presence of CO and organic fragments adsorbed on the catalyst surface was seen. They suggested that this CO formed during decarbonylation and the organic fragments, partially 'self-poisons' the catalyst surface (to a certain degree) and hence prevents the reaction pathway of the undesired products.[31]

The work carried out by *Mori et al.*[28] also used sulphur-containing compounds as a catalyst poison to achieve chemoselective hydrogenation between different types of

reducible functionalities. Their work showed that by poisoning the Pd/C catalyst with diphenyl sulphide (Ph_2S), a moderate decline in the activity of the catalyst occurred, whilst chemoselective hydrogenation of the desired compounds, in the presence of other reducible functionalities, was obtained.[28] This work demonstrates how the poisoning deactivation mechanism can be used to direct the selectivity to the desired products without significant loss of catalytic activity. *Padley et al.*[29] have shown that both sulphur dioxide and thiophene influence the adsorption of CO on Cu/SiO_2 differently. The information from this study provides an insight into the adsorption of carbonyl groups and the influence of sulphur-containing compounds on the activity of the catalyst. The work has shown that sulphur dioxide does not inhibit CO adsorption, whereas thiophene does block the adsorption of CO on the Cu^0.[29] Other hydrogenation systems have shown that thiophene causes the greatest deactivation, indicating that thiophene is the more influential catalyst poison compared to other sulphur-containing compounds.[36] The poisoning of the M^0 sites by thiophene was also shown in another study by *Bailie et al.*[26] Heterocyclic compounds such as cyclopentadiene, furan and pyrrole were able to poison the M^0 sites as well.[26] The poisoning of the catalysts by sulphur-containing compounds can be reduced by alkali-doping of the catalyst.[36] *Besson* and *Gallezot*[5] state that the effects of sulphur poisoning on copper hydrogenation catalysts can be cancelled with the use of a ZnO support.[5]

Englisch et al.[14] also showed that the catalyst may deactivate due to the presence of long organic molecules that are adsorbed on the catalyst. Their work stated that long organic molecules can only be partially removed by purging with He or by reduction at 400 °C.[14] Another study into the hydrogenation of crotonaldehyde was carried out by *Rodrigues et al.*[37] using used copper-based catalysts. The study showed that the conversion rate of crotonaldehyde decreased with time-on-stream as a result of the formation of carbonaceous species on the catalyst surface. The presence of coke formation during the hydrogenation of crotonaldehdye was confirmed using TPO.[37]

The hydrogenation of CO, at high temperatures, using Ni/SiO_2 was investigated by *Agnelli and Mirodatos*[38]. The results of their study showed that the catalyst deactivated primarily due to the formation of stable carbonaceous deposits on the metal particles. Using TPH, the type of carbon deposit was deduced. Previous work has shown that this carbonaceous species are in the form of surface nickel carbide.[39] To obtain a more stable

catalyst for the reaction, copper was added to the catalyst ($NiCu/SiO_2$). The CO hydrogenation using the $NiCu/SiO_2$ catalyst showed that only catalysts with high copper concentrations were able to avoid deactivation, but this caused a decrease in the conversion of CO.[38] The blocking of the active metal sites by nonreactive species of the dehydrogenated residue or by reaction products (carbonaceous species) has also been shown to be the cause of catalyst deactivation by *Ali et al.*[40] in a study of the hydrogenation of aromatics on modified platinum-alumina catalysts.

3.2. Fouling

Fouling is a physical mechanism of catalyst deactivation where active sites and/or pores are blocked by the physical deposition of species from the fluid phase onto the catalyst surface.[2] As a result of these occurrences, a noticeable amount of the pore volume is occupied causing the distortion of the pore structure.[6] This indicates that a complete analysis and proper understanding of the catalyst's pore structure and layout of the pore spaces is required to ascertain the presence of deactivation by fouling, as well as to understand the foulant's influence on catalyst reactivity.[6]

The primary example of fouling is the mechanical deposits of carbon and coke (formed by unwanted polymerization and dehydrogenation of the organic feed or formed product molecules) in porous catalysts.[2, 3] Other examples of fouling include the deposition of large molecules formed by free radical mechanisms, deposition of undesired by-products formed during the reaction and deposition of oligomerisation and alkylation products.[3] The deposition of these species has the ability to hinder reactant access to and product desorption from the catalyst surface.[5]

Zhu and *Hofmann*[41] investigated the deactivation of $Ni/SiO_2/Al_2O_3$ used in the hydrogenation of 3-hydroxypropanal to 1,3-propanediol. It was found that the deactivation of this catalyst was due to the adsorption of by-products and possibly the impurities present in the feedstock. Due to a decreased mesopore radius, specific area and radius distribution, *Zhu* and *Hofmann*[41] concluded that the main cause of the deactivation of the catalyst was due to pore blockage by higher molecular species. The work carried out by *Zhao et al.*[42] investigated the deactivation of the $Ni/K_2O\text{-}La_2O_3\text{-}SiO_2$

catalyst for the hydrogenation of *m*-nitrobenzene to *m*-phenylenediamine.[42] They also found that the main contributing factor to its deactivation was surface coverage and pore blockage with bulky molecular species. However, this conclusion was reached from the results obtained from the N_2 adsorption-desorption, TG/DTA and SEM-EDX.[42]

A catalytic and ATR-IR study was performed by *Burgerner et al.*[12] in order to establish the nature of catalyst deactivation of Pd/Al_2O_3 during the hydrogenation of citronellal. It was found that the chief contributor to the irreversible deactivation of the catalyst was the blocking of active sites by heavier oligomeric surface products.[12] Other studies of hydrogenation systems and non-hydrogenation systems have also shown catalyst deactivation due to coking.[11, 22, 26, 27, 43-57] *Yeong et al.*[43] have shown that organic deposits on the $Pd/\gamma\text{-}Al_2O_3$ surface can be removed by treating the catalyst in air at 130 °C whilst *Peña et al.*[48] propose catalyst aging ($Ni/NiAl_2O_4$) as a means to reduce coke formation. At different temperatures, the type of coke species formed is different, thus, depending on the stability of the coke species, H_2 gasification can used to remove the coke formed.[53] Essentially, the blocking of catalytic sites by chemisorption of hydrocarbons, surface carbides or relatively reactive films can be reversed in H_2, steam, CO_2 or oxygen. If this route cannot be applied, a suitable regeneration procedure must be used.[1, 2]

3.3. Leaching

Leaching is a deactivation mechanism which results in the loss of the active phase. It is a phenomenon most common for liquid phase reactions[58, 59] and is often reversible. The leaching of the metal atoms is dependent on the pH, oxidation potential and chelating properties of the reaction medium, as well as on bulk and surface metal properties.[3, 42]

Gallezot et al.[7] utilized metal-promoted Raney nickel catalysts for the hydrogenation of glucose. It was shown that the catalyst underwent deactivation after successive recycling due to the loss of the promoters.[7]

In addition to the fouling deactivation mechanism discussed in Section 3.2, *Zhao et al.*[42] detected the presence of nickel in the test solution. Such results indicate that a leaching

mechanism exists in this catalytic system. This loss of active metal (Ni) was attributed to the dissolution of the acidic silica support in the basic medium.[42]

The dual effect of water on a catalyst was demonstrated in the study performed by *Ma et al.*[20] in the production of hydrogen peroxide from carbon monoxide, water and oxygen. A novel alumina-supported nickel catalyst was used for the investigation. Water caused poisoning of the catalyst by reacting with the active NiO to produce the catalytically inactive $Ni(OH)_2$ specie which reacts with the phosphorous acid (present in the reaction mixture) to produce a salt, Ni_3PO_4. This salt partially dissolves in the media and thus surface Ni atoms are lost.[20]

In addition to the poisoning by the carboxylic acid (discussed in Section 3.1), *Hoffer et al.*[10] showed that the acidity of the reaction mixture is increased due to the presence of the acid causing the dissolution of the Ni into the product mixture. This result was confirmed by using ICP-OES and the decrease in the BET surface area.[10]

3.4. Mechanical Stress

A catalyst can deactivate mechanically where the catalytic material is lost due to attrition or abrasion or there may be loss of the surface area due to crushing. Such deactivation mechanisms have been found to be irreversible. Since a catalyst can deactivate *via* this pathway, it becomes important to ensure that the catalyst is able to withstand mechanical stresses it will encounter under the reaction conditions. The mechanical strength of the catalyst is influenced by the shape of the catalyst particles and its porosity.[3]

A catalyst can be crushed during the transport and loading of the catalyst particles in the reactor and depending on the reactor used, it will be introduced to varying mechanical stresses. Packed bed reactors and fixed-bed reactors are prone to mechanical stresses due to temperature changes and fluidized-bed reactors will always encounter attrition.[3]

In addition to the fouling and leaching deactivation mechanisms (Section 3.2 and 3.3), *Zhao et al.*[42] found that the catalyst used in the hydrogenation of *m*-dinitrobenzene to *m*-phenylenediamine was prone to mechanical abrasion. The loss of the active species from

the support indicated that the catalyst had broken up and the SEM image of the used catalyst showed the presence of smaller particles. This confirmed that the catalyst underwent mechanical deactivation as a result of the collision of particles with each other and with the reactor walls.[42]

3.5. Sintering

Sintering is an irreversible deactivation mechanism that occurs in both supported and unsupported catalysts. The mechanism involved in the sintering of unsupported catalysts is the reduction of the active surface area due to the influence of agglomeration and coalescence of small metal crystallites into larger ones with lower surface-to-volume ratios.[1] The growth of the particles can occur *via* crystallite migration, followed by coalescence or Ostwald ripening.[60] The deactivation of a catalyst by sintering shows a loss of surface area due to the distortion and collapse of the pore structure.[6] Sintering can occur when there are thermal effects, such as excesses in temperature, or other consequent chemical interactions which result in the solid phases of the catalyst becoming soft, or melting or possibly restructuring.[6] Temperature, atmosphere, metal type, metal dispersion, promoters or impurities, support surface area, texture and porosity of the supported metal catalyst each have their own influence on the rate at which the catalyst will sinter.[2] Studies carried out by *Huang et al.*[61] and *Mandreoli et al.*[56] have shown that high temperatures introduce catalyst deactivation due to sintering. Catalyst deactivation by this mechanism should best be avoided since the spent catalyst cannot be regenerated.

In addition to the sulfolene hydrogen discussed in Section 3.1, *Wu et al.*[23] also looked at the hydrogenation of acetophenone using the NiB/MgO catalyst. Deactivation of the catalyst set in after the seventh recycle run of the catalyst. Using HRTEM and H_2 chemisorption, it was seen that there was a destruction of pore structure and loss of surface concentration of Ni after the seventh recycle hydrogenation, thus causing deactivation.[23] These results imply that the catalyst may have sintered, although the authors do not mention this. Similarly, *Pillai et al.*[62] showed that the loss of metal surface area (after a number of runs) was the cause of catalyst deactivation during the hydrogenation of maleic anhydride.

The sintering of supported nickel catalysts for steam reforming reactions is useful to show the effects of sintering. *Sehested*[63] has stated that the sintering of a catalyst can influence coking, sulphur poisoning and catalyst activity, thus showing mutual dependency.[60, 63] Studies have shown that the sintering of these supported nickel catalysts is influenced by the amount of active metal in the catalyst[64], however, the size of the particles after sintering showed no strong dependency on metal loading and surface area of the support.[64] *Lif et al.*[65] have shown that the higher surface area Ni on γ-alumina is more resistant to sintering than the transalumina or α-alumina supported Ni. Similarly, the loss of Pd during the hydrogenation of nitrobenzene was overcome by using Pd supported on γ-alumina (prepared *via* the impregnation method).[43] This occurrence is primarily due to the stronger support-metal interaction existing in the Ni on γ-alumina catalyst.[65] Other parameters that influence the sintering of steam-reforming catalysts are temperature, steam and hydrogen pressure and surface area of the support.[60] The solvent used for the reaction has also been shown to influence sintering, with highly polar solvents being able to promote this deactivation mechanism.[58] *Sehested et al.*[66] have shown that the rate of sintering increased in the presence of steam, as well as at higher temperatures (greater than 700 °C). *Rasmussen et al.*[67] have shown that the rate of sintering is affected by the mechanism of particle growth occurring at different temperatures. This was also observed by *Sehested et al.*[60], who also showed that the rate of sintering increased upon adding a potassium promoter to the catalyst and by poisoning of the catalyst with sulphur.

Together with the high temperature CO hydrogenation (Section 3.1), *Agnelli and Mirodatos*[38] also studied the effects of copper addition to Ni/SiO_2 at low temperatures. Their work shows that sintering of the active nickel phase is the main cause of deactivation at low temperatures. However, this deactivation can be avoided by adding low concentrations of copper to the Ni/SiO_2 catalyst without significant change to the conversion of CO.[38] Other studies have also shown the deactivation of the catalyst due to sintering.[22, 57, 68]

In the subsequent Chapters', the procedures used for this study as well as the information obtained from it, will be presented and discussed.

3.6. References

1. P. Forzatti and L. Lietta, *Catal. Today*, 1999, **52**, 165.
2. C. H. Bartholomew, *Appl. Catal. A: Gen.*, 2001, **212**, 17.
3. J. A. Moulijn, A. E. van Diepen and F. Kapteijnm, *Appl. Catal. A: Gen.*, 2001, **212**, 3.
4. M. V. Twigg and M. S. Spencer, *Appl. Catal. A: Gen.*, 2001, **212**, 161.
5. M. Besson and P. Gallezot, *Catal. Today*, 2003, **81**, 547.
6. R. Mann, *Catal. Today*, 1997, **37**, 331.
7. P. Gallezot, P. J. Cerino, B. Blanc, G. Flèche and P. Fuertesl, *J. Catal.*, 1994, **146**, 93.
8. R. Hughes, *Deactivation of Catalysts*, Academic Press, London, 1984.
9. C. N. Satterfield, *Heterogeneous Catalysis in Practice*, McGraw-Hill, New York, 1980.
10. B. W. Hoffer, E. Crezee, F. Devred, P. R. M. Mooijman, W. G. Sloof, P. J. Kooyman, A. D. van Langeveld, K. Kapteijn and J. A. Moulijn, *Appl. Catal. A: Gen.*, 2003, **253**, 437.
11. H. A. Abdullah, C. H. Rochester, J. A. Anderson, J. E. Bailie, N. V. Richardson and G. J. Hutchings, *Phys. Chem. Chem. Phys.*, 2000, **2**, 3952.
12. M. Burgerner, R. Wirz, T. Mallat and A. Baiker, *J. Catal.*, 2004, **228**, 152.
13. M. Englisch, V. S. Ranade and J. A. Lercher, *Appl. Catal. A: Gen.*, 1997, **163**, 111.
14. M. Englisch, A. Jentys and J. A. Lercher, *J. Catal.*, 1997, **166**, 25.
15. F. Coloma, J. Llorca, N. Homs, P. R. de la Piscina, F. Rodríguez-Reinoso and A. Sepúlveda-Escribano, *Phys. Chem. Chem. Phys.*, 2000, **2**, 3063.
16. F. Coloma, J. Narciso-Romero, A. Sepúlveda-Escribano and F. Rodíguez-Reinoso, *Carbon*, 1998, **36**, 1011.
17. A. Sepúlveda-Escribano, F. Coloma and F. Rodríguez-Reinoso, *J. Catal.*, 1998, **178**, 649.
18. W. B. Burford and J. C. W. Frazer, *J. Am. Chem. Soc.*, 1945, **67**, 331.
19. J. Chang, T. Lin and C. Cheng, *Ind. Eng. Chem. Res.*, 1997, **36**, 5096.
20. Z. Ma, R. Jia and C. Liu, *J. Mol. Catal. A: Chem.*, 2004, **210**, 157.
21. W. Wang, M. Qiao, H. Li, W. Dai and J. Deng, *Appl. Catal. A: Gen.*, 1998, **168**, 151.
22. X. Zhang, A. Ma, X. Mu and E. Min, *Catal. Today*, 2002, **74**, 77.
23. Z. Wu, M. Zhang, W. Lei, S. Mu and K. Tao, *J. Mol. Catal. A: Chem.*, 2007, **273**, 277.
24. X. Wang, G. Li and U. S. Ozkan, *J. Mol. Catal. A: Chem.*, 2004, **217**, 219.
25. X. Wang, R. Y. Saleh and U. S. Ozkan, *J. Catal.*, 2005, **231**, 20.
26. J. E. Bailie, G. J. Hutchings, H. A. Abdullah, J. A. Anderson and C. H. Rochester, *Phys. Chem. Chem. Phys.*, 2000, **2**, 283.

27. P. Mäki-Arvela, G. Martin, I. Simakova, A. Tokarev, J. Wärnå and J. Hemming, *Chem. Eng. J.*, 2009, **154**, 45.
28. A. Mori, T. Mizusaki, Y. Miyakawa, E. Ohashi, T. Haga, T. Maegawa, Y. Monguchi and H. Sajiki, *Tetrahedron*, 2006, **62**, 11925.
29. M. B. Padley, C. H. Rochester and G. J. Hutchings, *J. Chem. Soc. Faraday Trans.*, 1994, **90**, 203.
30. L. M. Porto and J. B. Butt, *Ind. Eng. Chem. Res.*, 2002, **41**, 5420.
31. A. Waghray and D. G. Balckmond, *J. Phys. Chem.*, 1993, **97**, 6002.
32. P. Costa, J. Lemberton, C. Potvin, J. Manoli, G. Perot, M. Breysse and G. Djega-Mariadassou, *Catal. Today*, 2001, **65**, 195.
33. J. Chang and S. Chang, *J. Catal.*, 1998, **176**, 42.
34. F. Pinna, F. Menegazzo, M. Signoretto, P. Canton, G. Fagherazzi and N. Pernicone, *Appl. Catal. A: Gen.*, 2001, **219**, 195.
35. J. C. Rodríquez, E. Romeo, J. L. G. Fierro, J. Santamaría and A. Monzón, *Catal. Today*, 1997, **37**, 255.
36. A.Díaz, J. A. Odriozola and M. Montes, *Appl. Catal. A: Gen.*, 1998, **166**, 163.
37. E. L. Rodrigues, A. J. Marchi, C. R. Apesteguia and J. M. C. Bueno, *Appl. Catal. A: Gen.*, 2005, **294**, 197.
38. M. Agnelli and C. Mirodatos, *J. Catal.*, 2000, **192**, 204.
39. M. Agnelli, H. M. Swaan, C. H. Marquez-Alvarez, G. A. Martin and C. Mirodatos, *J. Catal.*, 1998, **175**, 117.
40. A. A. Ali, L. I. Ali, S. M. Aboul-Fotouh and A. K. Aboul-Gheit, *Appl. Catal. A: Gen.*, 1998, **170**, 285.
41. X. D. Zhu and H. Hofmann, *Appl. Catal. A: Gen.*, 1997, **155**, 179.
42. L. Zhao, J. Chen and J. Zhang, *J. Mol. Catal. A: Chem.*, 2006, **246**, 140.
43. K. K. Yeong, A. Gavriilidis, R. Zapf and V. Hessel, *Catal. Today*, 2003, **81**, 641.
44. S. Lee, J. Kim, W. C. Shin, M. Choi and S. Choung, *J. Mol. Catal. A: Chem.*, 2009, **301**, 98.
45. J. M. Bonello, R. M. Lambert, N. Künzle and A. Baiker, *J. Am. Chem. Soc.*, 2000, **122**, 9864.
46. P. A. Rautanen, J. R. Aittamaa and A. O. I. Krause, *Chem. Eng. Sci.*, 2001, **56**, 1247.
47. T. Salmi, P. Mäki-Arvela, E. Toukoniitty, A. K. Neyestanaki, L. Tiainen, L. Lindfors, R. Sjöholm and E. Laine, *Appl. Catal. A: Gen.*, 2000, **196**, 93.

48. J. A. Peña, J. Herguido, C. Guimon, A. Monzón and J. Santamaría, *J. Catal.*, 1996, **159**, 313.
49. B. Campo, C. Petit and M. A. Volpe, *J. Catal.*, 2008, **254**, 71.
50. E. Klemm, B. Amon, H. Redlingshöfer, E. Dieterich and G. Emig, *Chem. Eng. Sci.*, 2001, **56**, 1347.
51. M. S. Lylykangas, P. A. Rautanen and A. O. I. Krause, *Ind. Eng. Chem. Res.*, 2004, **43**, 1641.
52. M. Larsson, J. Jansson and S. Asplund, *J. Catal.*, 1998, **178**, 49.
53. D. Duprez, K. Fadili and J. Barbier, *Ind. Eng. Chem. Res.*, 1997, **36**, 3180.
54. C. Moreno-Castilla, M. A. Alvarez-Merino, F. Carrasco-Martin and J. L. G. Fierro, *Langmuir*, 2001, **17**, 1752.
55. X. Ouyang and R. S. Besser, *Catal. Today*, 2003, **84**, 33.
56. M. Mandreoli, A. Vaccari, E. Veggetti, M. Jacquin, D. J. Jones and J. Roziere, *Appl. Catal. A: Gen.*, 2002, **231**, 263.
57. J. Mikkola, H. Vainio, T. Salmi, R. Sjöholm, T. Ollonqvist and J. Väyrynen, *Appl. Catal. A: Gen.*, 2000, **196**, 143.
58. J. Panpranot, K. Phandinthong, P. Praserthdam, M. Hasegawa, S. Fujita and M. Arai, *J. Mol. Catal. A: Chem.*, 2006, **253**, 20.
59. F. Zhao, M. Shirai, Y. Ikushima and M. Arai, *J. Mol. Catal. A: Chem.*, 2002, **180**, 211.
60. J. Sehested, J. A. P. Gelten and S. Helveg, *Appl. Catal. A: Gen.*, 2006, **309**, 237.
61. W. Huang, J. N. Kuhn, C. Tsung, Y. Zhang, S. E. Habas, P. Yang and G. A. Somorjai, *Nano Lett.*, 2008, **8**, 2027.
62. U. R. Pillai, E. Sahle-Demessie and D. Young, *Appl. Catal. B: Enviro.*, 2003, **43**, 131.
63. J. Sehested, *Catal. Today*, 2006, **111**, 103.
64. J. Sehested, A. Carlsson, T. V. W. Janssens, P. L. Hansen and A. K. Datye, *J. Catal.*, 2001, **197**, 2001.
65. J. Lif, I. Odenbrand and M. Skoglundh, *Appl. Catal. A: Gen.*, 2007, **317**, 62.
66. J. Sehested, J. A. P. Gelten, I. N. Remediakis, H. Bengaard and J. K. Nørskov, *J. Catal.*, 2004, **223**, 432.
67. F. B. Rasmussen, J. Sehested, H. T. Teunissen, A. M. Molenbroek and B. S. Clausen, *Appl. Catal. A: Gen.*, 2004, **267**, 165.
68. J. Hong, J. S. Hwang, K. Jun, J. C. Sur and K. Lee, *Appl. Catal. A: Gen.*, 2001, **218**, 53.

Chapter 4

Experimental

The synthesis and characterization of the supported CuO catalysts forms a vital part of this study. Correct and careful preparation of these catalysts is required to obtain the desired properties to yield the 'best' catalytic results. The necessity of catalyst characterization has been mentioned in Chapter 1. The information obtained from the characterization techniques explained in Section 1.6, provides insight into the various properties of the catalyst. In addition, it may possibly indicate the interactions that exist between the catalyst and reactants/products in the reaction system. Catalyst characterization is pivotal in a deactivation study since the various characterization techniques employed indicate the possible deactivation mechanism/s that exists in the reaction under study. In the sections to follow, the methodology used for each characterization analysis will be provided. In addition, the necessary information pertaining to the synthesis and the catalytic testing will be given.

4.1. Synthesis of Catalysts

The various synthesis routes to prepare supported catalysts were given in Section 1.3.2.4. For this study, two techniques were employed in the catalyst synthesis. These were the method of co-precipitation which was used to synthesize CuO/Cr_2O_3 and the wet impregnation method which was used to prepare CuO/SiO_2 and CuO/Al_2O_3. Since a suitable commercial chromia support could not be obtained, the method of co-precipitation was employed for synthesizing CuO/Cr_2O_3. For the other two catalysts, the correct oxide phases could not be obtained (after numerous attempts) using co-precipitation, thus wet-impregnation was used. The synthesis of the catalysts were based on the work done by *S.V. Gredig et al.*[1] and *K.K. Bando et al.*[2]. Their synthetic procedure was modified to obtain the desired catalyst requirements for this study. Each of these preparative methods is discussed below.

4.1.1. Synthesis of CuO/Cr_2O_3

The Cu/Cr_2O_3 catalyst was synthesized from the metal nitrate solutions (0.4 M) with sodium hydroxide (NaOH) at a constant temperature of 298 K and at a pH of approximately 7. The metal nitrate solutions were added dropwise to a round bottomed flask containing distilled water under vigorous stirring. At the same time, NaOH was added dropwise to regulate the pH to the desired value and assist in precipitation. The slurry was aged for half an hour at room temperature and constant pH. The resulting precipitate was filtered, washed with distilled water and dried overnight at 120 ℃. The dried catalyst was crushed and thereafter calcined in air for 8 hours at 550 ℃. The catalyst was pelletized and sieved to a particle size of 300 – 600 microns. For example, a 6.0 g of copper nitrate and 20.0 g of chromium nitrate was used to obtain a metal loading of approximately 26 wt % copper.

4.1.2. Synthesis of CuO/SiO_2 and CuO/Al_2O_3

A copper nitrate solution was prepared by dissolving the required amount of copper nitrate in sufficient water to allow dissolution of the metal salt. The solution was then added to the catalyst support under stirring. The slurry obtained was stirred for 24 hours. Thereafter, the water was slowly evaporated by gentle heating with stirring. The resulting solid obtained was oven-dried overnight at 120 ℃ and thereafter calcined in air for 8 hours at 600 ℃. The catalysts were pelletized and sieved to a particle size of 300 – 600 microns. For example, 9.0 g of copper nitrate and 7.5 g alumina were used to obtain a catalyst with approximately 25 wt % copper.

4.2. Catalyst Characterization

4.2.1. X-Ray Diffraction (XRD)

The identification of crystalline compounds was obtained by X-Ray diffraction (XRD) using a Bruker XRD diffractometer employing Cu K_α radiation (λ = 1.5418 Å). The samples were analyzed as powders and were packed into a glass sample holder with a cavity having dimensions of 20 x 16 x 0.5 mm. The operating conditions for the XRD were 45 kV

and 100 mA with a scanning rate of 0.5 deg/min slit (in 2θ) and divergence slit and scatter slit widths of 1°.

4.2.2 Scanning Electron Microscopy (SEM)

The surface morphology was obtained using SEM and a backscattered detector was used to obtain backscattered SEM images to determine the location of the elements present in the material. Elemental composition scanning (EDS) was used to determine the elements present and their distribution in the catalyst. Prior to the SEM and EDS analysis, the samples were mounted on an aluminium stub using double-sided carbon tape and subsequently gold splutter coated using a Polaron E5100 coating unit and carbon coated using a Jeol JEE-4C vacuum evaporator for the SEM and EDS analyses respectively. The secondary (normal) and backscattered SEM images were viewed on a Leo 1450 scanning electron microscope. The EDS composition scanning was done on a Jeol JSM-6100 scanning microscope fitted with a Bruker EDX detector and was analyzed using Esprit 1.8 software.

4.2.3. Transmission Electron Microscopy (TEM)

TEM was used for obtaining images, particle sizes and selected area electron diffraction (SAED) patterns for the catalyst samples. The images and SAED patterns were viewed on a Jeol JEM-1010 electron microscope. The images were captured and analyzed using iTEM software.

4.2.4. Inductively Coupled Plasma-Optical Emission Spectroscopy (ICP-OES)

The elemental composition of the catalysts was determined by ICP-OES on a Perkin Elmer Precisely Optical Emission Spectrometer Optima 5300 DV. Prior to analysis, the catalyst samples were digested with concentrated nitric acid. In addition, a set of copper standards in the appropriate concentration range were prepared and analyzed to obtain the calibration curve from which the copper concentration in the samples were interpolated.

4.2.5. Brunauer-Emmet-Teller (BET) surface area and pore volume

The specific surface area and pore volumes of the catalyst were obtained by using the BET nitrogen physisorption analysis. This was done on a Micrometrics Gemini instrument and involved degassing the sample overnight at 200 °C under nitrogen flow using the Micrometrics FlowPrep 060. The degassed samples were cooled to room temperature and weighed. The surface area measurements and total pore volume analyses were performed on these samples with nitrogen adsorbate at -196 °C.

4.2.6. Temperature Programmed Reduction (TPR) and Temperature Programmed Desorption (TPD)

TPR and TPD were carried out on a Micrometrics Autochem II Chemisorption Analyzer. For both the H_2-TPR and NH_3-TPD, the catalyst sample was placed on quartz wool located in a U-shaped quartz tube. Prior to both analyses, the samples were pre-treated with argon flowing at a rate of 30 mL/min until 350 °C at a rate of 20 °C/min. For the H_2-TPR, the pre-treated sample was then subjected to 5 % H_2 in argon flowing at a rate of 30 mL/min, whilst the temperature was linearly increased from 90 °C to 600 °C at a rate of 10 °C/min. The hydrogen consumption was monitored by a thermal conductivity detector. The amount of hydrogen consumed was used to determine the degree of reducibility for each catalyst. For the NH_3-TPD, the pre-treated sample was then reduced with 5 % H_2 in argon and thereafter treated with helium for one hour to remove excess hydrogen. A 4 % NH_3 in helium gas mixture was then passed through the system and allowed to adsorb onto the surface of the catalyst for half an hour. Helium gas was then passed through at a flow rate of 30 mL/min, whilst the temperature was linearly increased from 100 °C to 1000 °C at a rate of 10 °C/min. The amount of ammonia desorbed was monitored using a thermal conductivity detector and the values obtained were used to determine the acidity of the sample.

4.2.7. Thermogravimetric Analysis-Differential Scanning Calorimetry (TGA-DSC)

TGA-DSC was performed on the catalysts under a nitrogen atmosphere using a SDT Q 600 TGA-DSC instrument. The temperature was increased from room temperature to 1050 °C

at a rate of 10 °C/min. For spent catalyst characterization, these conditions were used under static air as well.

4.2.8. Infra-red (IR) spectroscopy

Infra-red (IR) spectra were obtained using a Perkin Elmer Precisely, Universal ATR sampling accessory equipped with a diamond crystal. The powdered sample was placed on the crystal and a force was applied to ensure proper contact between the sample and the crystal. The spectra were edited and analyzed using Spectrum 100 software.

4.2.9. Catalyst characterization techniques used for the determination of catalyst deactivation mechanisms

Catalyst characterization provides vital information that can lead to the determination of which deactivation mechanism exists in the reaction system. In Table 4.1, the deactivation mechanisms that exist are listed and the characterization technique/s that has been used to show its presence is listed.

Table 4.1.: A list of the deactivation mechanisms and the corresponding characterization technique used to determine its presence

Deactivation mechanism	Characterization technique
Sintering	XRD Particle size measurements, TEM particle size measurements
Coking (deposition of polymeric compounds etc.)	BET surface area and pore size distribution (pore volume and pore radius), TGA/DSC, SEM
Leaching of active phase or support	ICP (shows a loss of wt% metal in used catalyst), SEM/EDS
Poisoning	XPS
Mechanical failure	SEM

4.3. Catalytic Testing

This section will be discussed in four parts: (a) reactor configuration; (b) packing of reactor tube; (c) experimental procedure for hydrogenation reactions and (d) product analysis and quantification.

4.3.1. Reactor configuration

The design of the reactor setup used in the catalytic testing is outlined in Figure 4.1. The pipe fittings and tubing used for the setup was stainless steel (grade 316) and were supplied by Swagelok®. Since the reaction investigated was a high pressure hydrogenation system, it was essential that the fittings, tubing and other parts used in the setup were stainless steel (grade 316). This was to ensure that the reactor setup complied with South African safety regulations.

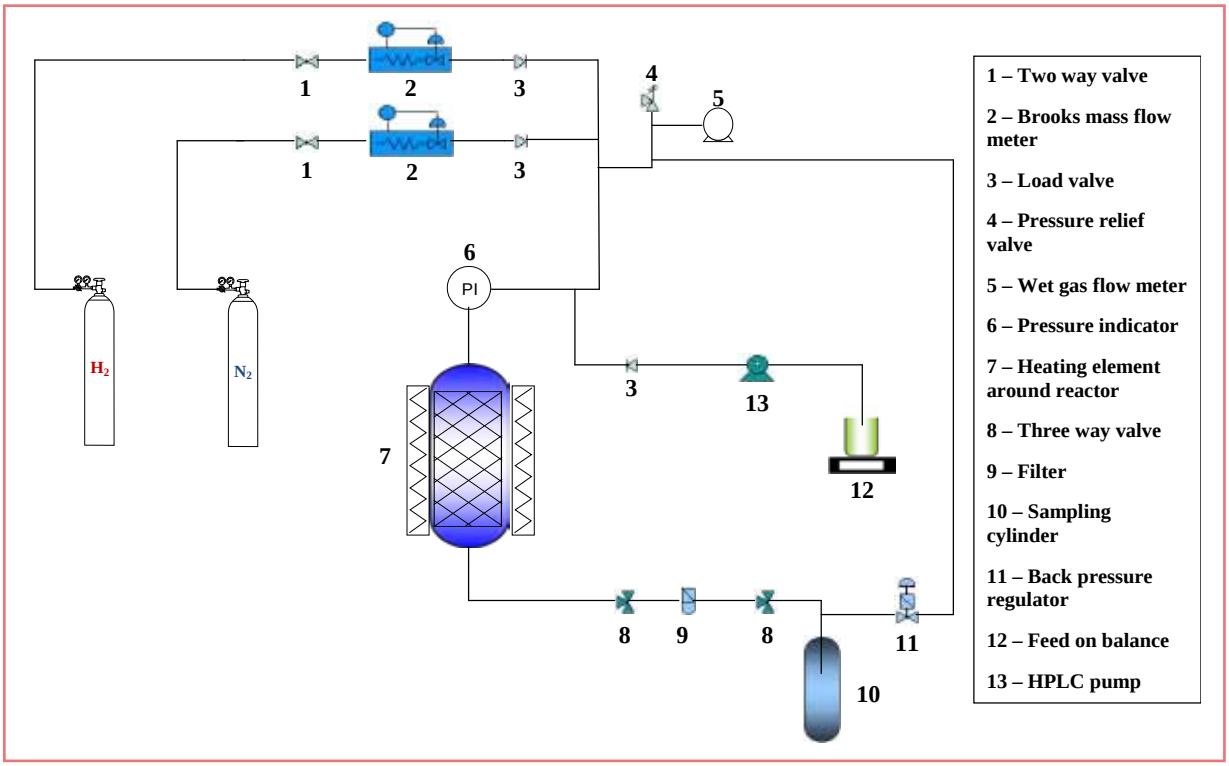

Figure 4.1: Reactor design

The hydrogen and nitrogen used were sourced from Afrox BOC Special Gases and were delivered to the system *via* a gas cylinder. These gas cylinders were controlled by

Swagelok® high pressure regulators. The gases were passed through ½ inch stainless steel tubing which was then reduced to ¼ inch stainless steel tubing before the entering the reactor system. The gas leaving through the regulators entered a two way valve before entering the Brooks mass flow meters. The amount of gas entering the reactor was controlled by means of a Brooks control box and Brooks mass flow meters (0 – 300 ml/min) which were calibrated before use. A load valve was positioned after the mass flow meters to prevent any back flow of the gases to the mass flow meters. The gas was then allowed to pass to the fixed bed reactor. This gas was also connected to a pressure relief valve (100 bar), which was positioned at the off gas exit by means of a t-piece.

The liquid feed was introduced to the reactor by means of a LabAlliance Series II isocratic HPLC pump (minimum flow rate of 0.01 ml/min and maximum flow rate of 9.99 ml/min). Preceding the pump was a Teflon tube fitted with a filter through which the feed was drawn. This Teflon tube was placed into the feed vessel. An $^{1}/_{16}$ inch stainless tube was fitted at the outlet of the pump which then passed through a reducing union that lead to ¼ inch stainless steel tubing. A load valve was fitted at this position to prevent the back flow of any liquid. This liquid feed was then passed through the ¼ inch tubing leading to the entrance of the reactor. At this point the gas and liquid mixed forming a solution with gas bubbling through it. A Swagelok® pressure indicator was placed before the entrance of the reactor to monitor the pressure within the reactor system.

The product leaving the reactor tube was first passed through a three way valve before entering a 2 micron filter. The product was then passed through a second three way valve before entering a 500 mL sampling cylinder. A t-piece was placed at the entrance of the sampling cylinder that allowed for the liquid product to enter into the cylinder and the off gas to pass to a Swagelok® back pressure regulator. The back pressure regulator maintained the pressure within the system to the desired value. The gas leaving the back pressure regulator was then passed through the ¼ inch stainless exit pipe which was connected to the pressure relief valve mentioned earlier. This gas then entered a Ritter drum type wet gas flow meter (TG1 – model 5 with a PVC drum and casing) which allowed for the determination of the quantity of off gas flowing during the run time of the experiment. This wet gas flow meter can measure up to 120 L/hr and was calibrated prior to its use.

A stainless steel (grade 316) tube with an inner diameter of 15 mm and a length of 325 mm was used as the reactor tube. This tube was fitted into a stainless steel (grade 316) block and was held in place by means of bolts which was torque to the desired value. The inlet tube and exit tube of the system was connected to the reactor tube using stainless steel nuts and ferrules that connected to a t-piece and reducing union respectively. The temperature change across the catalyst bed was monitored using a sliding thermocouple which was positioned at the centre of the bed. This was achieved by placing a movable $^{1}/_{16}$ inch thermocouple inside an $^{1}/_{8}$ inch stainless steel thermowell. This thermowell was placed in a fixed position within the reactor by means of a stainless steel male run tee. This complete setup was tested for leaks prior to the start-up of the reactor.

4.3.2. Packing of reactor tube

An illustration of a packed reactor is shown in Figure A 1 (Appendix A). The technique used for packing the reactor is also given in the Appendix (Section A 1, Appendix A).

Prior to packing the reactor with the catalyst, the reactor tube was packed with carborundum and subjected to a temperature profiling experiment. In this experiment the reactor block was set to a specific temperature and the temperature within the reactor was measured at specific lengths across the thermocouple. The hottest region of the reactor was then determined and catalyst was packed in this region for all subsequent catalytic testing reactions.

At the end of each catalytic testing experiment, the reactor tube was emptied before being washed with acetone and water. The tube was then oven dried at 120 °C before being used again.

4.3.3. Experimental procedure for the hydrogenation reactions

The procedure followed for the catalytic testing comprised of four parts:

(a) Pressure testing
(b) Activation with nitrogen
(c) Hydrogen switch over and hydrogen activation
(d) Catalytic reactions

4.3.3.1. Pressure testing

Prior to any reaction the system was subjected to a pressure test to check for any leaks. Once the reactor was torque to the desired value (explained in Section A 2, Appendix A), the back pressure regulator was closed and the system was pressurized to 60 bar using nitrogen. The system was allowed to remain at this pressure for 1 hour. After this period, the pressure within the system was observed. A drop of more than 1 bar during this time indicated a leak within the system. Once the test was complete the system was depressurized slowly using the backpressure regulator.

4.3.3.2. Activation using nitrogen

During the process of activation and the hydrogen switch over, the back pressure regulator was kept open. The flow rate of nitrogen was set to the required amount on the Brooks control box. At this time, the temperature was slowly increased until it reached 170 °C. The system was kept under these conditions overnight.

4.3.3.3. Hydrogen switch over and hydrogen activation

Before introducing hydrogen into the system, the temperature was dropped to 130 °C and was allowed to stabilize. The hydrogen flow was then started at the required value. Once the system stabilized, the nitrogen flow was decreased accordingly and allowed to stabilize. This process was repeated until the maximum required hydrogen flow rate was reached. The temperature was then increased to 200 °C and allowed to activate overnight.

4.3.3.4. Catalytic reactions

Before the commencement of each reaction the back pressure regulator was closed. The temperature was then decreased to the value required for the reaction, whilst the system was also pressurized to 60 bar. The HPLC pump was set to the required feed flow rate and the hydrogen flow rate was set to the required amount. The pump and hydrogen flow was then started. The reaction was allowed to proceed for approximately 28 hours. The liquid product formed was collected in the sampling cylinder and was sampled in 1.5 hour intervals. Due to the high exotherm associated with the hydrogenation of octanal, a 10 wt % octanal in octanol (diluent) was used as the fresh feed.

The product was injected into a Perkin Elmer Clarus 500 with a FID using a 1 µL SGE liquid syringe. A Petro-Elite column (length = 50 m and diameter = 200 µm) was used for the analyses. The column was initially held at 40 °C for five minutes and was then ramped to 240 °C at a rate of 3 °C/min and was held at this temperature for twenty minutes. The signal from the gas chromatograph was acquired and analyzed using TotalChrom software. The products from the reaction were identified using a Perkin Elmer Clarus 500 GC with a Perkin Elmer 560S MS fitted with a photo ionization detector (PID). The MS was operated in the positive electron ionization mode (EI+) and the GC programme was as outlined above. The signal from the GC-MS analysis was acquired and analyzed using TurboMass version 5.4.2 software.

For the water-impact studies, the above procedure was followed, but once the steady state conditions were obtained, the water-spiked feed (1.8 wt % water in fresh feed) was passed through the system. The sampling procedure and analysis was the same for the all reactions.

4.3.4. Product analysis and quantification

Two separate mass flow meters were used to control the amount of hydrogen and nitrogen entering the reactor. A top loading weighing balance was used to determine the mass of feed that flowed into the reactor over a period of time. The amount of feed that entered the reactor for a specific run time was determined by the difference in mass between the previous run and the subsequent run.

The products formed from the reaction were only liquid phase products. This product was injected into the GC and analyzed using a FID. The quantification of the components found from the GC analysis was determined by means of a relative response factor (RRF). Errors can occur in the peak area determined for each component as a result of injection differences and detector response. It therefore becomes essential to determine RRF values for each component to correct for the errors/discrepancies.

The peak areas determined for each component in the product mixture was multiplied by its corresponding response factor. This yielded a corrected peak area (CP). The CP values for each component were summed up to get a total corrected peak area (TCP). The mass % of each component was determined by taking the ratio of CP to TCP. These values were then utilized to calculate selectivity. The conversion was based on the mass drained. The quantification procedure was deemed valid if the mass balance was within the range of 100 ± 2 %. The experiments were found to show good repeatability.

The **conversion of octanal** was given by: *100 x [(Liquid in x mass % octanal in feed) – (Liquid out x mass % octanal in product)/(Liquid in x mass % octanal in feed)].* Since the main product formed in the reaction was also used as a diluent in the feed, the mass % values obtained from the GC analysis had to be further analyzed to correctly differentiate between reactant components and product components. This was achieved by using the statistical function *VLOOKUP*. After this determination the mass % for the products formed from the reaction were defined excluding the contribution from the feed. These mass % were multiplied by the total peak area and the peak area formed for that component due to the reaction only (RP) was determined. These RP values were summed up to obtained the total peak area due to components formed from the reaction (RTP). The **selectivity** was then determined using: *RP/RTP*.

4.4. References

1. S. V. Gredig, R. Maurer, R. A. Koeppel and A. Baiker, *J. Mol. Catal. A: Chem.*, 1997, **127**, 133.
2. K. K. Bando, K. Sayama, H. Kusama, K. Okabe and H. Arakawa, *Appl. Catal. A: Gen.*, 1997, **165**, 391.

Chapter 5

Results and Discussion: Catalyst Characterization

The results obtained using the characterization techniques outlined in Chapter 4 are reported and discussed hereunder. The information presented below is that for the 'fresh' catalyst, i.e. the catalyst that has not been used in the catalytic reaction.

5.1. X-Ray Diffraction (XRD)

The diffractograms for CuO/Al_2O_3, CuO/SiO_2 and CuO/Cr_2O_3 are shown in Figures 5.1 (a), (c) and (d) respectively. Each diffractogram displays peaks corresponding to the tenorite CuO phase (JCPDS 5-0661).

Individual peaks corresponding to gamma alumina (γ-Al_2O_3) are not seen in the diffractogram for CuO/Al_2O_3 (Figure 5.1 (a)). This is most probably due to the overlap of these peaks with those of the CuO, since the JCPDS files for each compound list similar d-spacing values. It may also be that the size of the alumina particles is small. This will then make it difficult to detect the alumina using XRD or a low intensity signal will be obtained that may be 'over-powered' by the higher intensity signals. Upon examining the diffractogram of γ-Al_2O_3 (Figure 5.1 (b)), broad low intensity peaks are seen. The position of these peaks coincides with the high intensity CuO peaks thus confirming the overlap of these peaks with those of CuO. In addition, the low intensity of the peaks confirms the presence of small sized crystallites, whilst the broadness of the peaks indicates the poor crystallinity of the alumina.

The diffractogram for CuO/SiO_2 (Figure 5.1 (c)) does not show characteristic silica peaks. However, a 'bump' is seen in the region of 15 – 25 degree 2 theta. This indicates that the support has an amorphous character. Low intensity CuO peaks are observed, however, these are primarily due to the presence of the amorphous silica.

In addition to the CuO phase peaks seen in the XRD pattern for CuO/Cr_2O_3 (Figure 5.1 (d)); peaks corresponding to the copper chromium oxide ($CuCr_2O_4$) phase (JCPDS 5-0657 and 21-0874) are also present.

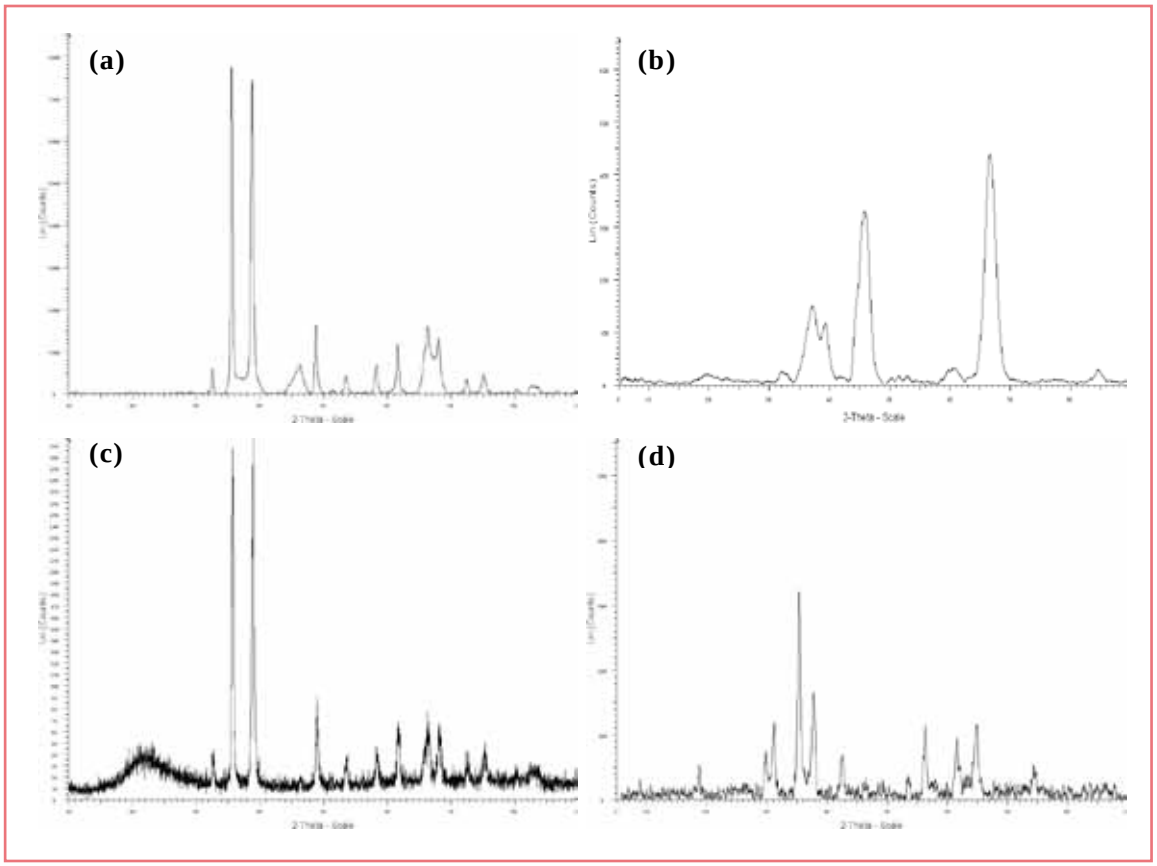

Figure 5.1: Diffractograms of (a) CuO/Al_2O_3; (b) Al_2O_3 support; (c) CuO/SiO_2 and (d) CuO/Cr_2O_3

In addition to the observations mentioned above, the diffractogram for CuO/Cr_2O_3 displays broad, low intensity peaks. This indicates that the CuO/Cr_2O_3 catalyst is less crystalline and is comprised of smaller crystallites.[1] The crystallite size (*d*) was calculated using the Scherrer equation, whilst the full width at half maximum (FWHM) was determined using EVA software. The Scherrer equation is given by Equation 5.1.[2] These values gave a quantitative means of validating the crystallinity and the CuO crystallite size of the catalysts. The FWHM and the crystallite sizes are given in Table 5.1. The particle shape factor was taken as 0.89 from literature[2] and because the crystallite size of CuO in each catalyst was being compared to each other.

Crystallite Size (d) = $K\lambda/\beta\cos\theta$ . . . . . **Equation 5.1**

where K = particle shape factor (taken as 0.89)[2]

λ = X-Ray wavelength (1.5418 Å for Cu K_α radiation)

β = FWHM in radians

θ = Braggs angle or peak position

Table 5.1: Showing the FWHM values and the XRD crystallite size for CuO at the highest intensity peak

Catalyst	FWHM/°	XRD crystallite size/nm
CuO/Al_2O_3	0.335 (1.11)[a]	49.2 (7.34)[a]
CuO/SiO_2	0.300	51.4
CuO/Cr_2O_3	0.516	42.8

[a] FWHM and crystallite size for γ-Al_2O_3 listed in parenthesis

From Table 5.1 it is seen that CuO/Cr_2O_3 possesses the greatest FWHM (0.516°), whilst CuO/SiO_2 possesses the lowest FWHM (0.300°). These values, as well as the crystallite sizes, confirm that the CuO/Cr_2O_3 consists of smaller CuO crystallites and is less crystalline compared to the other two catalysts. It is thus deduced that the XRD crystallite size of CuO and FWHM increases in the following manner: $CuO/Cr_2O_3 < CuO/Al_2O_3 < CuO/SiO_2$. The FWHM for alumina (1.11°) confirms the poor crystallinity of the alumina, whilst the crystallite size (7.24 nm) confirms that the alumina is comprised of small sized crystallites.

5.2. Scanning Electron Microscopy (SEM)

The SEM images of CuO supported on alumina (CuO/Al_2O_3) are shown in Figures 5.2 (a) – (b). These images show that the catalyst is made up of 'stacked' particles with some regions having 'flower-like' particles existing amongst them. All these features put together create a 'rough' surface morphology.

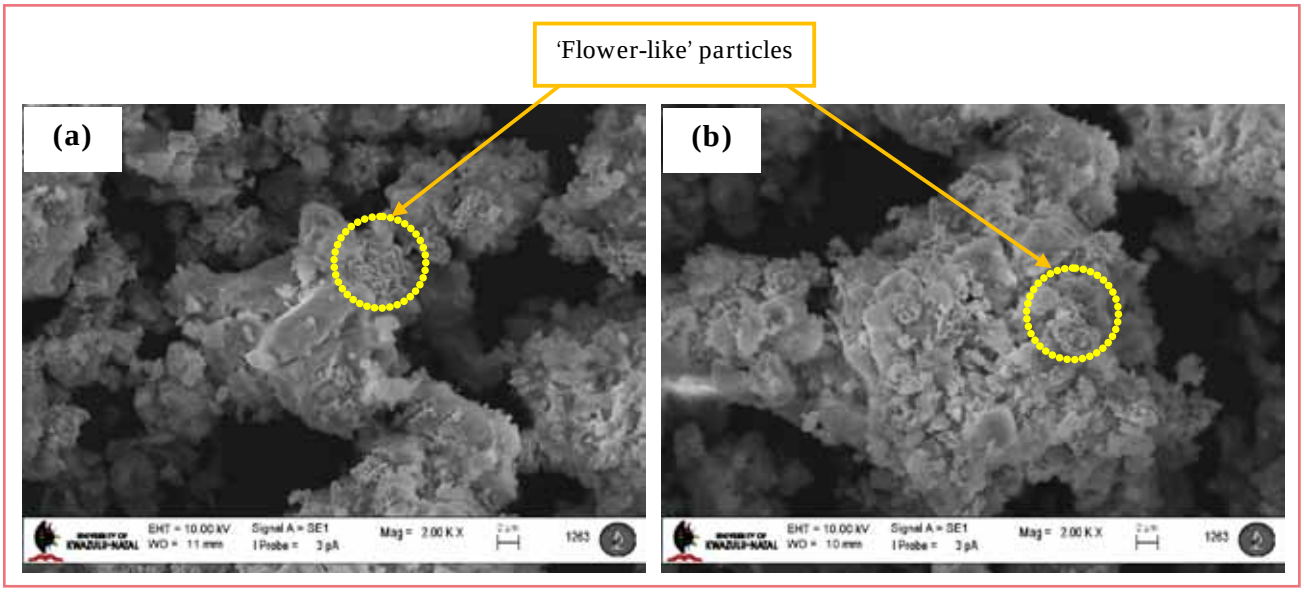

Figure 5.2 (a) – (b): SEM images of CuO/Al_2O_3

The backscattered SEM images for this catalyst are shown in Figures 5.3 (a) – (b). As stated in Chapter 1, Section 1.4.3, those elements with the higher atomic number will appear brighter in the backscattered SEM image. Thus, in the images shown in Figure 5.3, the brighter regions of the catalyst are due to the CuO particles and the darker/grey regions correspond to the alumina particles. The CuO particles formed clusters and appear to be present on the surface of the alumina particles.

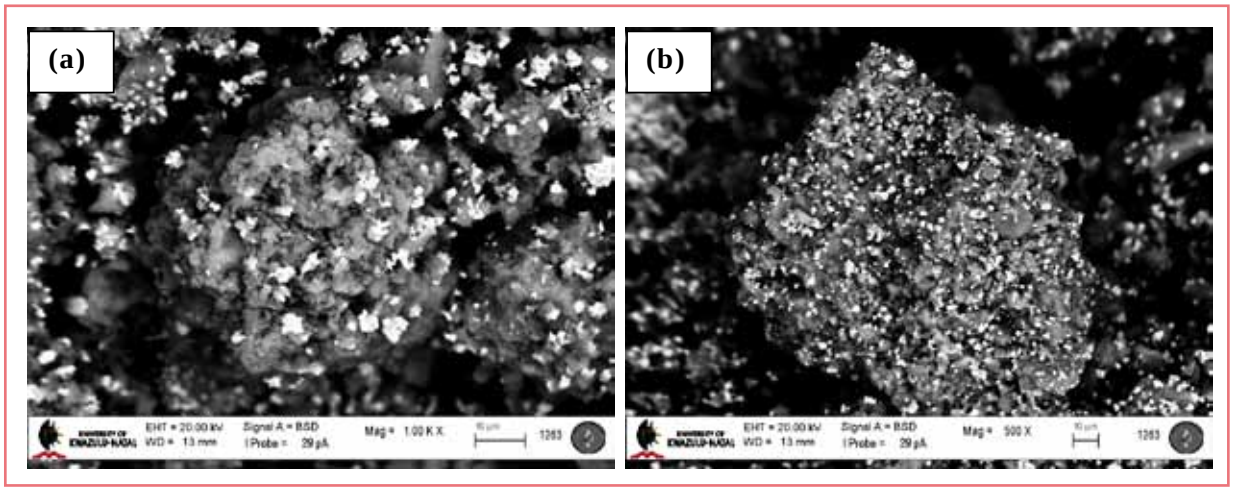

Figure 5.3 (a) – (b): Backscattered SEM images of CuO/Al_2O_3

The EDS composition scanning data for CuO/Al_2O_3 is shown in Figure 5.4 (a) – (d). The map data of the combination of the individual maps (Figure 5.4(b)) shows the presence of Cu-rich particles (CuO) on the Al-rich particle's surface (Al_2O_3). The individual Cu map shows that there are local concentrations of the Cu due to the clustering of the CuO and it is these 'clusters' that display a 'scattered' distribution relative to the alumina as seen in Figure 5.4 (b).

The SEM images of CuO supported on silica (CuO/SiO_2) are shown in Figures 5.5 (a) – (b). These images show the presence of sponge-like particles that have a flakey surface morphology. Some particles that possess a 'globular-like' appearance are also seen. As with the CuO/Al_2O_3 catalyst, this catalyst displays a rough surface morphology, however, the appearance of the particles differs noticeably from that of the former mentioned catalyst.

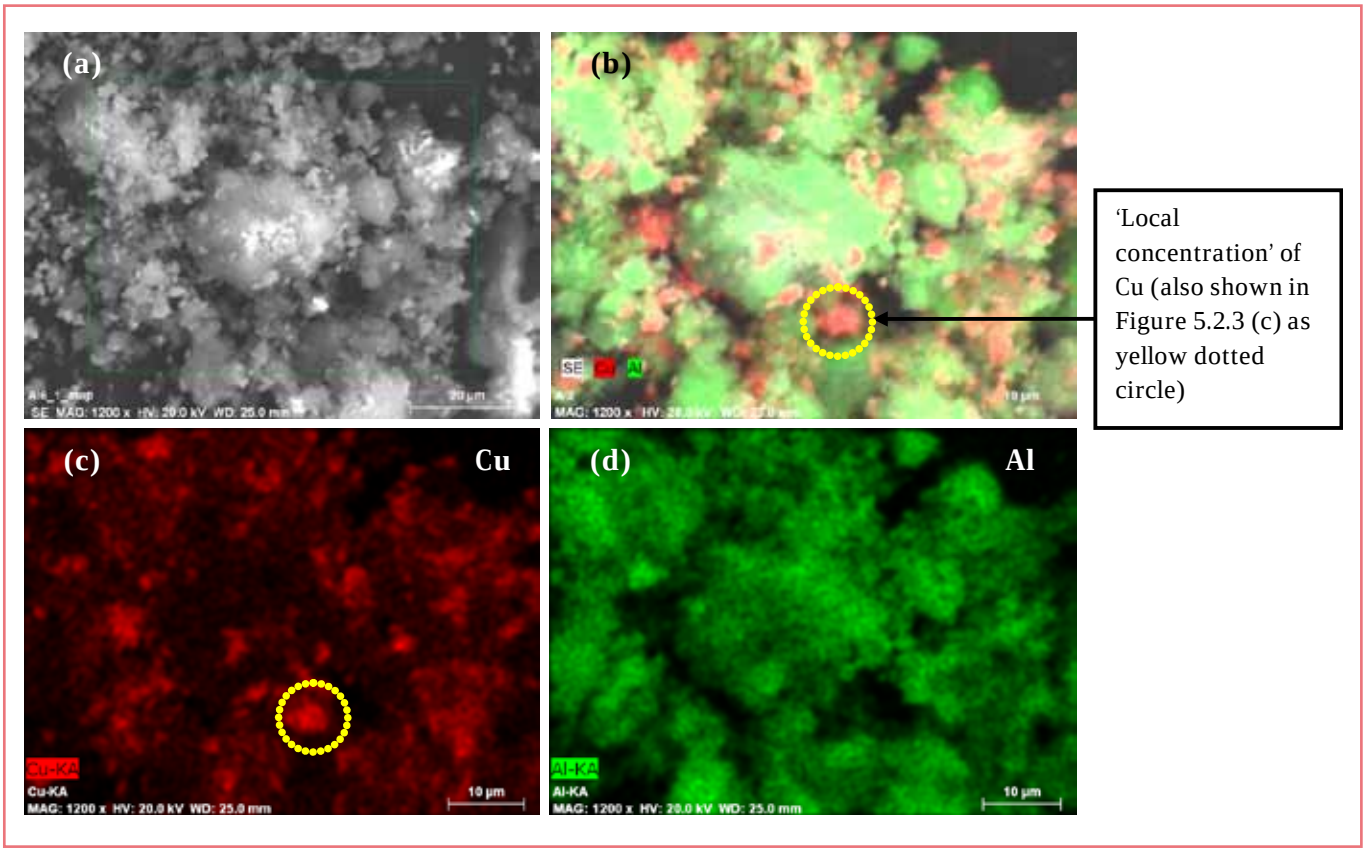

Figure 5.4: (a) Secondary SEM image and (b) – (d) EDS composition map data for CuO/Al_2O_3

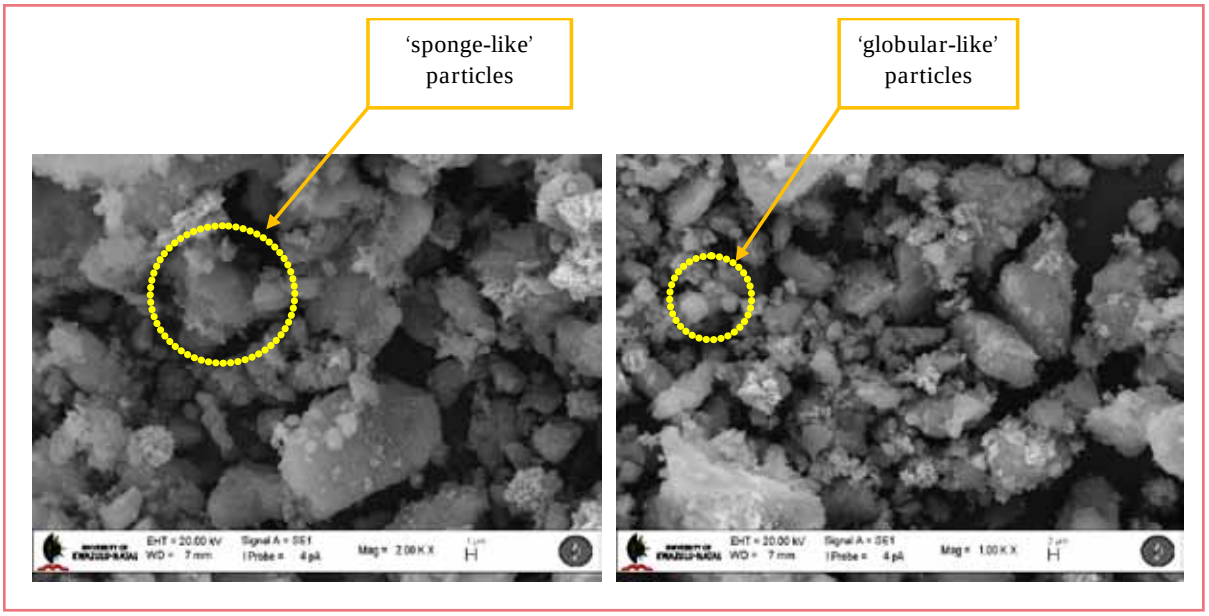

Figure 5.5 (a) – (b): SEM images of CuO/SiO_2

The backscattered SEM images for the CuO/SiO_2 catalyst are shown in Figures 5.6 (a) and (b). In a similar fashion as the former discussed catalyst, the CuO particles tend to exist as clusters on the surface of the silica particles. However, in contrast to the clusters of CuO on the alumina, the clusters of CuO on the silica surface appear to have a more spherically defined shape. In comparing the SEM and the backscattered SEM images of the silica supported CuO, it becomes apparent that some of the 'globular-like' particles seen in the SEM image are due to the CuO particles.

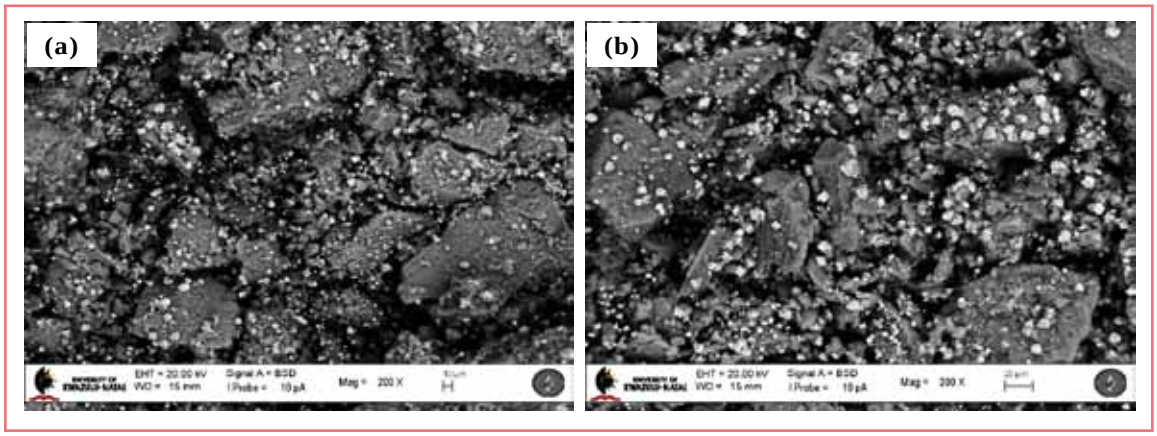

Figure 5.6 (a) – (b): Backscattered SEM images of CuO/SiO_2

From the elemental map data for CuO/SiO_2 as shown in Figures 5.7 (a) – (d), it is seen that the Cu-rich particles are not highly dispersed relative to the silica support; instead a scattered distribution exists. The clusters of CuO are also observed in the map data for Cu (Figure 5.7 (c)). Even though a scattered distribution is seen for the alumina-supported and silica-supported catalysts, the manner in which this type of distribution appears differs between the two catalysts. This may be attributed to the different supports influencing the distribution (the same wet impregnation method preparative method was followed for the two). In addition to these observations, it is seen, upon comparing the individual maps for Cu and Si, that there are some Cu-rich particles that exist unsupported by the silica particles.

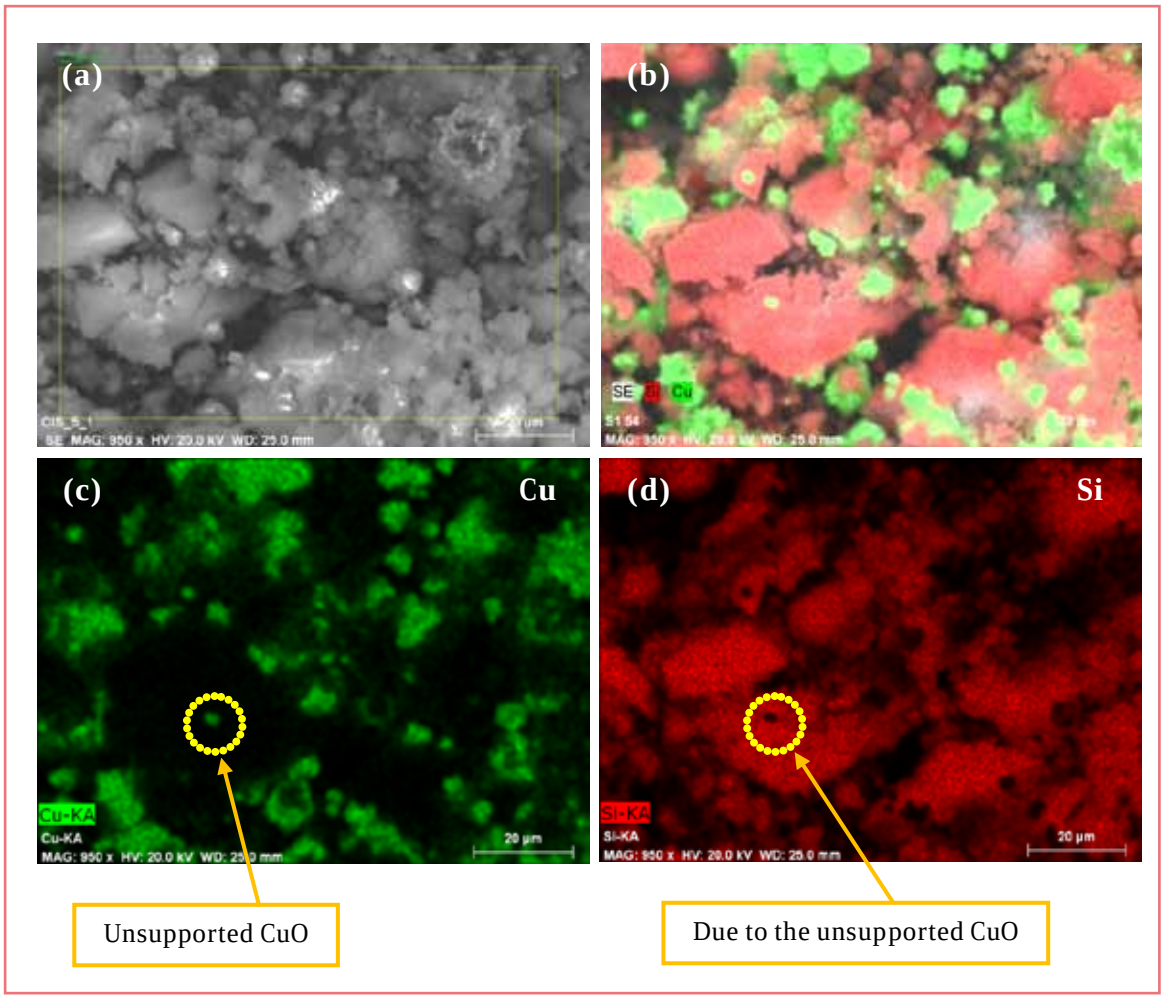

Figure 5.7: (a) Secondary SEM image and (b) – (d) EDS composition map data for CuO/SiO_2

The SEM images for the CuO supported on chromia are shown in Figures 5.8 (a) – (b). The images show the presence of irregularly shaped particles that display a 'mould-like' surface morphology. The appearance of the catalyst particles does not share any obvious similarities with the CuO/SiO_2 and the CuO/Al_2O_3 catalysts.

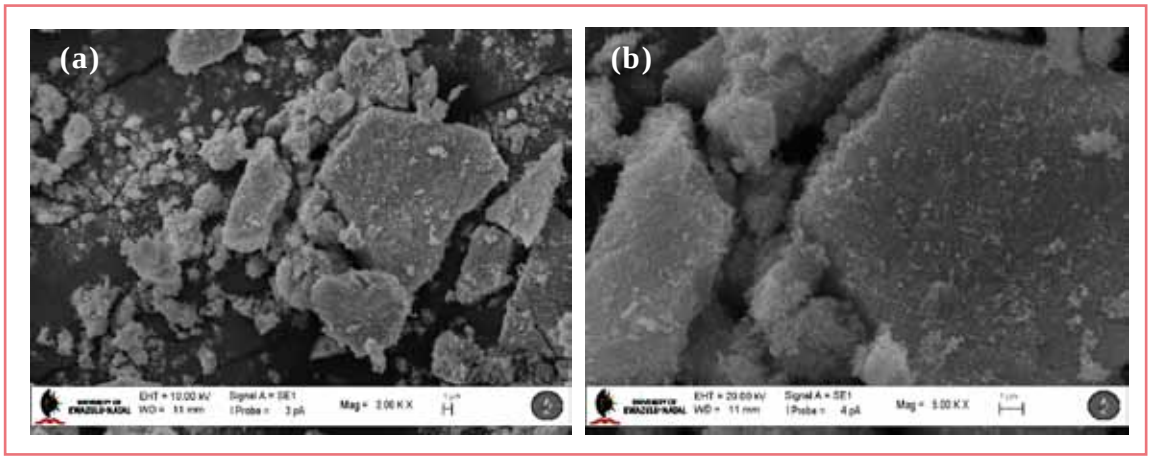

Figure 5.8 (a) – (b): SEM images of CuO/Cr_2O_3

The backscattered SEM image of the CuO/Cr_2O_3 catalyst is shown in Figure 5.9 and the entire surface of the particles appears brighter. This is due to the similarity in atomic number between Cu and Cr, causing these elements to backscatter electrons to nearly the same degree. Thus it is difficult to say with absolute certainty that the brightness seen is solely due to the CuO particles, since Cr-containing particles will also contribute to the brightness.

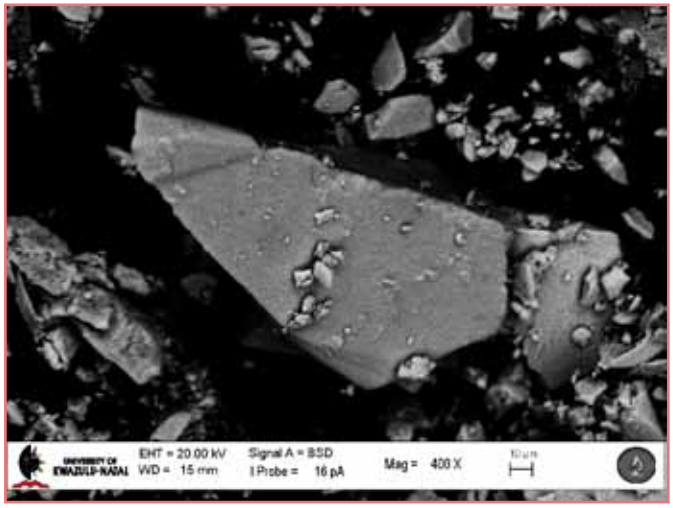

Figure 5.9: Backscattered SEM image of CuO/Cr_2O_3

The EDS composition scanning data is shown in Figures 5.10 (a) – (d). The map data (Figures 5.10 (a) – (c)) show that there is a homogeneous distribution of both the Cu and Cr, as well as a uniform dispersion of Cu relative to the Cr. This collectively indicates a high degree of dispersion in this catalyst. It is probable that this dispersion characteristic of the CuO/Cr_2O_3 catalyst is primarily due to the method of co-precipitation utilized for its synthesis. Much like the SEM and backscattered SEM images for the CuO/Cr_2O_3, the EDS composition scanning data does not display any similarities with the two former discussed catalysts.

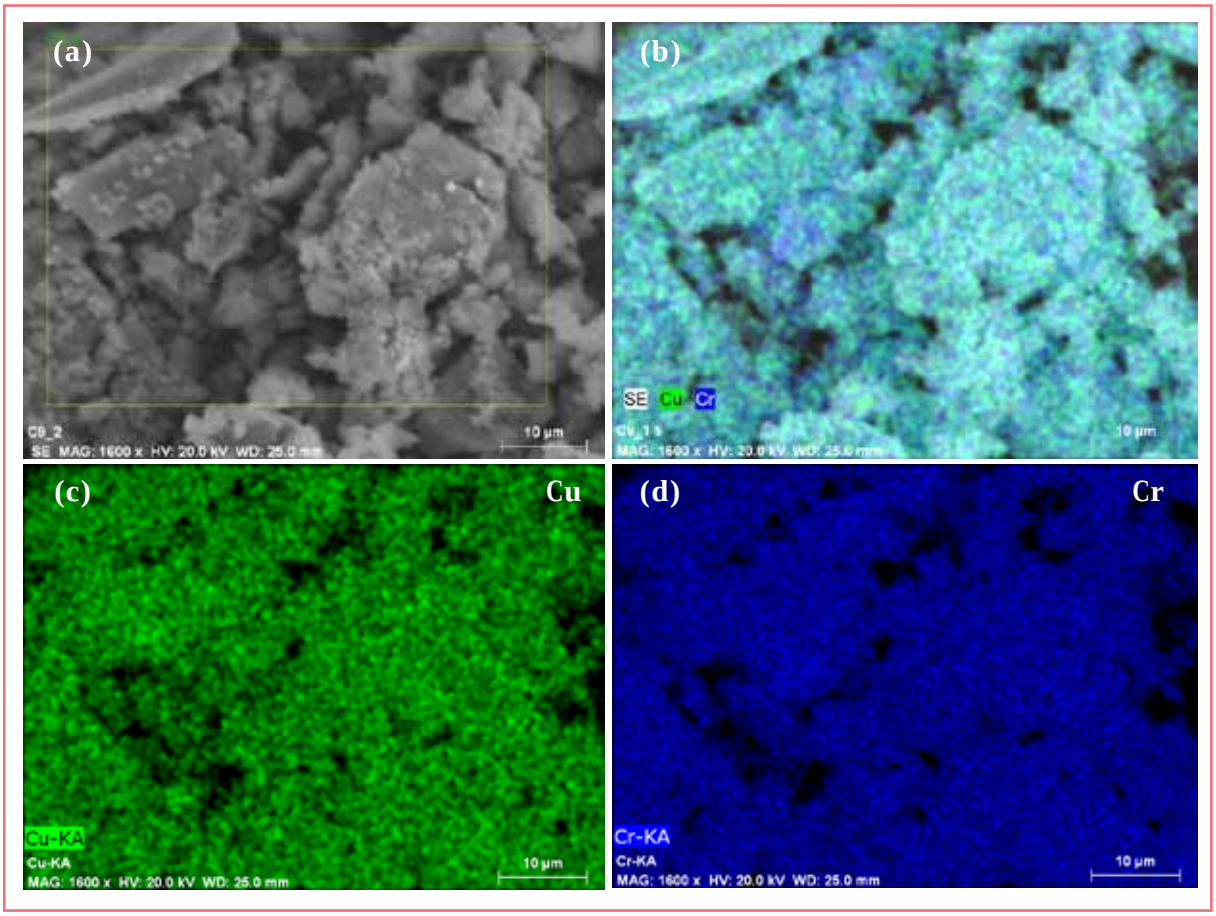

Figure 5.10: (a) Secondary SEM image and (b) – (d) EDS composition map data for CuO/Cr_2O_3. The color of the image seen in Figure (b) above is created by the superimposition of the images in Figures (a), (c) and (d)

5.3. Transmission Electron Microscopy (TEM)

The TEM images for CuO/Al_2O_3 are shown in Figure 5.11 (a) – (c). The images in Figures (a) and (b) show the presence of irregularly structured particles, as well as rod-like particles. As can be seen, these particles vary in size and this is confirmed by the TEM particle size analysis of these particles. Table 5.2 lists the particle size values obtained. The range of particle sizes was found to be 7 – 44 nm with the mean particle size being 16 nm. The particle size of 44 nm was due some of the rod-like particles, whilst other rod-like particles had sizes in the range of 9 – 12 nm. The irregularly shaped particles displayed particle sizes in the range of 15 – 30 nm. An interesting feature seen in Figure 5.11 (c) is the presence of deformed spherically shaped particles with particle sizes between 6 – 27 nm. These particles appear to be along the surface edge of a 'networked family' of rod-like and irregularly shaped particles.

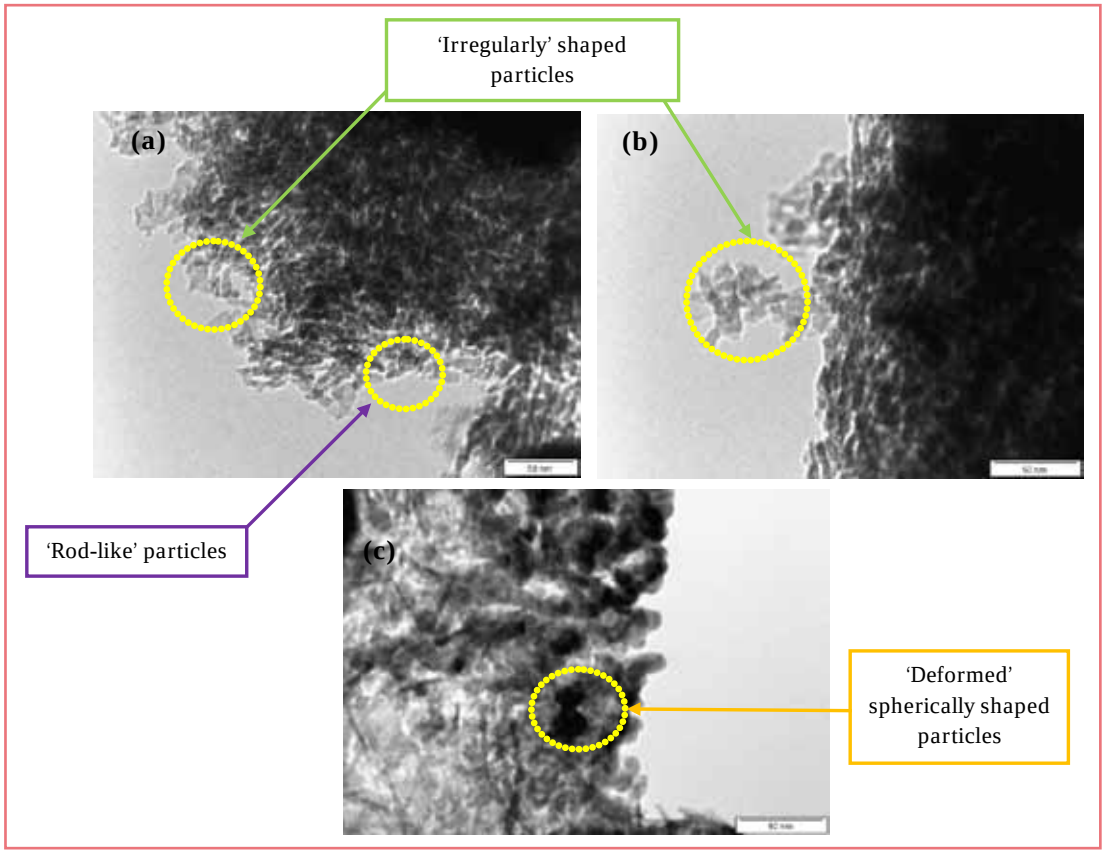

Figure 5.11 (a) – (c): TEM images of CuO/Al_2O_3

The selected area electron diffraction pattern (SADP) for this catalyst is shown in Figure 5.12 below. As stated in Chapter 1, Section 1.4.3, the electron diffraction patterns may be used to determine crystallographic information about the sample. The appearance of rings in a SADP generally indicates the presence of polycrystalline materials[3, 4], however it has been shown that these rings may also correspond to an amorphous state of the material.[5, 6] The presence of spots in a SADP is indicative of crystalline phases.[3-6]

It therefore becomes evident that the spots present in the SADP shown in Figure 5.12 are due to crystalline material and can most likely be attributed to CuO, since it was found to be highly crystalline by XRD. The ring pattern indicates the presence of polycrystalline material, as well as some amorphous nature, since XRD showed the evidence of poorly crystalline alumina phases. A range of particle sizes was determined by TEM (7 – 44 nm) and this supports the polycrystalline nature of the catalyst. In addition, it is seen that the rings are comprised of spots creating a 'spotty ring pattern'. This indicates that the size of the crystallites that give rise to the diffraction pattern is small. These observations are coherent with the particle size analysis and XRD observations discussed above that showed the size of the particles to be small. A similar SADP which displayed both rings and spots for alumina supported CuO was seen by *Jena et al.*[4]

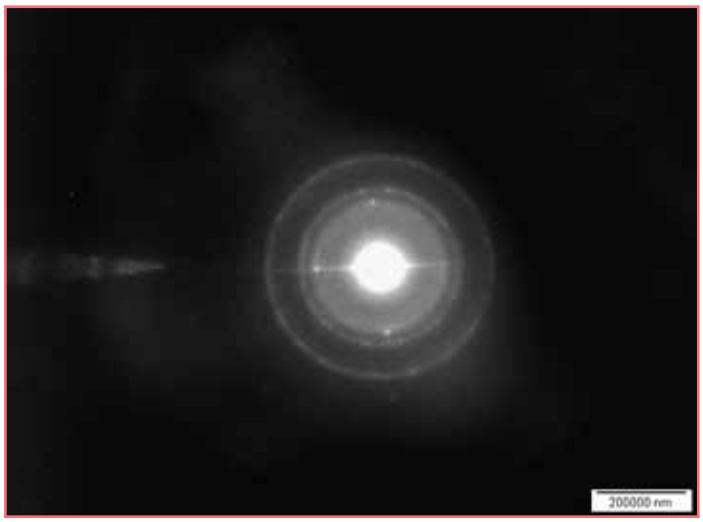

Figure 5.12: SADP of CuO/Al_2O_3

The TEM image for CuO/SiO_2 is shown in Figure 5.13. This image shows the presence of fairly spherically shaped particles as well as the presence of darker spots within the

matrix of these particles. A variety of particle sizes is seen for this catalyst and the particle size analysis showed the range of particle sizes to be 12 – 61 nm with the average particle size being 30 nm. The average particle size for the darker spots was found to be 2 nm and the range of particle size was determined to be 1 – 3 nm indicating very little variance. These particle size values are summarized in Table 5.2 below.

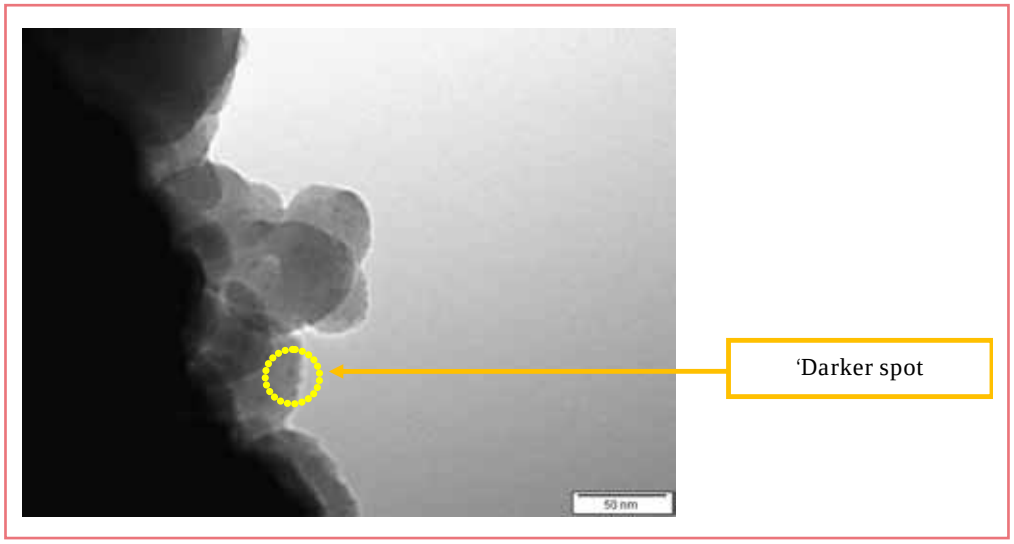

Figure 5.13: TEM image for CuO/SiO_2

Table 5.2: A summary of the range and average particle sizes determined for each catalyst

Catalyst	Average Particle Size/nm	Range of Particle sizes/nm
CuO/Al_2O_3	16	7 – 44
CuO/SiO_2	30	12 – 61 (dark spots: 1 – 3)
CuO/Cr_2O_3	17	6 – 43

The SADP for the silica supported CuO is shown in Figure 5.14. This pattern shows the presence of spots and a faint halo ring which confirms the presence of crystalline and amorphous material respectively. As discussed for the SADP of CuO/Al_2O_3, the spots indicate the presence of the crystalline CuO (since XRD showed this compound to be crystalline), whilst the faint halo ring occurs as a result of the amorphous silica (as determined by XRD). Such interpretations of electron diffraction patterns have been

outlined by *Lee et al.*[5] and *Zhong et al.*[6] in their characterization of amorphous lead oxide nanotubes and amorphous Ni-B alloy nanoparticles, respectively.

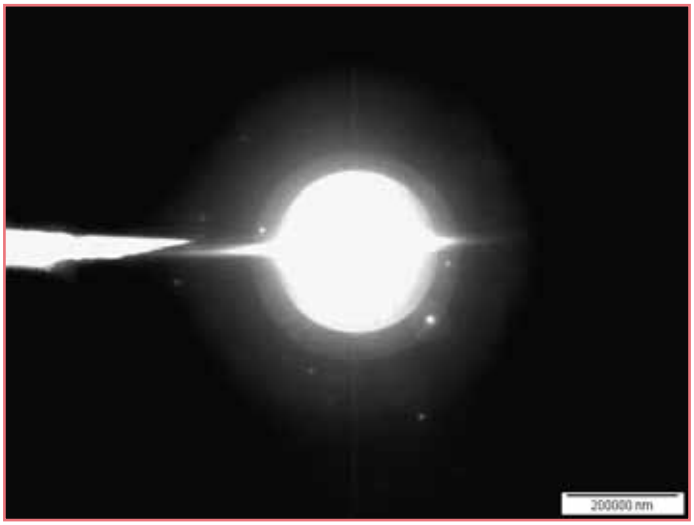

Figure 5.14: SADP of CuO/SiO_2

The TEM image for CuO supported on chromia is shown in Figure 5.15 and shows the presence of irregularly spherical particles and square shaped particles. A range of particle sizes from 6 nm to 43 nm exists for this catalyst, as determined by the particle size analysis, resulting in an average particle size of 17 nm. These particle size values are also tabulated in Table 5.2 above.

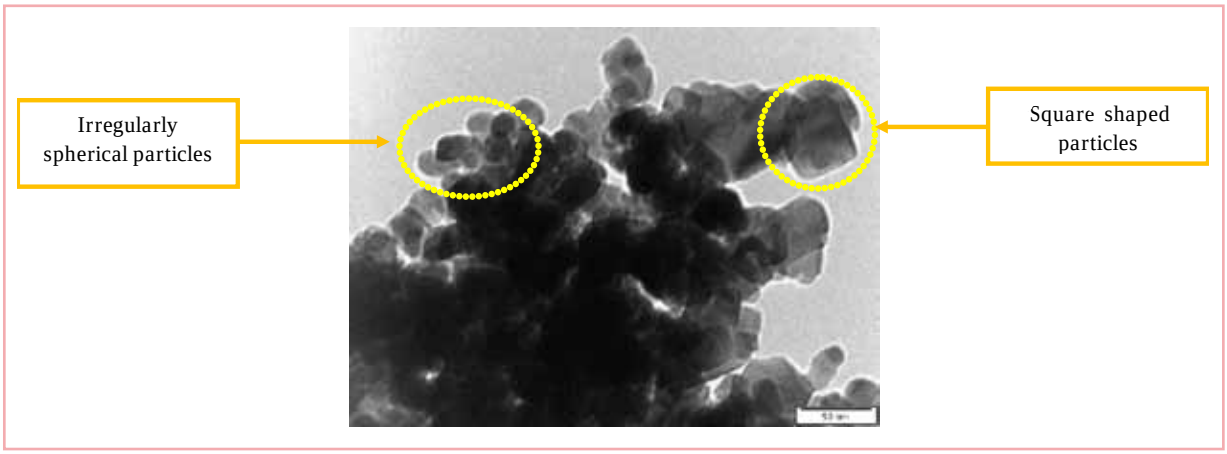

Figure 5.15: TEM image for CuO/Cr_2O_3

The SADP for chromia supported catalyst is shown in Figure 5.16. There are spots, rings and a spotty ring pattern in this electron diffraction pattern. As stated in the discussion on the SADP for each of the two former discussed catalysts, the presence of the spots confirms that crystalline material is present in the catalyst, the rings indicate the presence of polycrystalline material (supported by the range of particles sizes determined using TEM), whilst small particles are known to be present in the catalyst, since a spotty ring pattern is observed. This observation confirms that the low intensity peaks seen in the XRD diffractogram are due to small sized particles. Since the XRD showed that both CuO and $CuCr_2O_4$ are the crystalline phases present in the catalyst, it cannot be said, without further in-depth analysis, which compound is responsible for the spots seen in the SADP.

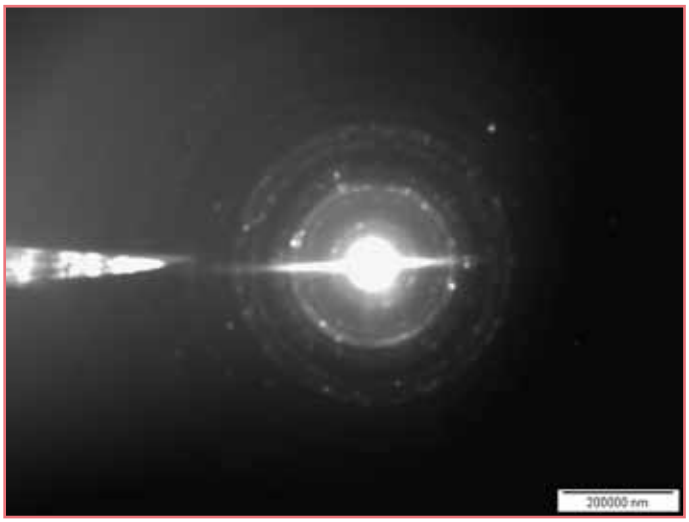

Figure 5.16: SADP for CuO/Cr_2O_3

The particle size values for each catalyst (as discussed above) are summarized in Table 5.2 above. There are no similarities between the XRD crystallite sizes and the TEM particle sizes. This is expected since the crystallite size is a volume averaged size across the entire sample, whilst the particle size is a number averaged size of a localized area that is viewed. In addition, particles can be comprised of a number of crystallites.[7]

5.4. Inductively Coupled Plasma-Optical Emission Spectroscopy (ICP-OES)

The copper loading for each catalyst is listed in Table 5.3. The target weight % of copper was 25 wt%. As can be seen the alumina and silica supported CuO is slightly below this value (23.5 and 24.8 wt% respectively) and this may be related to the capacity of metal oxide loading that a particular support can take. The theoretical amount of copper salt required to get a loading of 25 wt% was used in the syntheses. Upon increasing the mass of copper salt used, it was observed that there was a negligible increase in the copper loading, hence it was determined that approximately 25 wt% copper was the maximum loading that could be reached for these supports. The copper loading for the CuO/Cr_2O_3 catalyst was found to be 26.3 wt %. The copper content in the catalyst is dependent upon the reactions occurring during the preparation (the precipitation process) and the amount of each metal salt available for the reaction. It is observed, from each replicate analysis of the metal content, that there are regions of the catalyst that show a loading of 25 wt% Cu; however, since the loading represented in Table 5.3 is an average, it took into account the variations from each replicate and yielded a Cu loading of 26.3 wt%.

Table 5.3: A list of the copper loadings in each catalyst

Catalyst	Cu loading/wt %
CuO/Al_2O_3	23.5
CuO/SiO_2	24.8
CuO/Cr_2O_3	26.3

5.5. Brunauer-Emmet-Teller (BET) Analysis

The analysis of a catalyst using the BET technique can be comprised of two parts: (a) surface area and (b) pore volume. The surface area measurements provide the total surface area of the catalyst and the pore volume determined is the total pore volume. The total surface area measurement includes the internal and external surfaces. The total pore volume is an indication of the total internal volume per unit mass of catalyst and is indicative of the amount of the bulk volume of the catalyst that is occupied by pores (void space). What is important to note is that the total pore volume determined includes the

pore volume that may be completely enclosed and thus cannot be accessed by the reactant molecules during the catalytic testing reactions.[8] In addition, the pore volume of a catalyst can further be characterized by the size of the pores. Three pore types exist in this respect: (a) macropores (greater than 50 nm), (b) mesopores (between 2 – 50 nm) and micropores (less than 2 nm).[8]

The BET surface area measurements are listed in Table 5.4 below. It can be seen that the surface area for each catalyst decreases according to the following: $CuO/Al_2O_3 > CuO/SiO_2 > CuO/Cr_2O_3$. It cannot be said that the low surface area of CuO/Cr_2O_3 is due to high crystallinity since the XRD data (FWHM values) showed this catalyst to possess the lowest crystallinity. In addition, no relation can be made between the particle size and the BET surface area. This is because similar average particle sizes were obtained for CuO/Al_2O_3 and CuO/Cr_2O_3, whilst the BET surface areas for these catalysts were significantly different.

The CuO/Al_2O_3 and CuO/SiO_2 were prepared using high surface area alumina and silica, respectively. Since the alumina had the higher surface area (216 m^2/g) compared to the silica (155 m^2/g), it resulted in the CuO/Al_2O_3 having the largest surface area. After the impregnation of these supports with CuO, there was a reduction in the surface area of approximately 40% for each catalyst. This indicates that a similar effect was induced by the CuO on the surface area of both supports. It should be noted neither the SADP nor the XRD diffractograms of CuO/Al_2O_3 showed indication of the presence of amorphous phases, thus it cannot be said that the high surface area of this catalyst is due to amorphous phases. However, since both the SADP and XRD of CuO/SiO_2 support silica being amorphous, it can be said the high surface area of this catalyst indicates its amorphous nature.

The pore volume for each catalyst is shown in Table 5.4. The decrease in surface area after the addition of CuO may be due to the occupation of some pores in the support by the CuO.[9] This is confirmed by the decrease in the pore volume of the supported catalyst in comparison to the support only. The high surface areas of both CuO/Al_2O_3 and CuO/SiO_2 indicate that these catalysts may be porous, since high surface area catalysts are often found to be porous[8]. This is confirmed by the total pore volumes found for these catalysts. The trend observed for the total pore volumes in decreasing order is CuO/Al_2O_3

≈ CuO/SiO_2 > CuO/Cr_2O_3. This indicates that the higher surface area catalysts tend to possess greater pore volumes. Since the alumina and silica supports both initially had similar total pore volumes and the alumina and silica supported CuO also have similar pore volumes, the CuO on the alumina and silica occupied pores in the support to almost the same degree.

Table 5.4: A list of the BET surface areas and total pore volumes for each catalyst

Catalyst	BET surface area/m^2 g^{-1}	Total pore volume/cm^3 g^{-1}
CuO/Al_2O_3	128.8	0.43 (0.65)[a]
CuO/SiO_2	99.4	0.48 (0.66)[a]
CuO/Cr_2O_3	25.3	0.37

[a] Total pore volume of supports only is listed in parenthesis

5.6. Temperature Programmed Reduction (TPR)

The TPR profiles for CuO/Al_2O_3, CuO/SiO_2 and CuO/Cr_2O_3 are presented in Figures 5.17(a), (b) and (c) respectively. The data obtained from these profiles (temperature at maximum and degree of reducibility values) are tabulated in Table 5.5. Since the reasoning governing the temperature at which a reduction peak is observed is often related to the support and its influence on the CuO, it was decided to perform a TPR analysis on unsupported CuO (which is also referred to as bulk CuO) in order to fully ascertain the effect the support had on the reduction of the CuO. The TPR profile for the unsupported CuO (bulk) is shown in Figure 5.17 (d), whilst the data are summarized in Table 5.5 as well.

The TPR profile of unsupported CuO (as shown in Figure 5.17(d)) displays a reduction peak at 416 °C that corresponds to the reduction of bulk CuO. The broadness of the peak is mainly due to large clusters of CuO with varying sizes[10] and is an indication of the difficulty associated with the reduction of unsupported CuO. The larger CuO clusters present a smaller reactive surface area for reduction to occur thus accounting for the difficulty associated with the reduction of unsupported CuO.

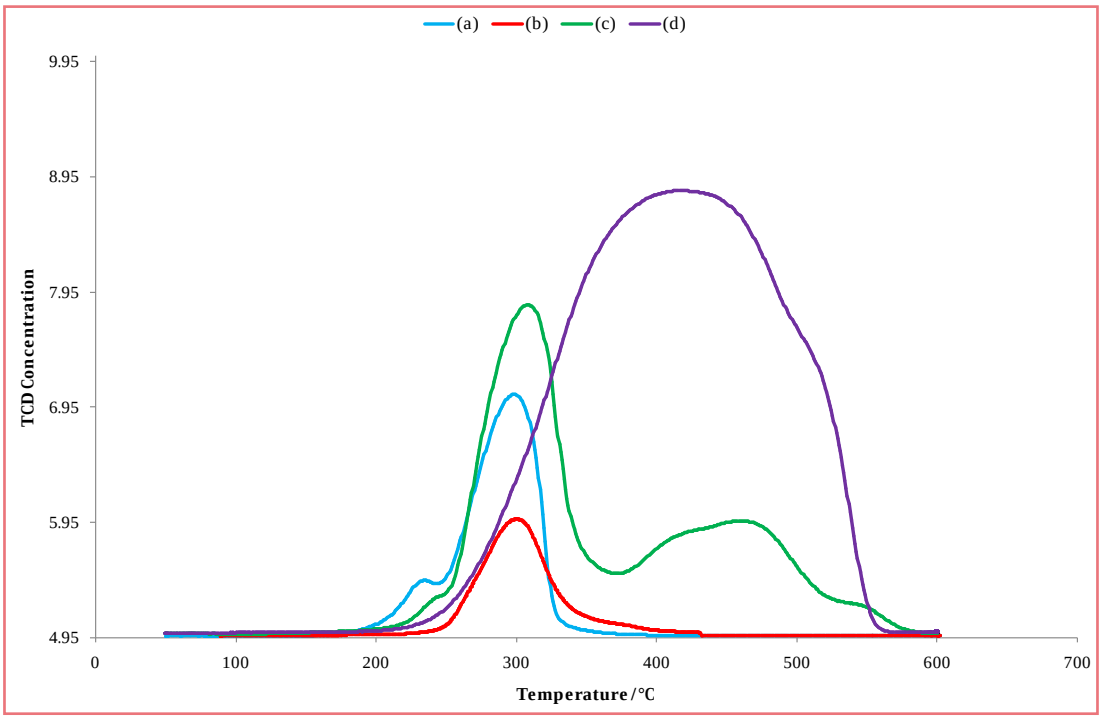

Figure 5.17: TPR Profile of (a) CuO/Al_2O_3; (b) CuO/SiO_2; (c) CuO/Cr_2O_3 and (d) Unsupported CuO

Table 5.5: List of temperature at maximum (T_m), degree of reduction and average oxidation state of Cu for different catalysts as determined by H_2-TPR

Catalyst	Temperature at maximum (T_m) /°C	Degree of reducibility /%[a]	Average Oxidation state of Cu based on H_2 consumed[b]
Unsupported CuO (Bulk)	416	--	--
CuO/Al_2O_3	231, 298	84.4	0.3
CuO/Cr_2O_3	308, 468, shoulder peaks at 240 and 541	85.8*	0.3
CuO/SiO_2	300	75.1	0.5

[a] Determined using the equation: *moles H_2 consumed / moles reducible Cu x 100*

[b] Determined based on the assumption that: *moles H_2 consumed = 2 electrons required for reduction to Cu^0* and using the equation: *Oxidation state of Cu before reduction – (moles H_2 consumed x 2 electrons/moles reducible Cu)*

* Based on first reduction peak only

The reduction peak seen for CuO/Al_2O_3 at 231 °C and the first shoulder peak for CuO/Cr_2O_3 seen at 240 °C corresponds to the reduction of highly dispersed CuO. The reduction peaks at 298 °C, 308 °C and 300 °C for CuO supported on alumina, chromia and silica, respectively, corresponds to the reduction of bulk CuO that interacts with the support.[11-13] It is uncertain as to what species is being reduced to give the second reduction peak seen at 468 °C as well as the shoulder peak at 541 °C for CuO/Cr_2O_3. Further investigation involving H_2 *in situ* XRD was used to determine the species being reduced at these temperatures. The diffractogram obtained from the H_2 *in situ* XRD is presented in Figure A 3 (Appendix A). It is seen that the phase changes observed between 465 – 468 °C and 539 – 542 °C are due to the reduction of Cr_2O_3 and $CuCr_2O_4$ respectively. It is uncertain as to what phase the Cr_2O_3 phase is being reduced to, since XRD does not show peaks corresponding to chromium in an oxidation state less than +3. The reduction of $CuCr_2O_4$ is to Cu^0 (due to the appearance of Cu^0 and Cr_2O_3 peaks at 542 °C) and due to its spinel structure, this reduction occurs at a high temperature.

It is observed that the T_m value obtained for unsupported CuO is much higher than those of the supported CuO. Regardless of the support, the supported catalysts investigated displayed reduction temperatures lower than that of the unsupported CuO. A possible explanation for the 'enhanced' reducibility of supported CuO is that there is an increased dispersion of the supported oxide, providing a larger reactive surface area and therefore a higher concentration of defects at which reduction can start.[14]

The degree of reducibility for CuO/Al_2O_3 and CuO/Cr_2O_3 is 84 % and 86 % respectively whilst that of CuO/SiO_2 is 75 %. The degree of reducibility for CuO/Cr_2O_3 was based on the first reduction peak, since this was the only peak that represented the reduction of the CuO to Cu^0. However, for the other catalysts the degree of reducibility was based on all peaks in the TPR profile, since these peaks corresponded to the reduction of CuO to Cu^0. The degree of reducibility obtained for the catalysts indicates that there remains a percentage of CuO that is not reduced. It is possible that there is some CuO that may be surrounded by an environment that does not allow it to be available for reduction, thus accounting for the degree of reducibility being less than 100 %. For CuO supported on alumina and silica, this can be linked to the presence of the clusters of CuO as seen in the backscattered SEM (Figure 5.3 and 5.6 (a) – (b)) and EDS composition scanning map data (Figure 5.4 and 5.7 (b) – (c)). Once the 'outer core' of the CuO cluster is reduced, it

encapsulates the 'inner core' CuO. It therefore creates a 'boundary wall' through which the hydrogen atoms cannot pass, leaving the 'inner core' CuO inaccessible to the hydrogen and thus unreduced. The lower degree of reducibility of CuO/SiO_2 is probably due to the presence of a greater amount of clusters than the alumina supported catalyst (as observed in the backscattered SEM images).

The average oxidation state of Cu after the H_2-reduction is listed in Table 5.5. This value indicates that for CuO supported on alumina, silica and chromia, the exposed Cu^{2+} species present was reduced to the zero oxidation state (Cu^0).[15] The slight deviation in this value from the expected value of zero is attributed to the degree of reducibility being less than 100%. In comparing the degree of reducibility obtained for each catalyst (Table 5.5) to the oxidation states determined (Table 5.5), it is seen that the higher the degree of reducibility the closer to zero the oxidation state will be (as for CuO/Al_2O_3 and CuO/Cr_2O_3). Thus, both the degree of reducibility and the average oxidation state from the amount of H_2 consumed can indicate whether the total amount of CuO present in the catalyst is reduced. The presence of the characteristic Cu^0 phase peaks in the H_2 *in situ* diffractograms (Figure A 2 – 4 in Appendix A) confirms the reduction of CuO to Cu^0. However, the H_2 *in situ* diffractograms for CuO/Cr_2O_3 (Figure A 3, Appendix A 1) also reveal the presence of characteristic Cu_2O phases. This indicates that the reduction of Cu^{2+} is to the Cu^{+1} oxidation state as well. In addition, the appearance of some CuO phase peaks in the H_2 *in situ* diffractograms of the three catalysts (Figure A 2 – 4 in Appendix A) indicates the incomplete reduction of the total amount of CuO available for reduction.

5.7. Temperature Programmed Desorption (TPD)

The TPD profiles for CuO/Al_2O_3, CuO/SiO_2 and CuO/Cr_2O_3 are shown in Figure 5.18 (a), (b) and (c) respectively. The temperature at the maximum, as well as the acid strength and acidity of the catalysts, are presented in Table 5.6. As stated in Section 4.2 in Chapter 4, the amount of ammonia desorbed was used to determine the acidity of the catalyst. The temperature at which the peak maximum (T_m) occurs is indicative of the acid strength of the sample.[16] The acid strength of the catalysts is described by three regions, namely, weak; medium and strong acid sites[16-18] over the temperature range 200 – 310 °C; 310 – 500 °C and 500 – 1000 °C respectively

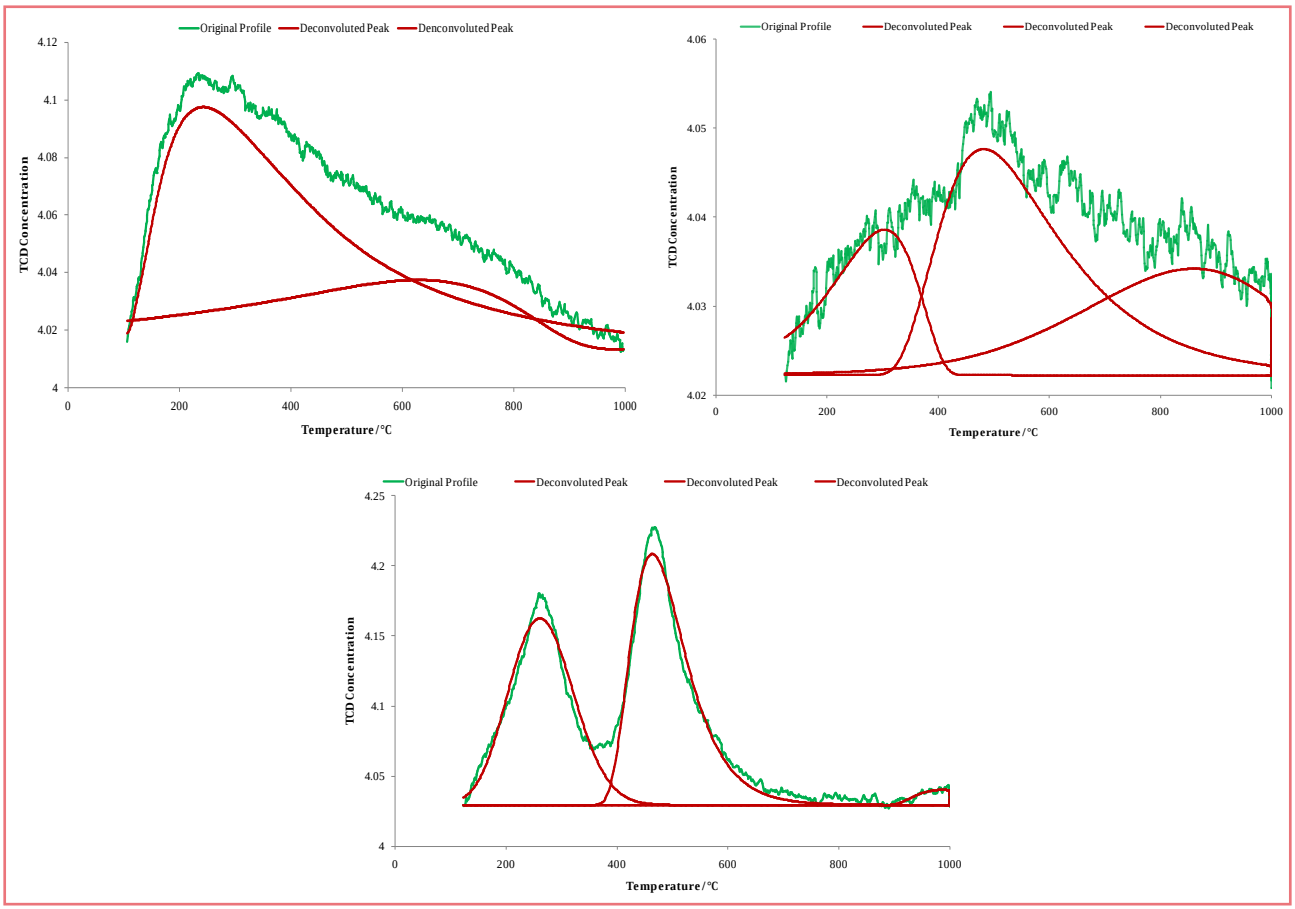

Figure 5.18: TPD Profile of (a) CuO/Al_2O_3; (b) CuO/SiO_2 and (c) CuO/Cr_2O_3

Table 5.6: A list showing the acid strength and acidity of each catalyst

Catalyst	Acid Strength Temperature/°C			Acid Sites concentration/µmol g^{-1}_{cat}			
	T_m at A[a]	T_m at B[a]	T_m at C[a]	Acidity at A	Acidity at B	Acidity at C	Total Acidity[b]
CuO/Al_2O_3	244	--	636	1288	--	504	1791
CuO/SiO_2	303	482	860	154	382	263	799
CuO/Cr_2O_3	261	464	987	847	1014	78	1938

[a] A = Weak Acid Site (200 – 310 °C); B = Medium Acid Site (310 – 500 °C) and C = Strong Acid Site (500 – 1000 °C)

[b] Determined using the equation: *Acidity = mol NH_3 desorbed / mass of catalyst used* [18]

The data listed in Table 5.6 show that the alumina supported CuO has both weak and strong acid sites, whilst CuO/SiO_2 and CuO/Cr_2O_3 show the presence of weak, medium and strong acid sites. With the exclusion of the weak acid sites, it is observed that the acid

strength based on the T_m values in decreasing order is: CuO/Cr_2O_3 > CuO/SiO_2 > CuO/Al_2O_3, whilst for the weak acid sites it is seen that the silica supported catalyst displays the greater 'weak acid strength'. From the total acidity values, the observed trend in decreasing order is: CuO/Cr_2O_3 > CuO/Al_2O_3 > CuO/SiO_2.

It is known that the acid sites that make up a catalyst may be divided into two types, namely, Lewis acid sites and Brønsted acid sites. *Camiloti et al.*[19] states that the desorption of ammonia at lower temperatures is due to Lewis acid sites. A more conclusive proof of the presence of Lewis acid sites and Brønsted acid sites is obtained upon examining the reaction network of the catalytic reaction. The presence of products that are formed by reactions that are typically characterized by Lewis acids (electron pair acceptors) indicates that the catalyst is comprised of Lewis acid sites, whilst the presence of products that are formed from the acid-catalyzed (H^+) reactions indicates that the catalyst contains Brønsted acid sites (proton (H^+) donors).

5.8. Thermogravimetric Analysis-Differential Scanning Calorimetry (TGA-DSC)

The TGA-DSC curves (under N_2) for CuO/Al_2O_3, CuO/SiO_2 and CuO/Cr_2O_3, as well as for unsupported CuO are presented in Figures 5.19 (a), (b), (c) and (d), respectively. A summary of some of the information extracted from these curves is given in Table 5.7. The TGA-DSC curves were divided into three regions. These regions were:

(a) Initial stage, occurring from room temperature to 200°C
(b) Intermediate stage, occurring between 200 - 770°C and
(c) Final stage, occurring from 770 - 1000°C.

The TGA-DSC curves for each of the catalysts show a similar profile, however, differences arise in the weight percent loss, as well as in the onset temperature for the weight loss seen above approximately 770 °C in the TGA curve.

The TGA curves also show a decrease in the weight from the start temperature to 200 °C (initial stage) and from 200 °C to the onset temperature of the reduction of CuO

(intermediate stage). The weight loss observed in the initial stage is often attributed to the loss of carbon dioxide (CO_2) and water (H_2O) that is adsorbed weakly to the catalyst.[20] The weight loss seen in the intermediate stage is possibly due to the loss of CO_2 without H_2O.[20] However, for CuO/Cr_2O_3, it is also possible for the weight loss seen in the intermediate stage to be due to dehydroxylation.[21] The weight losses in the initial and intermediate stages are tabulated in Table 5.7.

In comparing the weight loss for each catalyst in the initial stage, it is seen that the weight % lost increases in the order $CuO < CuO/SiO_2 < CuO/Cr_2O_3 < CuO/Al_2O_3$. The unsupported CuO displayed the lowest weight loss, indicating that the weight loss in this region may be a function of the support. It is probable that the supports have an increased ability to adsorb H_2O and CO_2, thus accounting for the data. However, as stated in Section 4.1 in Chapter 4, CuO/Cr_2O_3 was not prepared by using Cr_2O_3 as a support. Hence, as a result of the synthesis (method of co-precipitation), it is possible for the catalyst to contain interlayer water molecules or hydroxyls. Hence, the weight loss in the initial stage could be due to these interlayer water molecules and physically adsorbed water.[21] Thus, the weight loss does not solely reflect the ability of the catalyst to adsorb H_2O and CO_2. The trend observed for the initial stage also applies to the intermediate stage.

Table 5.7: The weight losses seen for the Initial and intermediate Stages of the TGA-DSC curve for each catalyst

Catalyst	Initial Stage (room temperature – 200 °C)	Intermediate Stage (200 °C – Final stage)
	Weight Loss/%	Weight Loss/%
CuO/Al_2O_3	6.6	3.2
CuO/Cr_2O_3	2.1	1.3
CuO/SiO_2	1.2	0.6
Unsupported CuO	0.3	0.3

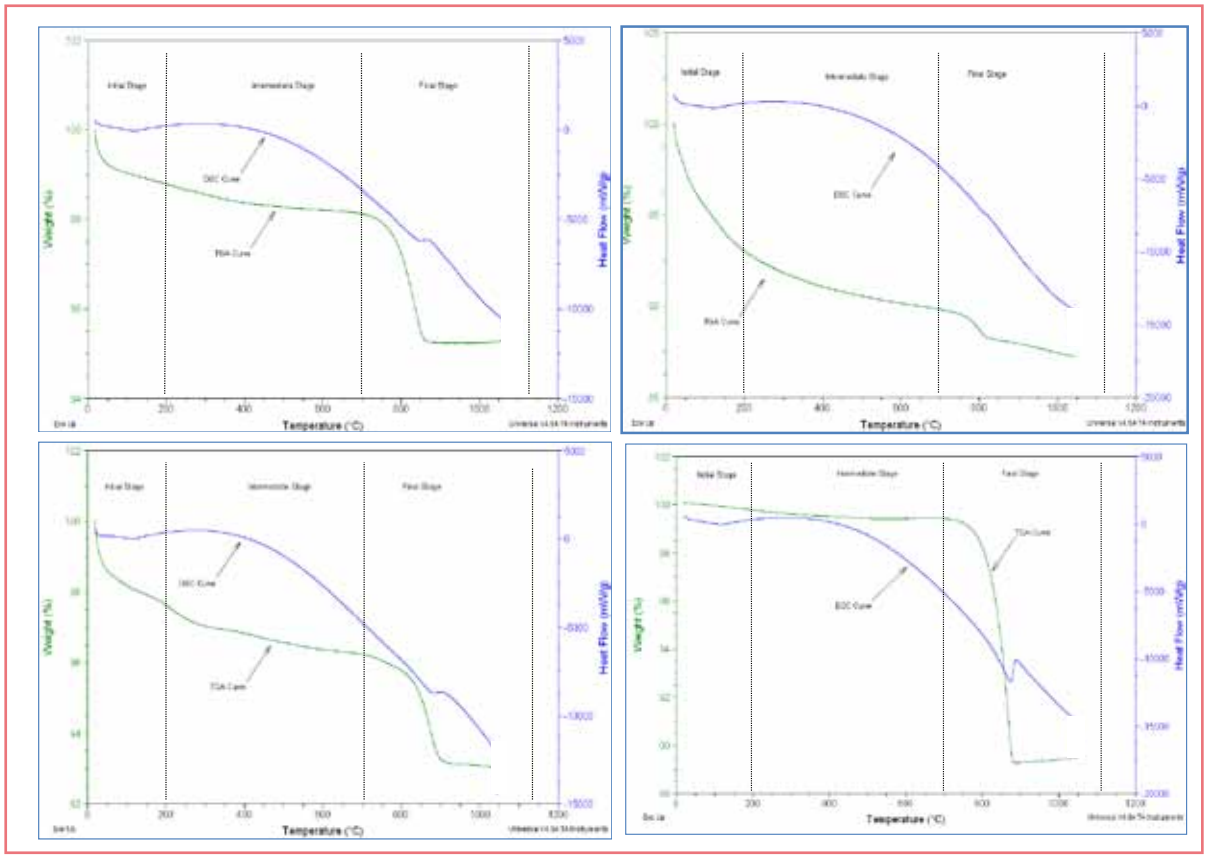

Figure 5.19: TGA-DSC curves of (a) CuO/Al_2O_3; (b) CuO/SiO_2; (c) CuO/Cr_2O_3 and (d) unsupported CuO

The weight loss occurring in the final region (770 - 1000°C) is said to be due to the release of O_2 from the reduction of CuO.[20] The data extracted from the TGA-DSC curve for the final stage for each catalyst is presented in Table 5.8.

Table 5.8: A summary of the onset temperature and weight percent (wt %) loss for each catalyst in the final stage

Catalyst	Onset Temperature / °C	Weight Loss / %
CuO/Al_2O_3	768.0	2.0
CuO/SiO_2	856.0	3.0
CuO/Cr_2O_3	895.0	3.2
Unsupported CuO	878.5	10.0

Utilizing the data listed in Table 5.8, it can be deduced that the general trend of the onset temperature, in increasing order, is: CuO/Al_2O_3 < CuO/SiO_2 < unsupported CuO < CuO/Cr_2O_3. With the exception of the chromia supported catalyst, this trend is consistent with that seen for the T_m values from the TPR analysis, in which it was shown that the general trend for the T_m values in increasing order is: CuO/Al_2O_3 < CuO/SiO_2 < CuO/Cr_2O_3 < unsupported CuO. As with the T_m value trend from TPR, the observed trend for the onset temperature in the TGA may be attributed to the effect of the support on the CuO and the strength of the CuO bond. Since the reduction of the CuO is dependent on the energy gained from heating, it can be said that the lower the onset temperature, the more easily the Cu to oxygen bond breaks. Thus, it may be said that the support influences the CuO bond such that it makes it more susceptible to bond breakage. The onset temperature for the chromia supported CuO is the highest compared to the other three samples and may be due to the existence of a metal-metal bond (Cu bonded to Cr in the $CuCr_2O_4$), which requires a greater amount of energy to dissociate. In addition, due to the absence of a support in the unsupported CuO, the onset temperature is higher than the alumina and silica supported catalysts. The differences seen in the weight loss values are related to the amount of copper present in the catalysts. From the ICP analysis it is seen that the copper loadings increase according to: CuO/Al_2O_3 < CuO/SiO_2 ≈ CuO/Cr_2O_3. Thus, since the alumina supported catalysts contained the least amount of copper, it displayed the smallest weight loss, whilst CuO/SiO_2 and CuO/Cr_2O_3 contained similar higher amounts of copper (to within experimental error) and displayed the higher weight losses.

The DSC curves for each of the catalysts show broad exotherms from ~ 110 °C to ~ 890 °C. No change is observed in the heat flow between 900 – 950 °C, thereafter the heat flow decreases indicating the occurrence of an endothermic process.

5.9. Infrared Spectroscopy (IR)

The IR spectra for CuO/Al_2O_3, CuO/SiO_2 and CuO/Cr_2O_3, as well as for alumina, silica and unsupported CuO are presented in Figures 5.20 (a), (b), (c), (d), (e) and (f) respectively. The IR spectra for unsupported CuO and the alumina and silica supports were obtained in order to fully ascertain the bands responsible for the oxides due to the copper and that of the supports. However, despite determining the regions at which CuO bands will appear (from the IR spectra of unsupported CuO) it is difficult to determine these characteristic absorptions, since the support displays bands in the same region but with a greater degree of absorption. The summary of the wavenumbers obtained from the IR spectrum of each catalyst/compound is listed in Table 5.9.

The broad band observed above 3200 cm^{-1} are assigned to hydroxyl groups that exhibit hydrogen bonding amongst the hydroxyls and is therefore attributed to water molecules.[22] For the CuO/SiO_2 catalyst, the appearance of this band is said to be characteristic of molecular water physisorbed to silica.[23] Although the band at 3358 cm^{-1} for the CuO/Cr_2O_3 is due to a hydroxyl group, it is a sharp, narrow band and is characteristic of isolated hydroxyls[22] or free hydroxyls (hydroxyls not involved in hydrogen bonding)[24]. This may be due to the sodium hydroxide (used for the synthesis) not being removed by washing or calcination. The bands that occur between the wavenumbers 1600 – 1636 cm^{-1} are indicative of asymmetric O-C-O stretching that is due to bidentate carbonate formation, as a result of carbon dioxide adsorption to the surface of the catalyst/compound.[25, 26] However, it is also possible for the band between 1634 – 1636 cm^{-1} to be due to the bending mode of water.[21, 27]

The absence of the characteristic water and carbon dioxide bands in the spectrum of unsupported CuO indicates that there is little or no water and carbon dioxide adsorbed to the compound. This confirms the observations made from TGA-DSC analysis. In addition, the appearance of the water band in the IR spectra for the alumina and silica supports confirms the observations made from the TGA-DSC analysis which showed that the unsupported CuO had the lowest weight loss, thus attributing the weight loss in this region to be a function of the support.

The bands seen in the 400 – 600 cm^{-1} region in the IR spectrum of unsupported CuO have been shown to be characteristic of CuO.[28] The bands that occur at 818 and 500 cm^{-1} in the IR spectrum of γ-alumina indicate the ionic character of the metal-oxygen (Al-O) bonds.[29] Similarly, the bands seen at 800 cm^{-1} in the IR spectrum of silica are indicative of the ionic character of the Si-O bond.[29] These bands characteristic of the alumina and silica supports are observed in the IR spectra of the alumina and silica supported CuO catalysts as well. The slight shift in the wavenumber of the bands in the IR spectra of the supported CuO catalyst from that seen for the supports alone, is due to the influence of the CuO on the environment surrounding the support. The peaks seen between 990 and 449 cm^{-1} in the IR spectrum of CuO/Cr_2O_3 are characteristic of metal oxides, but it is difficult to assign a particular peak to the CuO or the chromium oxide. In general, the peaks occurring between 990 – 884 cm^{-1} are attributed to the metal-oxide (M=O) stretching, whilst the peaks occurring below 884 cm^{-1} may be assigned to the M=O and M-O vibrations of hydrated surface metal oxide species.[29, 30]

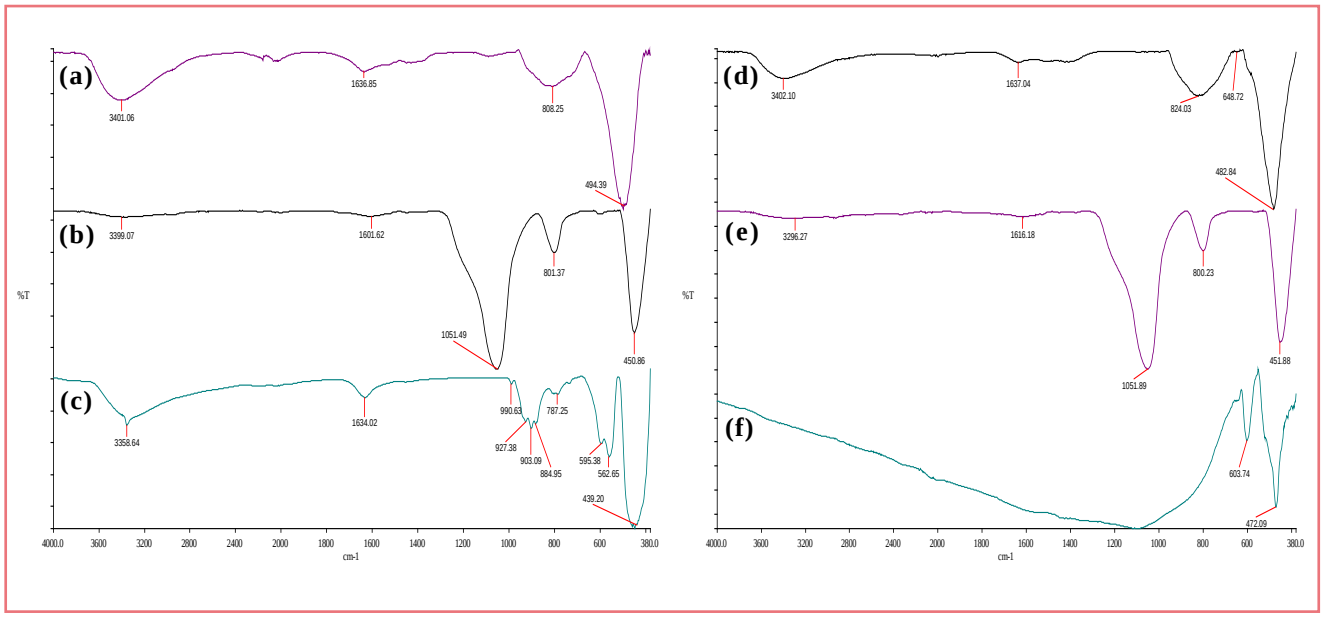

Figure 5.20: IR spectra of (a) CuO/Al_2O_3; (b) CuO/SiO_2; (c) CuO/Cr_2O_3; (d) Alumina; (e) Silica and (f) unsupported CuO

Table 5.9: A list of the wavenumbers observed in the IR spectrum of each compound

Catalyst/Compound	Wavenumber/cm $^{-1}$
Unsupported CuO	1100; 603; 472; 395
Gamma Alumina	3413; 1636; 818; 500
Silica	3296; 1616; 1051; 800; 451
CuO/Al_2O_3	3402; 1637; 824; 482
CuO/SiO_2	3399; 1601; 1051; 801; 450
CuO/Cr_2O_3	3358; 2167; 1634; 990; 927; 903; 884; 787; 595; 562; 449

5.10. References

1. *X-Ray Diffraction*, www.panalytical.com/index.cfm?pid=866, Accessed 11/10/2009, 2009.
2. P. W. Park and J. S. Ledford, *Appl. Catal. B: Enviro.*, 1998, **15**, 221.
3. J. J. Bozzola and L. D. Russell, *Electron Microscopy: Principles and techniques for biologists*, Jones and Bartlett Publishers, Boston, 1992.
4. P. K. Jena, E. A. Brocchi and M. S. Motta, *Mater. Sci and Eng. A*, 2001, **313**, 180.
5. J. Lee, S. Sim, K. Kim, K. Cho and S. Kim, *Mater. Sci. and Eng. B*, 2005, **122**, 85.
6. G. Q. Zhong, H. L. Zhou and Y. Q. Jia, *J. Alloys and Comp.*, 2008, **465**, L 1.
7. D. Ozkaya, *Platinum Metals Rev.*, 2008, **52**, 61.
8. J. Haber, *Pure & Appl. Chem.*, 1991, **63**, 1227.
9. H. Chang, M. A. Saleque, W. Hsu and W. Lin, *J. Mol. Catal. A: Chem*, 1996, **109**, 249.
10. S. Valange, J. Barrault, A. Derouault and Z. Gabelica, *Microporous and Mesoporous Mat.*, 2001, **44 - 45**, 211.
11. L. Chen, T. Horiuchi, T. osaki and T. Mori, *Appl. Catal. B: Environ*, 1999, **23**, 259.
12. M. Luo, P. Fang, M. He and Y. Xie, *J. Mol. Catal. A: Chem.*, 2005, **239**, 243.
13. R. Zhou, T. Yu, X. Jiang, F. Chen and X. Zheng, *Appl. Surf. Sci.*, 1999, **148**, 263.
14. P. A. Barnes, M. Tiernan and G. Parkes, *J. Therm. Anal. Cal.*, 1999, **56**, 733.
15. J. Guzman and B. C. Gates, *J. Phys. Chem. B*, 2002, **107**, 2242.
16. A. M. Venezia, V. L. Parola, B. Pawelec and J. L. G. Fierro, *Appl. Catal. A: Gen.*, 2004, **264**, 43.
17. M. H. O. Nunes, V. T. d. Silva and M. Schmal, *Appl. Catal. A: Gen.*, 2005, **148**.
18. G. V. Sagar, P. V. R. Rao, C. S. Srikanth and K. V. R. Chary, *J. Phys. Chem. B*, 2006, **110**, 13881.
19. A. M. Camiloti, S. L. Jahn, N. D. Velasco, L. F. Moura and D. Cardoso, *Appl. Catal. A: Gen.*, 1999, **182**, 107.
20. P. H. Matter, D. J. Braden and U. S. Ozkan, *J. Catal.*, 2004, **223**, 340.
21. M. Crivello, C. Pérez, J. Fernández, G. Eimer, E. Herrero, S. Casuscelli and E. Rodríguez-Castellón, *Appl. Catal. A: Gen.*, 2007, **317**, 11.
22. S. Solar, *J. Phys. Chem.* , 1984, **88**, 5620.
23. G. J. Millar and C. H. Rochester, *J. Chem. Soc. Faraday Trans.*, 1992, **88**, 1477.
24. D. N. Kendall, *Applied Infrared Spectroscopy*, Reinhold Publishing Corporation, London, 1966.
25. V. K. Diez, C. R. Apesteguia and J. I. D. Cosmo, *Catal. Today*, 2000, **63**, 53.

26. T. Horiuchi, H. Hidaka, T. Fukui, Y. Kubo, M. Horio, K. Sukuzi and T. Mori, *Appl. Catal. A: Gen.*, 1998, **167**, 195.
27. M. J. Holgado, V. Rives and M. S. S. Román, *Appl. Catal. A: Gen.*, 2001, **214**, 219.
28. G. Papadimitropoulos, N. Vourdas, V. E. Vamvakas and D. Davazoglou, *Thin Solid Films*, 2006, **515**, 2428.
29. I. E. Wachs, *Catal. Today*, 1996, **27**, 437.
30. K. Nakamoto, *Infrared and Raman Spectra of Inorganic and Coordination compounds*, Third edn., Wiley-Inetrscience, John Wiley & Sons, New York, 1978.

Chapter 6

Results and Discussion: Catalytic Testing

The work carried out in this study involved an investigation of a reaction system used for the hydrogenation of octanal. The catalysts that were synthesized were CuO/Al_2O_3, CuO/SiO_2 and CuO/Cr_2O_3. The synthesis and characterization of these catalysts were discussed in Chapters 4 and 5 respectively.

The fresh feed used for the hydrogenation of octanal was 10 wt % octanal in octanol whilst a water-spiked feed with 1.8 wt % water in fresh feed was used for the water-impact study. The primary product of the reaction is octanol, which forms when octanal is hydrogenated. Other products formed during the reaction are mainly C16 and C24 heavies. Some alkanes, esters and ethers are also formed during the reaction.

The first part of the study was to establish whether the system remains at steady state for a period of approximately 28 hours. This initial study was carried out using CuO/Al_2O_3 as the catalyst. The effects of temperature and hydrogen/aldehyde ratios were investigated. The result of this study was used to determine the operating conditions for the subsequent catalytic testing.

In the second part of the study, the impact of water on the catalysts and the reaction was investigated. The water-spiked feed was introduced to the system once steady state was reached (unless otherwise stated). The effects on the conversion of octanal and the selectivity to octanol and the by-products were investigated. In addition, the effect of the water on the catalyst was examined, by the characterization of the used catalyst and comparing this to the fresh catalyst characterization and fresh feed catalyst characterization (catalyst used for the reaction with no water in the feed).

In the sections to follow the results obtained for the initial study, the water-impact study and used catalyst characterization will be presented and discussed (Sections 6.1, 6.2 and 6.3 respectively).

6.1. Initial Study

The catalyst characterization showed that CuO/Al_2O_3 possessed the highest surface area and the lowest reduction temperature in comparison to the other catalysts (CuO/SiO_2 and CuO/Cr_2O_3). These characteristics suggested that CuO/Al_2O_3 would be the most active catalyst in the hydrogenation reactions. It was for this reason that this catalyst was chosen for the initial study.

The initial study was used to determine the effect of temperature and hydrogen/aldehyde ratio on the steady state, catalytic activity and selectivity to octanol (desired product). The initial catalytic testing was carried out at 140, 160 and 180 °C using CuO/Al_2O_3. At 140 and 160 °C, the effect of the hydrogen/aldehyde ratio was investigated using a ratio of one and two.

6.1.1. Effect of temperature on octanal hydrogenation

Figures 6.1 (a) and (b) present the initial catalytic data obtained at 140, 160 and 180 °C and a hydrogen/aldehyde ratio of two. The reactions were carried out under these conditions for a period of 28 hours.

The conversion of octanal at each temperature as a function of time-on-stream is shown in Figure 6.1 (a). These results showed that the conversion at 160 and 180 °C is slightly higher (approximately 2 %) than at 140 °C. In addition, the conversion at 140 °C does not remain at steady state over 28 hours. However, the conversion at 160 and 180 °C reaches steady state after 3 hours, with a value of approximately 99 % and remains steady under these conditions even after 28 hours. There is an insignificant difference between the conversion at 160 and 180 °C, possibly because the catalyst is functioning at its maximum ability. These results indicate that by increasing the temperature, only a slight increase in conversion can be obtained.

The selectivity to octanol at each of the three temperatures is shown in Figure 6.1 (b). There are no significant differences seen in the selectivity and a value of approximately 97 % is maintained after 28 hours at each temperature. At 140 °C, the selectivity to octanol is not altered when the conversion of octanal decreases, indicating that this catalyst is highly specific and directs the reaction to the primary product (octanol).

Selectivity is affected by the adsorption of the carbonyl group (C=O) on the catalyst surface. The high selectivity to octanol indicates that the interaction of the carbonyl group (C=O) with the catalyst surface, is favored. The C=O group is made up of a π system due to the presence of the double bond. From molecular orbital theory, it is known that this molecule has a π^*_{CO}-orbital which is able to accept electrons. When this orbital is lowered and the backbonding interaction is favored, the adsorption of the C=O group occurs more easily. This then directs the selectivity to the primary product. The presence of Lewis acid sites can activate the carbonyl group and lower the π^*_{CO}-orbital. The active metal is enriched with electrons by interaction with a support which favors backbonding.[1] The former mentioned (interaction of the active metal with a support) is present in the catalyst and thus a high selectivity to octanol is obtained. In addition, the high selectivity to the octanol indicates that the octanal interacts strongly with the catalyst surface, which allows for the desorption of the octanol as soon as it is formed.

At 140 °C, the conversion fluctuated over time, whilst the conversion at 160 and 180 °C showed an insignificant difference, but there are higher operating costs associated with working at 180 °C. The temperature chosen for subsequent reactions was therefore 160 °C.

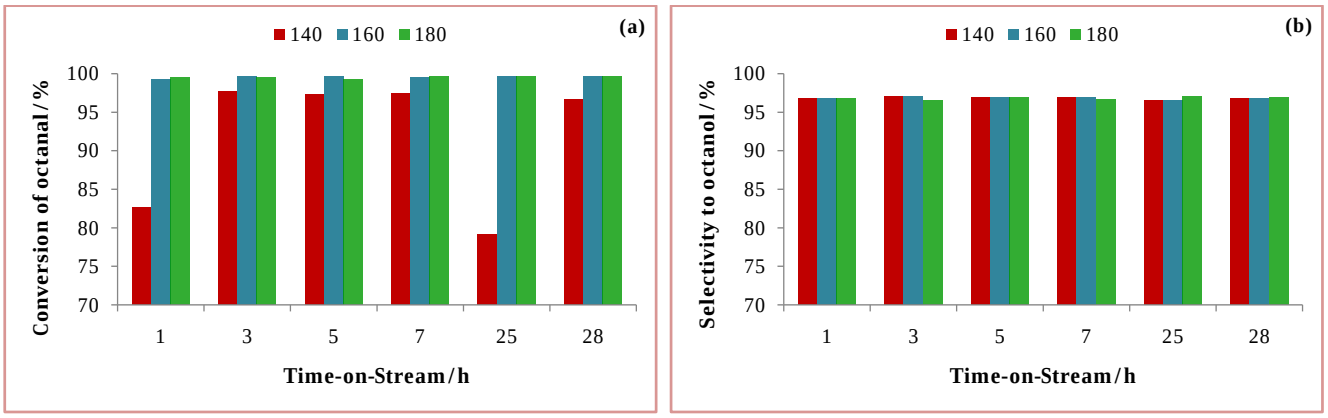

Figure 6.1: (a) Conversion of octanal and (b) Selectivity to octanol for the hydrogenation of octanal at 140; 160 and 180 °C

6.1.2. Effect of hydrogen/aldehyde ratio on octanal hydrogenation

The effect of the hydrogen/aldehyde ratio of one and two on the conversion of octanal and the selectivity to octanol at 160 °C is shown in Figure 6.2. The conversion at both ratio one and two reaches steady state after 5 hours and remains steady for the duration of the experiment (28 hours). The conversion at ratio one is approximately 98 %, whilst a conversion of 99 % is achieved at ratio two showing that there is minimal difference in the conversion at ratios one and two. The minor increase in conversion at ratio two indicates that the increase in hydrogen flow into the system does not significantly impact the hydrogenation of octanal at 160 °C. The stoichiometric amount of hydrogen required to hydrogenate one mole of octanal is one (as shown in Scheme 2.3 in Section 2.3.2.1), but there are other possible reactions in the system that require hydrogen (discussed in Section 6.1.3). Therefore, by using the stoichiometric hydrogen/aldehyde ratio of one for the reaction, it could result in a hydrogen deficiency as the reaction proceeded. This would be observed by a decrease in the conversion with time-on-stream. There was no indication of this occurrence, indicating that at 160 °C, there was a thermodynamic influence that favored the direct hydrogenation of octanal to octanol.

The selectivity to octanol at ratio one and two maintains a value of around 97.5 % and 97 %, respectively, with time-on-stream. This shows that the selectivity at ratio one is only slightly higher than at ratio two (approximately 0.5 %). The slight decrease in selectivity

at ratio two is due to the excess hydrogen in the system that allows for hydrogen consuming side reactions to occur.

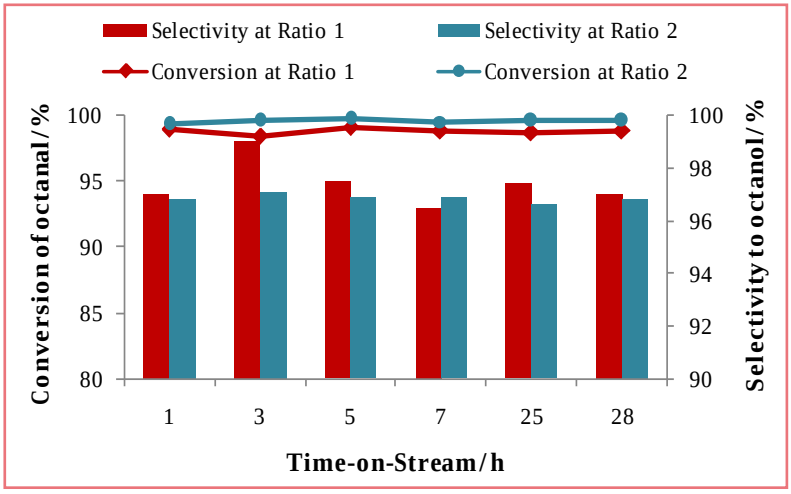

Figure 6.2: Conversion of octanal and selectivity to octanal at 160 °C and hydrogen/aldehyde ratios of one and two

Since the effect of the hydrogen/aldehyde ratio could not be properly determined at 160 °C, the reaction was carried out at 140 °C. From section 6.1.1, it was determined that at temperatures higher than 160 °C, the conversion of octanal is not significantly different, whilst at temperatures lower than 160 °C there is a slight decrease in the conversion. Hence, it was hoped that the influence of the hydrogen/aldehyde ratio could be seen at 140 °C.

The conversion of octanal and the selectivity to octanol at 140 °C and hydrogen/aldehyde ratios of one and two is shown in Figure 6.3. The conversion of octanal at ratio two decreases after 25 hours on stream reaching a value of 79 %, thereafter, it increases to 97 %. The conversion of octanal at ratio one remains at approximately 68 % for 5 hours; after which it gradually decreases to 42 % after 25 hours and remains at this value. As expected, the effect of the hydrogen/aldehyde ratio is clearly observed at 140 °C. This confirms that temperature does influence the hydrogenation of octanal and that at temperatures greater than 140 °C, thermodynamics significantly influence the reaction. The higher conversion obtained at ratio two indicates that an excess of hydrogen is required to obtain optimum/high conversions of the octanal. The lower conversion at ratio one confirms that operating at the stoichiometric hydrogen/aldehyde ratio results in

a hydrogen deficiency in the system. Operating under these conditions leaves octanal molecules adsorbed on the surface of the catalyst. As the reaction proceeds, the un-reacted octanal molecules accumulate on the catalyst surface and can undergo self-condensation to form C16 or C24 products, which can block the active sites for the hydrogenation of octanal. This accounts for the decrease in the conversion with time-on-stream (as observed in Figure 6.3). *Yeong et al.*[2] and *Bonello et al.*[3] have shown that under hydrogen starvation conditions, by-products form on the catalyst surface and due to the accumulation of these products, the catalyst loses its activity over time.

The selectivities to octanol at ratios one and two are not significantly different (approximately 0.7 % difference). The selectivity at ratio one maintains a value of nearly 97.6 % with time-on-stream, whilst at ratio two, the selectivity remains around 96.9 % after 28 hours. These selectivity trends are also observed for the reactions carried out at 160 °C. Thus, while conversion at ratio one and 140 °C is considerably lower than for the reactions carried out, the selectivity to octanol is similar to those obtained for all experiments under the different conditions. This shows the ability of the synthesized CuO/Al_2O_3 to preferentially form the desired product.

Since the low conversion of octanal and its decrease over time at a hydrogen/aldehyde ratio of one indicates that using this stoichiometric amount of hydrogen leads to the loss of activity over time, for further reactions a hydrogen/aldehyde ratio of two was used.

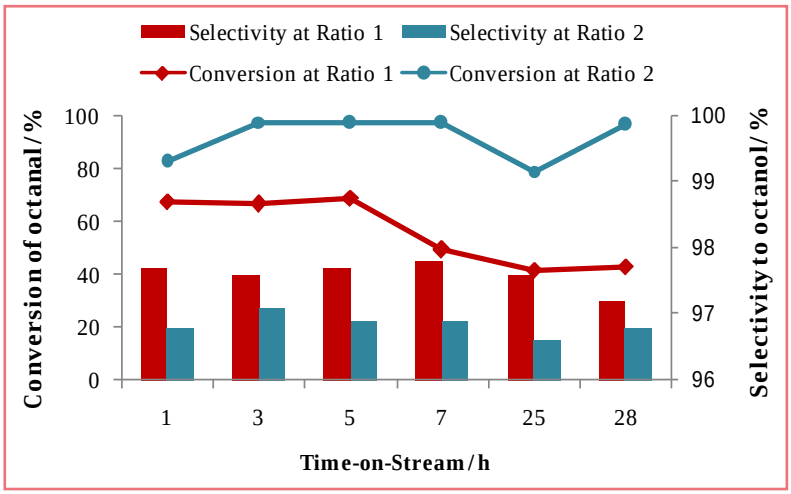

Figure 6.3: Conversion of octanal and selectivity to octanol at 140 °C and hydrogen/aldehyde ratios of one and two

6.1.3. Other products

The product network for the hydrogenation of octanal shows a similar profile across all reactions carried out. The by-products formed during the hydrogenation of octanal using CuO/Al_2O_3 under the conditions discussed in Sections 6.1.1 and 6.1.2 is shown in Figure 6.4.

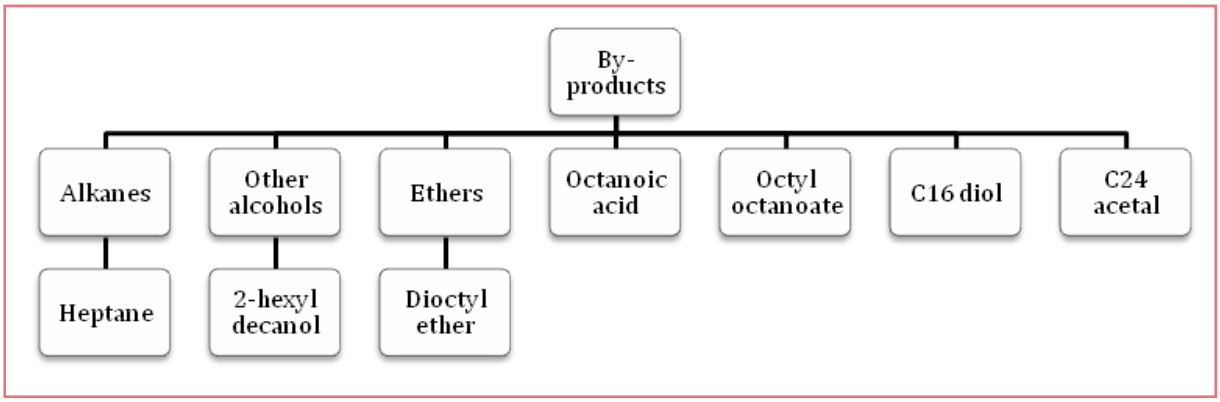

Figure 6.4: Graphical representation showing the by-products formed during the hydrogenation of octanal under various conditions

6.1.3.1. Reaction network in the hydrogenation of octanal

As already mentioned, the primary or desired reaction in the system is the hydrogenation of octanal to octanol. Scheme 2.3 in Section 2.3.2.1 shows the reaction by which it is formed. This is the main reaction in the reaction network and occurs when the carbonyl group on the octanal is hydrogenated to the hydroxyl group forming the corresponding alcohol, octanol.

As stated in Section 2.3.2.1, the major side reaction that is expected to occur in the system is the aldol condensation of two octanal molecules. The reactions that occur in the aldol condensation process are shown in Scheme 6.1. Such reactions are typically base-catalyzed; however, it is possible for acid-base bifunctional catalysts (such as supported alumina catalysts) to promote aldol condensation reactions. *Wang et al.*[4] proposed a mechanism for aldol condensation over acid-base sites.[4] This mechanism, modified for octanal as the feed, is shown in Scheme 6.2.

In aldol condensation, the two octanal molecules react to form a C16 aldol intermediate. This compound is unstable and can follow one of two reaction routes as shown in Scheme 6.1. The first reaction route that the C16 aldol can undergo is hydrogenation to the C16 diol which can be dehydrated to form a C16 unsaturated alcohol, which in turn can be hydrogenated to form a C16 saturated alcohol. The second reaction route that the aldol intermediate can undergo is a dehydration reaction to form an α, β-unsaturated aldehyde (C16 unsaturated aldehyde). As shown in Scheme 6.1, this C16 unsaturated aldehyde can undergo hydrogenation to form the saturated aldehyde, which can be further hydrogenated to form the C16 saturated alcohol. The C16 saturated aldehyde and alcohol can react with an octanol and octanal molecule, respectively, to form C24 esters. Only the C16 diol and the C16 saturated alcohol (2-hexyl decanol) were found as products from the hydrogenation of octanal using CuO/Al_2O_3 (as shown in Figure 6.4).

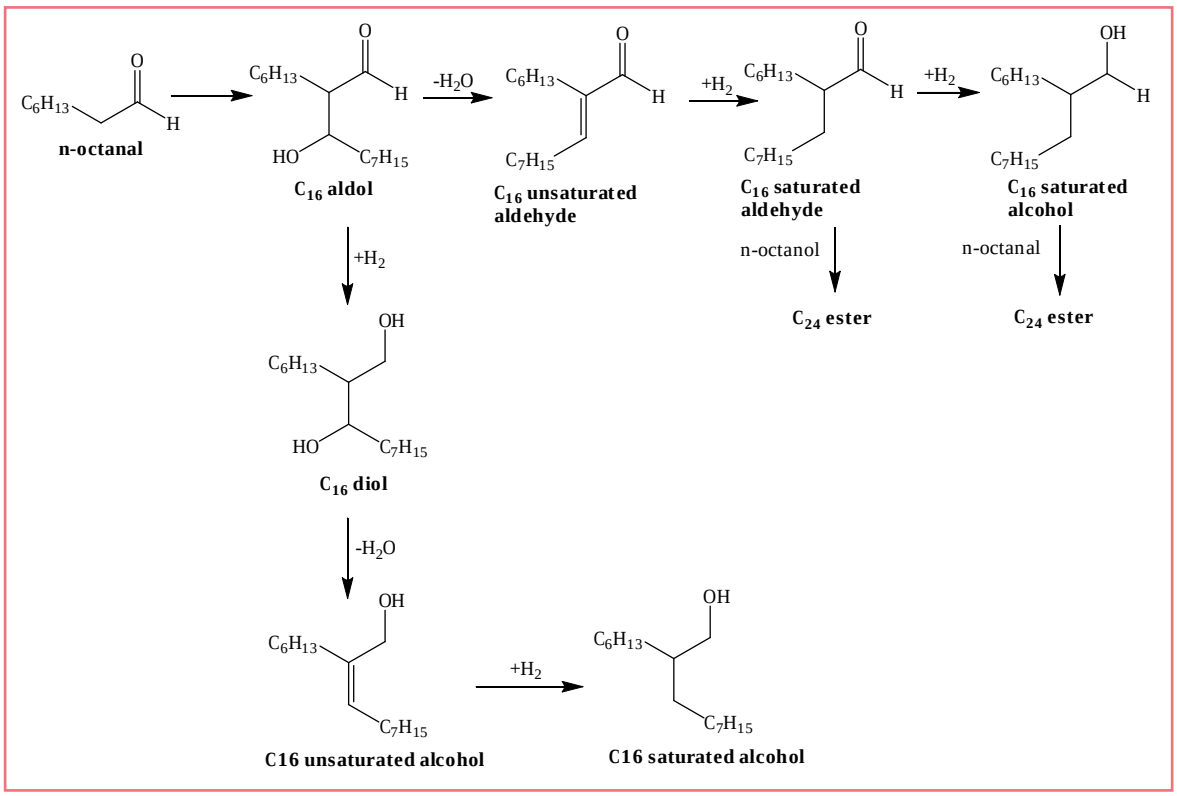

Scheme 6.1: Possible products formed from the aldol condensation of octanal (Adapted from *Wang et al.*[4])

As stated earlier, the presence of both acid and base sites can favor the formation of aldol condensation products. Scheme 6.2 shows the role these sites may play in the formation of the C16 aldol intermediate. Since alumina is amphoteric, an alumina supported catalyst

can promote the aldol condensation reaction. In this mechanism, the weak base sites remove one hydrogen atom from the α-carbon to form a carbanion which is the nucleophile in the reaction. The weak acid sites are responsible for protonating the carbonyl oxygen through polarization of the C–O bond, which results in a positively charged carbon atom (the electrophile). This electrophile is attacked by the nucleophile and the aldol intermediate is formed. This aldol intermediate can follow one of the two reaction routes discussed above. The presence of the C16 diol and the 2-hexyl decanol in the product stream indicate that using the alumina support does influence the formation of aldol condensation products.[4]

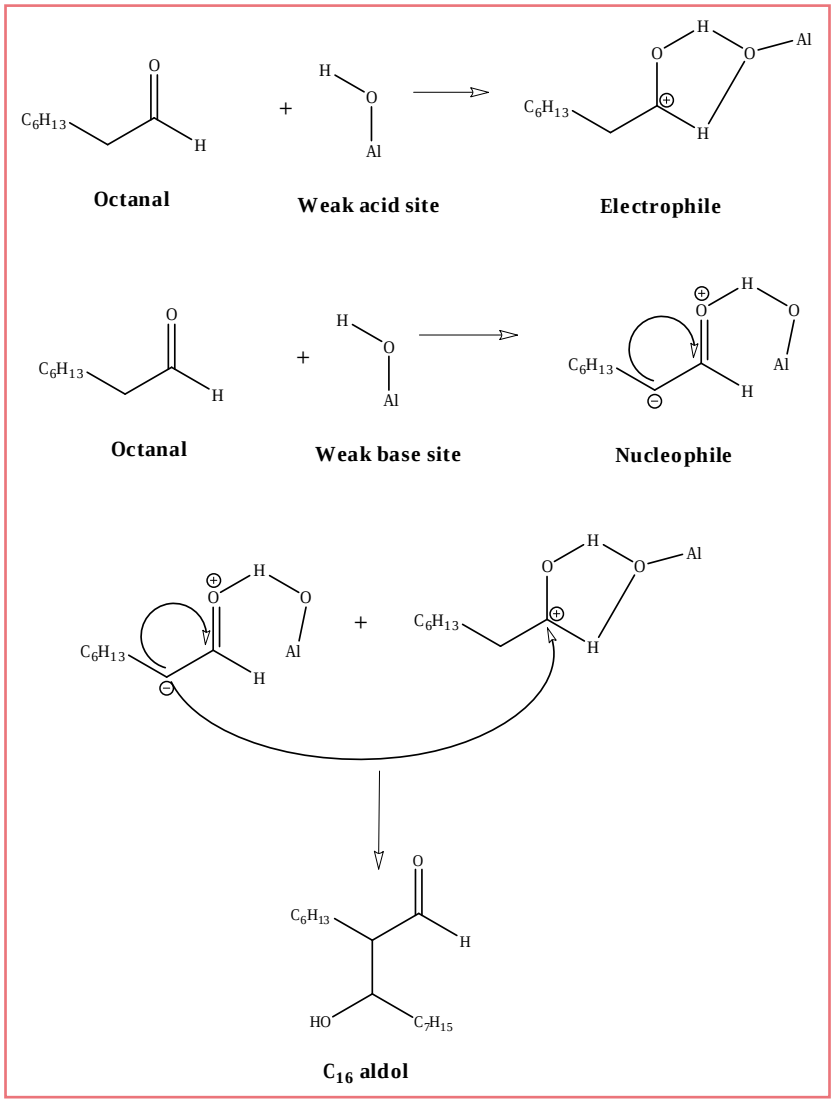

Scheme 6.2: Proposed mechanism for aldol condensation reactions over acid-base sites (Adapted from *Wang et al.*[4])

Aldol condensation can also occur between two octanol molecules. This reaction produces dioctyl ether, which can also be formed via the hydrocracking of a C24 acetal (its formation is discussed below). Octanol is also formed during this reaction. The presence of dioctyl ether in the product stream indicates that either one or both of these reactions occurs in the system. The dioctyl ether can undergo a hydrocracking reaction in which octane and octanol are the products. However, octane was not found in the product stream, hence the former mentioned reaction does not occur to any detectable extent.

Acetal formation is another prominent side reaction in this reaction network. This reaction occurs between aldehyde and alcohol species. In order for this reaction to occur, an acid site is required to protonate the carbonyl oxygen on the octanal molecule. Scheme 6.4 shows the formation of the C24 acetal from octanal and octanol. When the addition reaction occurs between the protonated octanal and the octanol, a hemiacetal intermediate is formed, which exists in equilibrium with the oxonium ion (formed upon dehydration of the hemiacetal). However, due to the instability of the hemiacetal, it quickly undergoes a reaction with a second alcohol molecule to produce the C24 acetal. This compound was found as a product from the hydrogenation of octanal.

In Section 5.8 (Chapter 5), the catalyst was shown to have acid sites and the presence of the C24 acetal and the aldol condensation products indicates that the CuO/Al_2O_3 contains Brønsted acid sites, since H^+ is required for these products to form.

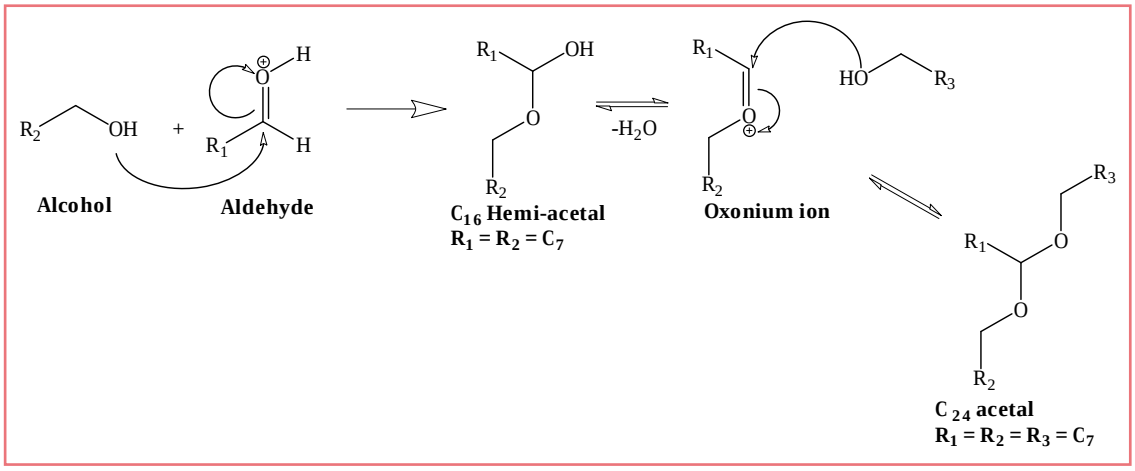

Scheme 6.3: Acetal formation from octanal and octanol (adapted from *Wang et al.*[4])

Water is a by-product formed as a result of the condensation reactions occurring in the system. Its presence creates an oxidizing atmosphere and results in the formation of octanoic acid. This can then lead to the production of octyl octanoate, from the esterification reaction occurring between octanol and octanoic acid. Octyl octanoate was found as a minor product in the hydrogenation of octanal; however, no octanoic acid was detected. The presence of the ester indicates that octanoic acid was produced but was completely consumed during the esterification. The octanoic acid and the octyl octanoate are expected to be minor reactions in the reaction network. In addition, light products such heptanes (found as shown in Figure 6.4), produced from the decarbonylation of octanal, may form a small component of the product distribution.[4]

6.1.3.2. Effect of temperature on the formation of other products

Figure 6.5 (a), (b) and (c) presents the by-products formed during the reaction and the selectivity at which they form. The major by-products in the reaction are the C16 diol and the C24 acetal, whilst minor by-products include octyl octanoate, heptane, dioctyl ether and 2-hexyl decanol. This was expected based on the work carried out by *Wang et al.*[4] on the hydrogenation of propanal and hexanal (discussed in Section 6.1.3.1). Of these two major by-products, the C16 diol is formed with the greatest selectivity (around 2 %). This is primarily due to the amphoteric alumina support, which was shown to influence the aldol condensation reaction (Section 6.1.3.1). The selectivity to the C24 acetal is seen to decrease by 0.2 % when the reaction is carried out at 180 °C, whilst at 140 and 160 °C, the selectivity remains at approximately 0.46 %. At 180 °C, the lower selectivity to the C24 acetal indicates that there are more acid sites available for other reactions.

The selectivity to octyl octanoate shows a minimal increase from 140 to 180 °C (from around 0.05 % at 140 °C to 0.47 % at 180 °C) which shows the temperature dependence of the ester forming reactions. In addition, the greater availability of acid sites at 180 °C, can favor the formation of the ester.

The selectivity to ethers remains at approximately 0.05 % at both 140 and 160 °C, whilst at 180 °C it shows a slight increase to 0.12 %. This may be attributed to an increase in the

hydrocracking of the C24 acetal at 180 °C. This can also account for the decrease in the C24 selectivity at 180 °C.

As with the selectivity to octanol (discussed in Section 6.1.1), there is little difference in the selectivity to the total by-products with time-on-stream. A total by-product selectivity of less than 3.5 % is maintained for the duration of the reaction at all temperatures. Slight changes in by-product selectivity with time-on-stream are only seen for the C24 acetal, octyl octanoate and ethers.

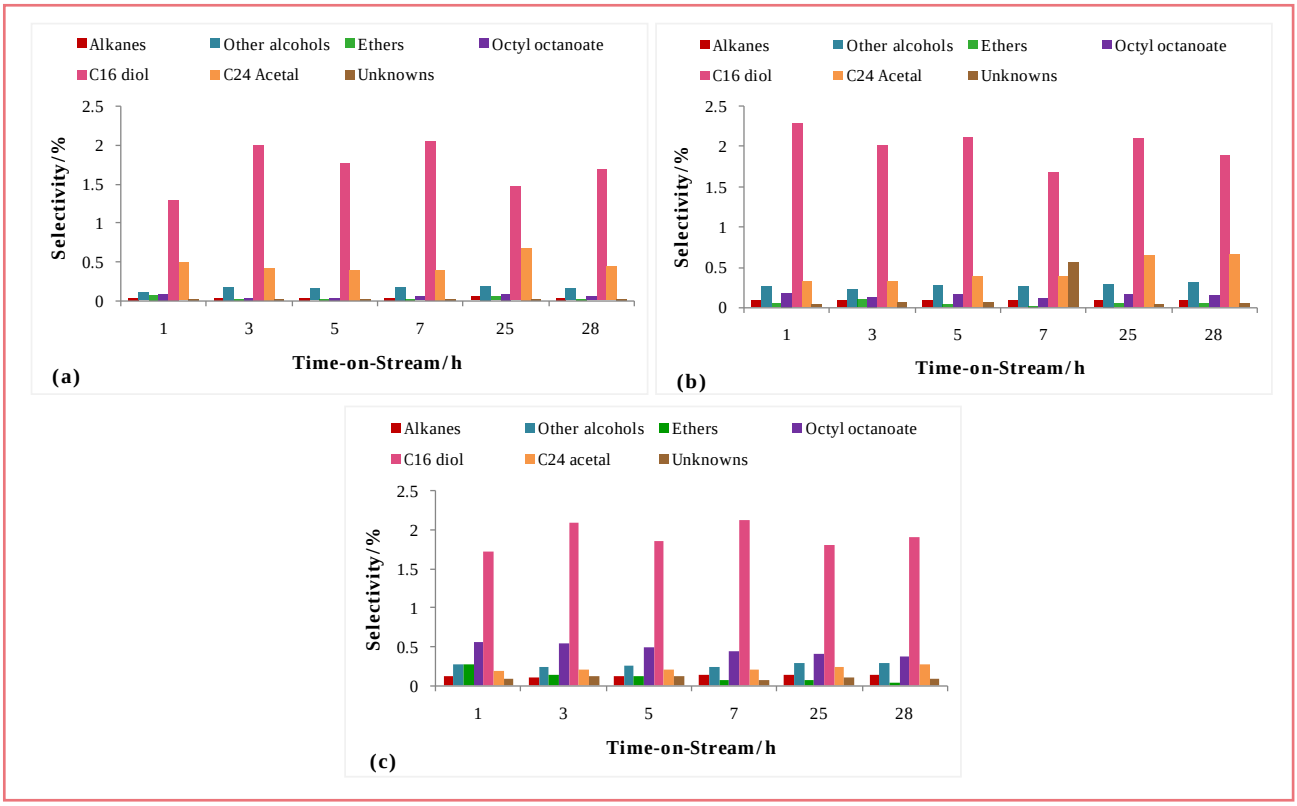

Figure 6.5: Selectivity to by-products formed during the hydrogenation of octanal at (a) 140 °C; (b) 160 °C and (c) 180 °C

6.1.3.3. Effect of hydrogen/aldehyde ratio on the formation of other products

Tables 6.1 and 6.2 show the selectivity obtained for the by-products at 140 and 160 °C and a hydrogen/aldehyde of one and two. At 160 °C, the selectivity to all by-products is only minimally higher at ratio two than at ratio one. This indicates that the hydrogen/aldehyde ratio effectively does not influence the formation of by-products at 160 °C (much like for the selectivity to octanol). At 140 °C, the selectivities to all by-

products, except the C16 diol and C24 acetal, show similar values at ratio one and two for the duration of the reaction.

At 140 °C and a hydrogen/aldehyde ratio of one, the selectivity to the C16 diol increases slightly, reaching approximately 2 % after 5 hours on stream. The selectivity is then observed to decrease reaching 0.25 % after 28 hours on stream. These changes in selectivity with time-on-stream can be attributed to the build-up of unreacted octanal and aldol condensation products on the catalyst, which then block active sites. Initially, the selectivity to the C24 acetal shows no change for 5 hours, however, when the selectivity to the C16 diol decreases, the selectivity to the C24 acetal is seen to increase slightly reaching a value of 1 % after 28 hours. This may be due to the availability of more acid sites, since the aldol condensation reactions occur to a lesser extent.

As stated in Section 6.1.2, investigating the effect of the hydrogen/aldehyde ratio at 140 °C shows the influence of the amount of hydrogen on the hydrogenation of octanal. Since the catalytic data show that an accumulation of reactant and/or product molecules occurs on the catalyst, operating the system using a hydrogen/aldehyde ratio of one may affect the deactivation studies since the lack of hydrogen in the system may lead to catalyst deactivation due to coking over time.

6.2. Water-impact studies

From the results of the initial study (discussed in Section 6.1), the operating conditions for the subsequent catalytic testing and water-impact studies were determined (160 °C and a hydrogen/aldehyde ratio of two). These conditions were used for further catalytic testing of all three catalysts (CuO/Al_2O_3; CuO/SiO_2 and CuO/Cr_2O_3).

As mentioned already, the water-impact studies were carried out by spiking the fresh feed with water. This was achieved by adding water to the fresh feed to obtain a concentration of 1.8 wt % water in the octanal feed. This concentration of water was found to be the maximum amount of water that can be added to the feed before phase separation occurred. The effects of the water on the conversion and selectivity were observed for each catalyst and are discussed hereunder.

Table 6.1: Selectivity to the by-products formed during the hydrogenation of octanal at 140 °C and hydrogen/aldehyde ratios of one and two

Time-on-Stream/h	Selectivity to by-products/%													
	Alkanes		*Other Alcohols*		*Ethers*		*Octyl octanoate*		*C16 diol*		*C24 acetal*		*Unknowns*	
	Ratio 1	**Ratio 2**	**Ratio 1**	**Ratio 2**	**Ratio 1**	**Ratio 2**	**Ratio 1**	**Ratio 2**	**Ratio 1**	**Ratio 2**	**Ratio 1**	**Ratio 2**	**Ratio 1**	**Ratio 2**
1	0.05	0.04	0.22	0.11	0.05	0.08	0.10	0.09	1.09	1.30	0.77	0.50	0.01	0.02
3	0.05	0.04	0.17	0.17	0.05	0.03	0.12	0.04	1.18	2.01	0.81	0.43	0.03	0.02
5	0.05	0.04	0.18	0.16	0.05	0.03	0.11	0.04	2.24	1.77	0.77	0.40	0.04	0.03
7	0.08	0.04	0.24	0.17	0.06	0.02	0.14	0.05	0.68	2.05	0.92	0.40	0.06	0.03
25	0.07	0.05	0.12	0.19	0.06	0.06	0.13	0.09	0.93	1.47	1.38	0.67	0.06	0.02
28	0.07	0.04	0.17	0.15	0.06	0.02	0.09	0.05	0.25	1.69	1.03	0.44	1.12	0.03

Table 6.2: Selectivity to the by-products formed during the hydrogenation of octanal at 160 °C and hydrogen/aldehyde ratios of one and two

Time-on-Stream/h	Selectivity to by-products/%													
	Alkanes		*Other Alcohols*		*Ethers*		*Octyl octanoate*		*C16 diol*		*C24 acetal*		*Unknowns*	
	Ratio 1	**Ratio 2**	**Ratio 1**	**Ratio 2**	**Ratio 1**	**Ratio 2**	**Ratio 1**	**Ratio 2**	**Ratio 1**	**Ratio 2**	**Ratio 1**	**Ratio 2**	**Ratio 1**	**Ratio 2**
1	0.04	0.08	0.23	0.26	0.99	0.05	0.25	0.18	0.89	2.29	0.58	0.32	0.06	0.04
3	0.08	0.08	0.23	0.23	0.11	0.10	0.00	0.13	0.00	2.01	0.00	0.32	0.55	0.07
5	0.07	0.08	0.21	0.27	0.08	0.03	0.20	0.16	1.46	2.11	0.46	0.39	0.05	0.07
7	0.04	0.08	0.17	0.26	0.12	0.02	0.20	0.12	2.03	1.68	0.89	0.39	0.06	0.57
25	0.07	0.08	0.19	0.29	0.06	0.05	0.17	0.16	1.78	2.10	0.26	0.65	0.03	0.04
28	0.06	0.08	0.26	0.30	0.04	0.05	0.19	0.15	2.18	1.89	0.30	0.66	0.03	0.05

6.2.1. Effect of water on the hydrogenation of octanal using CuO/Al_2O_3

Figure 6.6 shows the conversion of octanal and the selectivity to octanol when the reaction was carried out using the fresh feed and the water-spiked feed. The initial 30 hours on stream corresponds to the reaction using the fresh feed where steady state conditions were achieved and maintained. The conversion reached steady state after 1 hour on stream at a value of 99 % and remained steady at this value for 30 hours. After this time, the water-spiked feed was introduced into the system and the reaction was allowed to proceed for a further 74 hours. During this time, the conversion remained unchanged (99 %), indicating that the presence of water in the feed did not influence the activity of the catalyst. The selectivity to octanol reaches a value of approximately 96.9 % during the first 30 hours of the reaction. However, once the water-spiked feed was introduced into the system, the selectivity increases to around 98.4 % and remains at this value for the duration of the reaction.

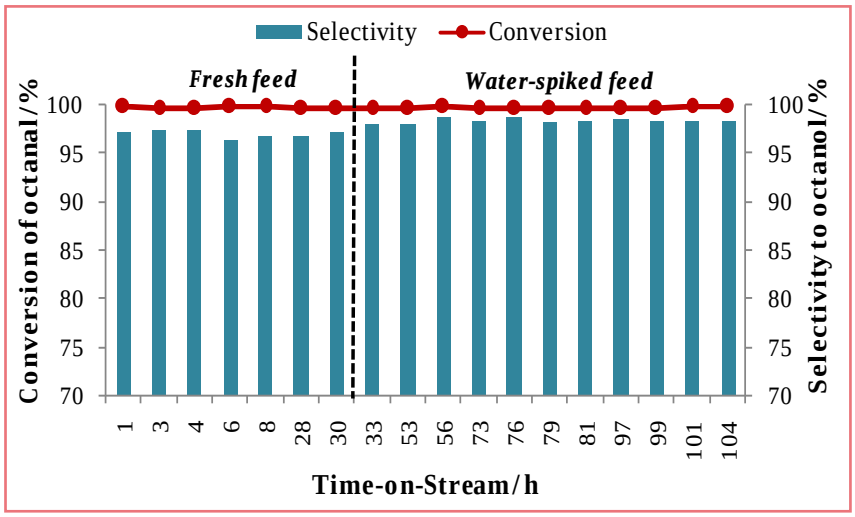

Figure 6.6: Conversion of octanal and the selectivity to octanol for the hydrogenation of octanal using the fresh feed and the water-spiked feed

With the increase in the selectivity to octanol, there is a decrease in the selectivity to certain by-products. The by-products formed during the reaction are as listed in Figure 6.7 and their formation has been discussed in Section 6.1.3.1. The selectivity to these by-products, formed during the reaction with the fresh feed and the water-spiked feed, is shown in Figure 6.7. The C16 diol is the major by-product formed during the reaction with a selectivity of approximately 2 %. However, upon the introduction of the water-

spiked feed, the selectivity decreases to around 1 %. Similarly, all other by-products, except the other alcohols, show a drop in selectivity when the water-spiked feed is used. The selectivity to alkanes, ethers and octyl octanoate drops to less than 0.06 %, whilst the selectivity to the C24 acetal and the unknowns reaches 0.14 % in the presence of the water-spiked feed. These selectivity trends indicate that the presence of water in the reactant stream can suppress the by-product formation and improve the selectivity to the octanol. Similar results were obtained by *Wang et al.*[4, 5] in their study on the hydrogenation of hexanal and propanal using sulphided Ni-Mo/Al_2O_3 as catalysts. Since the conversion of octanal remains unchanged and the selectivity to octanol is improved, after the introduction of the water-spiked feed, it indicates that the presence of water is beneficial to the hydrogenation of octanal.

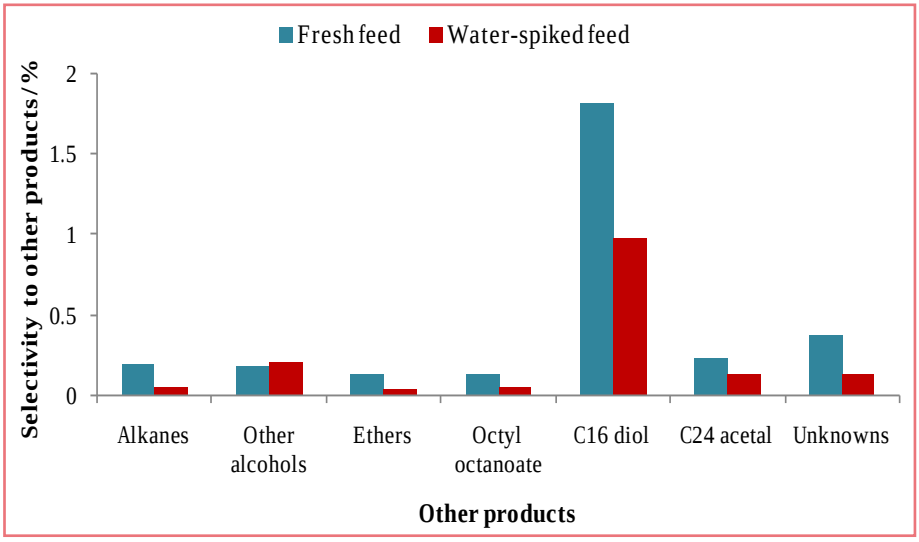

Figure 6.7: Selectivity to the various by-products formed during the hydrogenation of octanal using the fresh feed and the water-spiked feed

The reasoning that governs the observed selectivity trends in the presence of water can be explained by the presence of the alumina support. Alumina contains surface hydroxyls[6-11] and it is these groups that create weak acid and base sites. These acid-base sites are mainly responsible for the formation of heavies (as discussed in Section 6.1.3.1). Upon the introduction of the water-spiked feed, the water molecules can interact with the surface hydroxyls *via* hydrogen bonding (as illustrated in Figure 6.8) and possibly passivate them. Thus, the acid and base sites are no longer available to participate in the

formation of by-products and this accounts for the decrease in the selectivity to the by-products.[4]

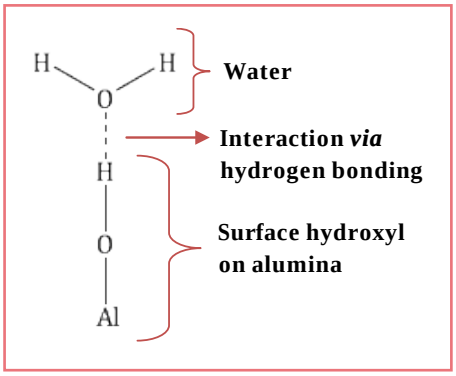

Figure 6.8: An illustration of the interaction between a water molecule and the surface hydroxyl on alumina (Adapted from *Thomas*[11])

The high conversion of octanal and selectivity to octanol obtained when using the fresh feed and the water-spiked feed indicate that this catalyst can be a suitable replacement for the industrially used copper chromite catalyst. This is primarily due to the environmentally unfriendly nature of the copper chromite catalyst, causing more restrictions being placed to reduce environmental pollution by the harmful chromium (VI) by-products formed when synthesizing and using this catalyst.[12, 13] *Pillai et al.*[12] state that patent literature suggests that aluminum-containing catalysts could be a promising alternative to the chromite catalysts and the above results agree with this suggestion.

6.2.2. Effect of water on the hydrogenation of octanal using CuO/Cr_2O_3

The conversion of octanal and the selectivity to octanol during the hydrogenation of octanal using fresh feed and water-spiked feed is shown in Figure 6.9. The conversion initially decreases from 89 % to 86 % and then increases to 99 % at 5 hours and remains steady at this value for 26 hours. The initial low conversion possibly suggests that the catalyst was not fully reduced prior to the start of the reaction. Hence, when the reaction was underway, some of the hydrogen present was initially used for further reduction of the CuO in the catalyst.

Upon introduction of the water-spiked feed, the conversion initially decreases to 94 % and thereafter reaches 99 % and remains at this value for the remaining period of the reaction. It is possible that the water oxidizes some of the Cu^0 present and this causes the drop in conversion. However, as the reaction proceeds, the reaction conditions cause the reduction of these re-oxidized species and do not allow for any further changes to occur. The selectivity to octanol reaches approximately 96.3 % during the first 31 hours of the reaction when using the fresh feed, whilst after introducing the water-spiked feed, only a minor increase in selectivity was observed (0.5 %).

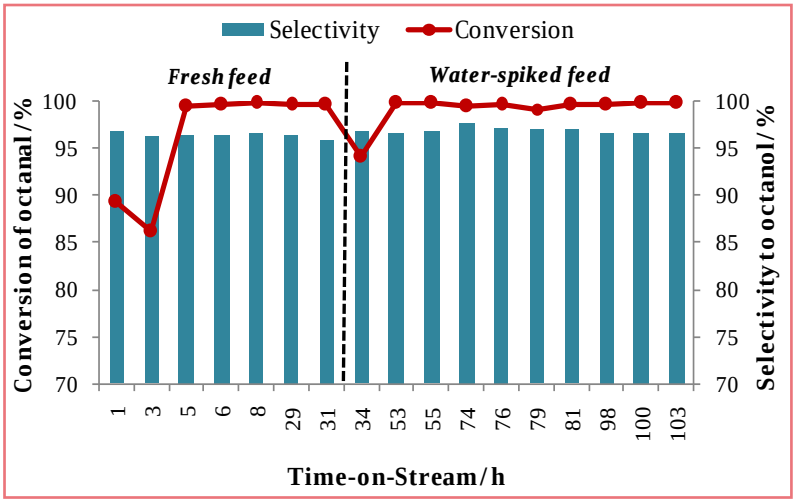

Figure 6.9: Conversion of octanal and selectivity to octanol for the hydrogenation of octanal using fresh feed and water-spiked feed

A similar conversion (99 %) was obtained for this reaction when using CuO/Al_2O_3 as the catalyst (Section 6.2.1). From the TPR data obtained from the fresh catalyst characterization, it was determined that CuO/Al_2O_3 and CuO/Cr_2O_3 had similar degree of reducibility of 84 and 86 %, respectively. This accounts for the similar activity of these catalysts during the hydrogenation reaction. In addition, the BET surface area for CuO/Cr_2O_3 is low (25.3 $m^2\ g^{-1}$) compared to the much higher surface area for CuO/Al_2O_3 (128.8 $m^2\ g^{-1}$) indicating that the surface area of the catalyst does not influence their activity to a great extent under these operating conditions.

The reaction network in the hydrogenation of octanal when CuO/Cr_2O_3 is used as the catalyst is the same as that obtained when using CuO/Al_2O_3 as the catalyst. The by-products formed in this reaction are as listed in Figure 6.10. The selectivity to these by-

products formed during the reaction with the fresh feed and the water-spiked feed, is shown in Figure 6.10. The major by-product formed during the reaction with the fresh feed and the water-spiked feed is the C16 diol. The selectivity to the C16 diol when using the fresh feed is around 2.2 %, whilst a selectivity of 2 % is reached when the reaction is carried out with the water-spiked feed. Similarly, all other by-products showed a minor change in the selectivity after introducing the water-spiked feed into the system.

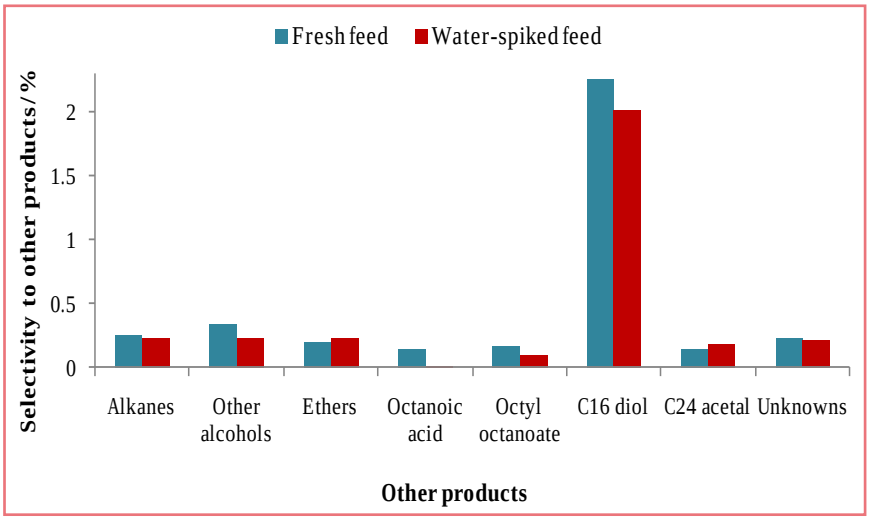

Figure 6.10: Selectivity to the various by-products formed during the hydrogenation of octanal using the fresh feed and the water-spiked feed

In Section 6.2.1, it was suggested that the presence of water in the feed stream can improve the selectivity to octanol by suppressing the formation of by-products (using CuO/Al_2O_3 as the catalyst). However, a key factor favoring this trend is believed to be the presence of surface hydroxyls on the catalyst support. Since a minor increase in the selectivity to octanol was obtained when using CuO/Cr_2O_3 as the catalyst, the effect of water on the hydrogenation of octanal is not as pronounced as when CuO/Al_2O_3 is used as the catalyst. It was expected for the trends observed with CuO/Al_2O_3 as the catalyst to be present for the reaction with CuO/Cr_2O_3 as the catalyst, since *Armistead et al.*[6] state that all metal oxides contain varying amounts of surface hydroxyls. Since only a minor change in the selectivity to octanol and the selectivity to the C16 diol and the C24 acetal (by-products mainly formed due to the presence of the support) is obtained, it indicates that this catalyst contains a low concentration of surface hydroxyls. However, since the C16 diol and the C24 acetal form with selectivity values similar to those obtained when using

CuO/Al_2O_3 as the catalyst, it implies that there may be partial passivation of the acid and base sites responsible for their formation. It may also be that these acid and base sites (which usually exist due to surface hydroxyls) may not have functional groups that can interact with the water *via* hydrogen bonding and cause the by-product formation to decrease and thus favor the selectivity to octanol. Since the conversion of octanal and the selectivity to octanol essentially remain unchanged after the introduction of the water-spiked feed, it indicates that the presence of water in the reactant stream does not influence the hydrogenation of octanal for this system.

6.2.3. Effect of water on the hydrogenation of octanal using CuO/SiO_2

The conversion of octanal and the selectivity to octanol for the reaction using fresh feed only are presented in Figure 6.11. The conversion of octanal is initially at 94 % and increases to 95 % after 3 hours. However, after this time, the conversion steadily decreases reaching approximately 22 % after 55 hours on stream. The initial conversion is lower than that achieved for the same reaction using CuO/Al_2O_3 and CuO/Cr_2O_3 and is most likely due to the degree of reducibility being much lower for CuO/SiO_2 (75 %) than for CuO/Al_2O_3 (84 %) and CuO/Cr_2O_3 (86 %). The selectivity to octanol also decreases with time-on-stream to 89 % after 55 hours. Since both conversion and selectivity to octanol decrease with time, it becomes evident, from the definition of catalyst deactivation (Chapter 3), that this catalyst undergoes this phenomenon.

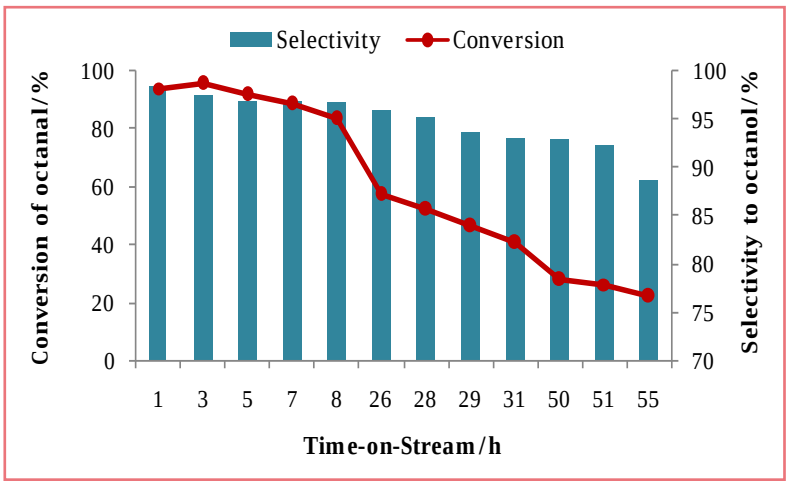

Figure 6.11: Conversion of octanal and selectivity to octanol during the hydrogenation of octanal using fresh feed

Figure 6.12 shows the selectivity to the various by-products formed during the reaction with fresh feed only. The reaction network in the hydrogenation of octanal using CuO/SiO_2 is similar to that obtained with CuO/Al_2O_3 and the by-products formed are as listed in Figure 6.12. The C16 diol is initially the major by-product formed, however, as the reaction progresses the selectivity to dioctyl ether (represented as ethers), C24 acetal and heptane (represented as alkanes) is seen to increase, whilst the selectivity to the C16 diol decreases. The selectivity to the C16 diol reaches approximately 2 % after 8 hours on stream, after which time it steadily decreases to 0 % by the end of the reaction. The selectivity to the C24 acetal is less than 0.1 % at the start of the reaction and it progressively increases to 7.5 % after 55 hours on stream. The selectivities to heptane and dioctyl ether show an overall increase of around 0.2 % by the end of the reaction. The increase in the selectivity to dioctyl ether may due to the increase in the hydrocracking of the C24 acetal, as more of this compound is formed during the course of reaction. It is also possible that the aldol condensation of octanol is favored, thus increasing the selectivity to dioctyl ether. The increase in the selectivity to the C24 acetal and heptane indicates that the conversion of octanal to octanol becomes less preferred as the reaction proceeds. This possibly implies that the required adsorption of octanal on the catalyst to allow for the hydrogenation to octanol becomes less favored during the course of the reaction.

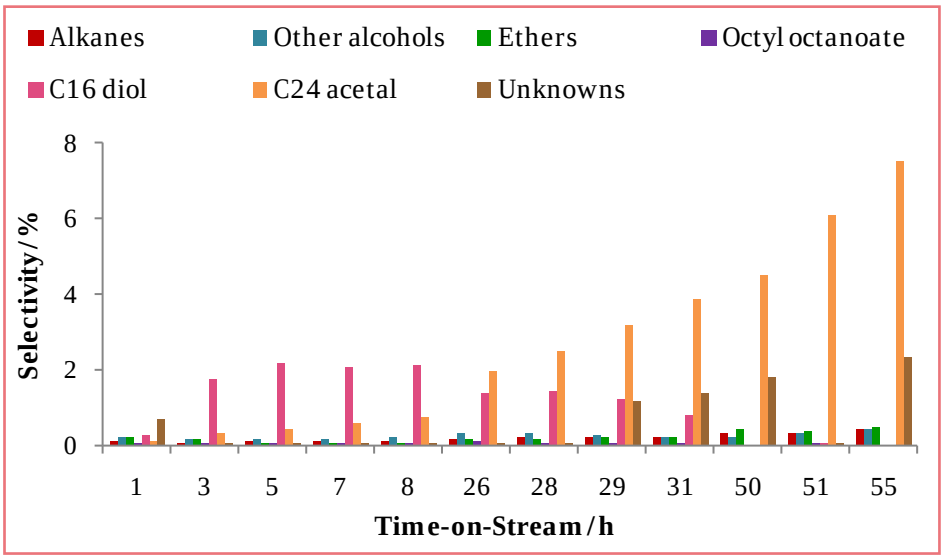

Figure 6.12: Selectivity to the various by-products formed during the hydrogenation of octanal using fresh feed

The trends observed with the conversion of octanal and the selectivity to octanol and the by-products (as discussed above) may be explained based on the surface charge of silica. Due to the nature of silica and its isoelectric point of 2 (the pH at which the surface of the metal oxide is not charged)[14], the adsorption of cations primarily occurs.[14] Since octanal has a positive dipole on the carbonyl carbon and a negative dipole on the carbonyl oxygen, the adsorption *via* the delta positive end will be more likely. The required orientation of octanal on the catalyst surface to promote the conversion of octanal to octanol is *via* the positive and negative ends. Hence, since the adsorption of cations is preferred, it is most likely that the probability of the required orientation of octanal to form octanol decreases as the reaction progresses. Furthermore, as the reaction proceeds, the surface of the silica becomes polarized and charged. As a result, the support no longer enriches the active metal with electrons and the backbonding (discussed in Section 6.1.1) is no longer favored. Since the adsorption of cations is preferred and the catalyst is comprised of acid sites (determined using NH_3-TPD, Section 5.7), the formation of the C24 acetal is promoted since the protonation of octanal yields a cation (Scheme 6.3). The decrease in the selectivity to the C16 diol supports the notion that cation adsorption is preferred since an octanal nucleophile must interact with the octanal electrophile on the catalyst so that aldol condensation of octanal can occur (Scheme 6.2). Due to the nature of the adsorption of octanal and the dipolar nature of octanol, desorption of octanol occurs much slower in comparison to the reactions using CuO/Al_2O_3 and CuO/Cr_2O_3. This allows for longer residence times and therefore the formation of the heavy by-products increases with time-on-stream. Since alumina and chromia have isoelectric points greater than 7 and can adsorb cations and anions[14], the effect of surface charge is not observed and catalyst deactivation does not occur.

Since steady state could not be reached and catalyst deactivation set in, the hydrogenation of octanal was carried out using water-spiked feed over fresh CuO/SiO_2. Figure 6.13 shows the conversion of octanal and the selectivity to octanol obtained during the reaction. The conversion is initially at 84 % and gradually decreases to 73 % after 55 hours on stream. This indicates that the presence of water in the feed does not prevent the catalyst deactivation but slows down the process. The selectivity to octanol reaches approximately 98 % and remains steady at this value for the duration of the reaction.

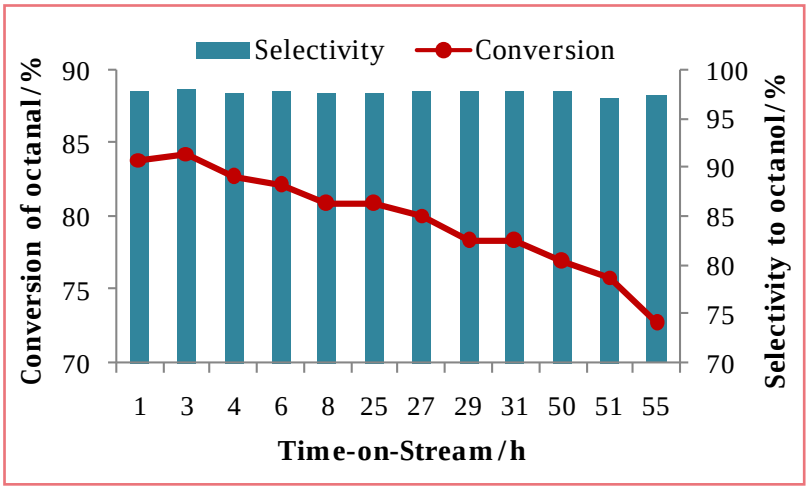

Figure 6.13: Conversion of octanal and the selectivity to octanol during the hydrogenation of octanal using water-spiked feed

The selectivity to the various by-products formed during the hydrogenation of octanal using fresh feed and water-spiked feed is shown in Figure 6.14. In the presence of the water-spiked feed, the C16 diol is the major by-product formed with a selectivity of around 1.3 %. The selectivity to all other by-products, in the presence of water, is less than 0.3 %. These selectivity values are similar to those obtained with CuO/Al_2O_3 and CuO/Cr_2O_3 using fresh feed only. This indicates that in the presence of water the catalyst is able to maintain a selectivity to octanol that is similar to that obtained with the more stable and active catalysts. In comparing these selectivity values with those obtained from the reaction with the fresh feed only (Figure 6.14), it is clearly seen that in the presence of water, the selectivity to all by-products, except the C16 diol, is noticeably reduced. These selectivity trends demonstrate the beneficial effect of water in the reactant stream.

The improved selectivity to octanol obtained in the presence of water can be explained using the argument presented in Section 6.2.1. As with Al_2O_3, silica contains surface hydroxyls[6, 8, 11, 15] (which allow for by-product formation) and the presence of water will passivate or neutralize these hydroxyls. Hence, the selectivity to octanol is improved by preventing by-product formation. Furthermore, the interaction of water with the surface hydroxyl would prevent any changes in the surface charge. This will allow for the adsorption of octanal to occur so that the conversion to octanol is promoted. Since a high

selectivity to octanol is maintained throughout the reaction, it indicates that the surface hydroxyls on silica are most likely responsible for the influence of surface charge and the trends observed during the reaction with the fresh feed. However, since there is still a decline in the conversion of octanal, it indicates that there is a catalyst deactivation mechanism that plays a significant role in the loss of catalytic activity. The decrease in the BET surface area and other changes in the used catalyst indicate that mechanical failure is most likely contributing to the loss of activity over time. The characterization of the used CuO/SiO_2 catalyst is discussed in greater detail in Section 6.3.

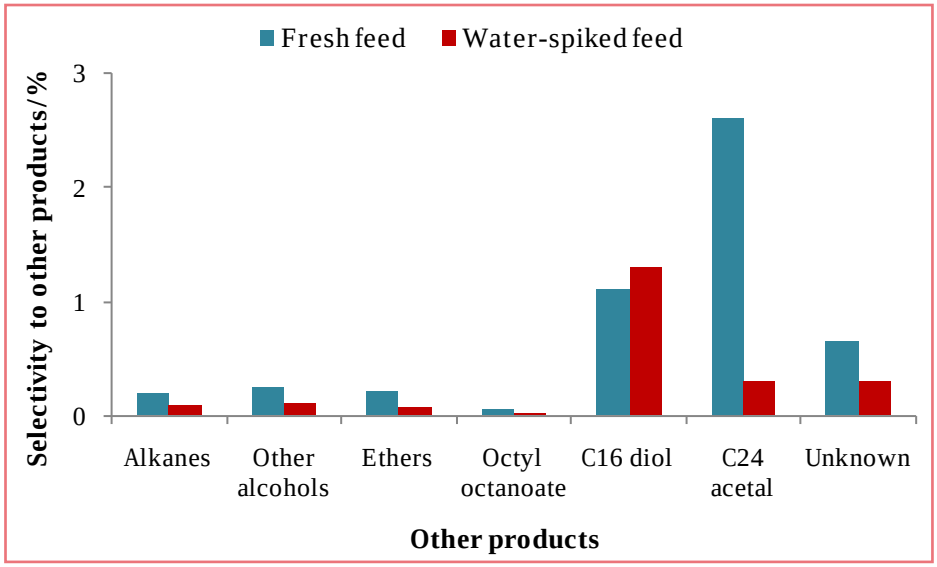

Figure 6.14: Selectivity to the various by-products formed during the hydrogenation of octanal using fresh feed and water-spiked feed

6.3. Used catalyst characterization

In order to establish the effect of the water on the catalyst, used catalyst characterization was necessary. The catalysts were characterized after the reactions with fresh feed only and the water-spiked feed. The characterization techniques used were XRD, SEM, EDS composition scanning, TEM, BET surface area and pore volume, TGA-DSC and IR. The information obtained from these techniques for each catalyst will be discussed and compared. Since these catalysts were characterized after the reaction, they mostly contained copper as Cu^0 and will no longer be referred to as supported CuO, but as supported Cu.

6.3.1. X-Ray Diffraction (XRD)

The diffractograms for the Cu/Al_2O_3, Cu/Cr_2O_3 and Cu/SiO_2 after the reaction with fresh feed and water-spiked feed are shown in Figures A 5 – 7 (Appendix A). These diffractograms show the presence of characteristic copper (Cu^0) peaks (JCPDS 4-0836) and some CuO peaks. In addition, the diffractogram for Cu/Cr_2O_3 (Figure A 6) reveals the presence of the $CuCr_2O_4$ (JCPDS 5-0657), Cr_2O_3 (JCPDS 6-0504) and Cu_2O (JCPDS 5-0667). These observations are in accordance with the data obtained from the H_2 *in situ* diffractogram.

The full width at half maximum (FWHM) and the XRD crystallite sizes are listed in Table 6.3. Due to the reduction of CuO to Cu^0, which is a smaller molecule, these values are expected to be lower than those of CuO. The FWHM for Cu/Al_2O_3 and Cu/SiO_2 used for the reaction with water-spiked feed are negligibly different to the values obtained for the catalysts used for the reactions with the fresh feed. However, a significant change is observed for the Cu/Cr_2O_3, where an increase of 0.5 ° is seen for the FWHM of the catalyst used for the reaction with water-spiked feed. This indicates that the catalyst suffered a loss of crystallinity during the reaction with the water-spiked feed. It is most likely that this occurrence is a result of the longer time-on-stream for the reaction with the water-spiked feed (104 hours) compared to the reaction with the fresh feed (28 hours). Despite the loss in crystallinity observed for this catalyst, the catalyst maintains a high activity and selectivity to the primary product. The crystallite size for the catalysts used for the reaction with the water-spiked feed is slightly smaller in comparison to the crystallite size of the catalyst used for the reaction with the fresh feed. The crystallite size of the Cu/Cr_2O_3 catalyst is of the smallest and a decrease of 5 nm is seen in the crystallite size of the catalyst used for the reaction with the water-spiked feed. These crystallite size and FWHM trends are most likely a consequence of the preparation method, since similar crystallite sizes and FWHM were obtained for the catalyst synthesized using the wet impregnation method (Cu/Al_2O_3 and Cu/SiO_2).

The catalytic testing using CuO/SiO_2 shows a decline in the conversion of octanal and the selectivity to octanol with time-on-stream (Section 6.2.3) when using fresh feed and a decline in the conversion when using the water-spiked feed. As mentioned in Section 6.2.3, these catalytic results indicate that a deactivation mechanism plays a role. Since the

crystallite size for the Cu/SiO_2 used for these reactions does not show an increase, it indicates that sintering does not play a role in the deactivation of the catalyst. Similarly, since negligible changes are observed in the crystallite size of the other catalysts after the reaction with fresh feed and water-spiked feed, it indicates that the presence of the water does not influence the size of Cu in the catalyst.

Table 6.3: Showing the FWHM values and the crystallite size of the highest intensity Cu peak for each catalyst after the reaction using fresh feed and water-spiked feed

Catalyst	FWHM/°	Crystallite size/nm
Cu/Al_2O_3 fresh feed	0.264	31.7
Cu/Al_2O_3 water-spiked feed	0.258	30.6
Cu/Cr_2O_3 fresh feed	0.799	11.5
Cu/Cr_2O_3 water-spiked feed	1.335	6.5
Cu/SiO_2 fresh feed	0.247	32.1
Cu/SiO_2 water-spiked feed	0.259	30.4

6.3.2. Scanning Electron Microscopy

The SEM images for Cu/Al_2O_3, Cu/Cr_2O_3 and Cu/SiO_2 after the reaction with the fresh feed and the water-spiked feed are shown in Figures A 8 and 9 (Appendix A) and Figure 6.15, respectively. These images show that the surface morphology of the used catalyst changed in comparison to the fresh catalyst (Figures 5.2, 5.5 and 5.8). In addition, minor differences are observed between the SEM image of the Cu/Al_2O_3 and Cu/Cr_2O_3 used for the reaction with the fresh feed and the water-spiked feed (Figure A 8 and 9 respectively). The SEM image of Cu/SiO_2 used for the reaction with the fresh feed (Figure 6.15 (a)) shows the presence of smaller particles, whilst the image of the catalyst used with the water-spiked feed (Figure 6.15 (b)) showed fewer small sized particles. This indicates that the Cu/SiO_2 used for the reaction with the fresh feed experienced mechanical failure causing the catalyst particles to break-up. Furthermore, since small sized particles are seen in the SEM image for Cu/SiO_2 used for the reaction with the water-spiked feed, it shows that mechanical failure persists in this reaction as well.

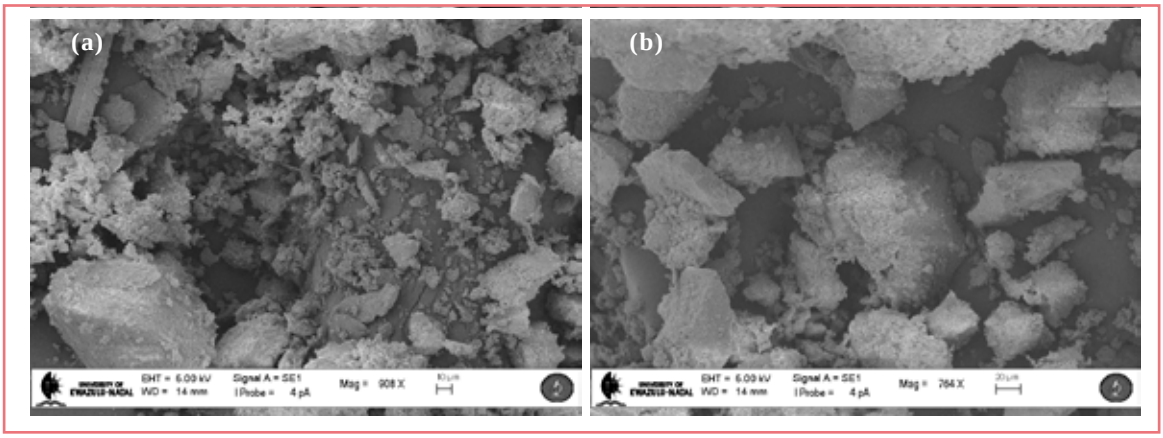

Figure 6.15: SEM image of Cu/SiO_2 after (a) the reaction with fresh feed and (b) reaction with the water-spiked feed

The EDS composition scanning map data for Cu/Al_2O_3, Cu/Cr_2O_3 and Cu/SiO_2 after the reaction with the fresh feed and the water-spiked feed are shown in Figures A 10 – 15 (Appendix A) respectively. These maps show that the distribution of the Cu-rich particles relative to the metal in the support is the same as for the fresh catalysts. This indicates that there was no migration of the active metal species during the course of the reaction and in the presence of water.

6.3.3. Transmission Electron Microscopy

The TEM images for Cu/Al_2O_3, Cu/Cr_2O_3 and Cu/SiO_2 after the reaction with the fresh feed and the water-spiked feed are shown in Figures A 16 – 18 (Appendix A) respectively. These images show that the particle shapes of the used catalysts are the same as those for the fresh catalysts. In addition, no differences are observed between the catalyst used for the reaction with the fresh feed and the catalyst used for the reaction with the water-spiked feed. This indicates that the reaction conditions, as well as the presence of water, do not impact the shape of the catalyst particles. The TEM particle sizes of each catalyst used for the various reactions are listed in Table A 1 (Appendix A). These values show that the particle sizes for the catalysts used in the reaction with the water-spiked feed are slightly lower than those for the catalysts used for the reaction with the fresh feed. Similar trends were observed with the XRD crystallite size. The smaller particle and crystallite size is most likely a consequence of the longer time-on-stream for the reaction

using the water-spiked feed. The changes observed in the particle size of the used catalysts from the fresh catalysts are mainly due to the reduction of the CuO to Cu^0, thus, the presence of water does not influence the catalyst shape and size.

6.3.4. Brunauer-Emmet-Teller (BET) Analysis

The BET surface area and the total pore volume measurements are listed in Table 6.4. The BET surface area for Cu/Al_2O_3 and Cu/Cr_2O_3 shows an increase in comparison to the value obtained for the fresh catalyst. This is primarily due to the decrease in the particle size of the used catalyst (discussed in Sections 6.3.1 and 6.3.3). In addition, a slightly higher surface area was obtained for these catalysts used for the reaction with the water-spiked feed due to the smaller particle sizes present in this catalyst. The total pore volumes of Cu/Al_2O_3 and Cu/Cr_2O_3 after the reaction with fresh feed and water-spiked feed are negligibly different to those obtained for the fresh catalyst. This indicates that pore plugging does not occur; hence fouling (deactivation mechanism discussed in Section 3.2) does not take place.

In contrast to the BET surface areas obtained for the two former mentioned catalysts, a decrease in the surface area is observed for Cu/SiO_2 used for the reaction with the fresh feed and the water-spiked feed. A surface area of 88 $m^2\ g^{-1}$ was obtained for the catalyst used in the reaction with the fresh feed (*versus* 99.4 $m^2\ g^{-1}$ for the fresh catalyst), whilst a surface area of 94 $m^2\ g^{-1}$ was obtained for the catalyst used in the reaction with the water-spiked feed. This decrease in surface area confirms that mechanical failure is the cause of the catalyst deactivation observed for the reaction with the fresh feed and water-spiked feed (Section 6.2.3). Since the deactivation was more rapid in the reaction with the fresh feed (conversion of 22 % and a selectivity to octanol of 89 % after 55 hours on stream) than in the reaction with the water-spiked feed (conversion of 73 % and a selectivity to octanol of 98 % after 55 hours on stream), the surface area is much lower for the catalyst used in the reaction with the fresh feed. In Chapter 3, it was deduced that a decrease in BET surface area can also indicate that leaching plays a role in catalyst deactivation. However, the ICP results (Table A 2, Appendix A) show that the amount of Cu in the used catalyst is the same as in the fresh catalyst. Thus, leaching does not influence the deactivation of Cu/SiO_2.

A slight decrease (0.1 cm^3 g^{-1}) in the total pore volume in the used catalysts (for both feeds) in comparison to the fresh catalyst indicates that there is some pore blockage occurring during the reaction with Cu/SiO_2 as the catalyst. Thus, it is possible that fouling may contribute to the deactivation of Cu/SiO_2 to a slight extent.

Table 6.4: A list of the BET surface areas and total pore volumes for each catalyst

Catalyst	BET surface area/m^2 g^{-1}	Total pore volume/cm^3 g^{-1}
Cu/Al_2O_3 fresh feed	141.7	0.39
Cu/Al_2O_3 water-spiked feed	143.9	0.42
Cu/Cr_2O_3 fresh feed	33.5	0.32
Cu/Cr_2O_3 water-spiked feed	36.0	0.26
Cu/SiO_2 fresh feed	88.4	0.34
Cu/SiO_2 water-spiked feed	94.3	0.36

6.3.5. Thermogravimetric Analysis-Differential Scanning Calorimetry (TGA-DSC)

The TGA-DSC curves for Cu/Al_2O_3, Cu/Cr_2O_3 and Cu/SiO_2 after the reaction with the fresh feed and the water-spiked feed are shown in Figures A 19 – 21 (Appendix A), respectively. The catalysts were analyzed under nitrogen and static air environments. The weight loss observed under a nitrogen environment is due to the loss of volatile organic species from the surface of the catalyst, whilst the weight loss observed under a static air environment is due to the loss of combustible organics or carbon deposits.[16, 17] The weight losses observed for each catalyst under the two environments are listed in Table 6.6.

The weight loss observed from room temperature (RT) to 200 °C is due to the loss of water adsorbed on the surface of the catalyst.[18] For Cu/Al_2O_3 and Cu/Cr_2O_3, the weight loss in this region is greater for the catalysts used for the reactions with the water-spiked feed than for the reactions with the fresh feed. This indicates that water remains on the surface of the catalyst after the reaction with the water-spiked feed. Despite this, the presence of the water does not negatively influence the activity of the catalyst and its

ability to direct the selectivity to octanol (Section 6.2). There is no difference between the weight loss seen in this region for Cu/SiO_2 used for the reaction with the fresh and water-spiked feed. Although the TGA weight loss for this catalyst does not show any indication of water remaining on the catalyst, beneficial effects were found when the reaction was carried out using the water-spiked feed. The weight % lost follows the same trend as for the fresh catalysts and increases in the order $CuO/SiO_2 < CuO/Cr_2O_3 < CuO/Al_2O_3$.

The second weight loss observed between 200 – 1000 °C is due to the loss of organic species remaining on the catalyst. The amount of combustible organics lost (determined under a static air atmosphere) is less than the amount of volatile organics lost (determined under a N_2 atmosphere), indicating that only some of the organic species present can be oxidized. Furthermore, since organic species were removed under both analysis atmospheres, it shows that a variety of organics with different properties remain on the catalyst after the reaction. The loss of volatile organics and the loss of combustible organics from the catalyst was seen to increase in the order $Cu/SiO_2 < Cu/Cr_2O_3 < Cu/Al_2O_3$. Although Cu/Cr_2O_3 and Cu/Al_2O_3 showed high weight losses (greater than 9 % under N_2 and greater than 4 % under static air), these catalysts did not show any change in total pore volume (Section 6.3.4), as well as no indication of catalyst deactivation during the reactions (Section 6.2). However, Cu/SiO_2 displayed the lowest weight losses under both N_2 and static air, also slight changes in the total pore volume were found, as was loss activity during the reactions. This indicates that there is no relationship between the activity of the catalyst and the presence of organics on the catalyst; hence fouling or coking is not a major contributing factor to the decline in catalytic activity.

The TGA curves for Cu/SiO_2 under a static air environment show a weight increase from 350 °C to 500 °C and these indicate the re-oxidation of the reduced Cu present in the catalyst. There is no weight change after 500 °C until 950 °C, where the weight loss is probably due to the loss of species that were removed from the catalyst but were then deposited on the catalyst again. This can occur in the static air environment, since there was no flowing air to carry the removed species out of the instrument. The re-oxidation observed in the TGA curves of Cu/SiO_2 is not seen in the TGA curves of the other two catalysts under static air. This possibly indicates that due to the mechanical failure of Cu/SiO_2, it causes the reduced copper to become more susceptible to re-oxidation.

The DSC curves obtained under a N_2 atmosphere show an endothermic peak during the initial weight loss region and thereafter the heat flow decreases. Under the static air environment, an exothermic peak is seen between 200 – 400 °C and is due to the re-oxidation of the reduced metal in the catalyst. After this exotherm, the heat flow is seen to decrease.

6.3.6. Infra-Red Spectroscopy (IR)

The IR spectra for Cu/Al_2O_3, Cu/Cr_2O_3 and Cu/SiO_2 after the reaction with the fresh feed and the water-spiked feed are shown in Figures A 22 – 24 (Appendix A), respectively. The summary of the wavenumbers obtained from the IR spectrum of each catalyst is listed in Table 6.5. The bands observed around 3400 cm^{-1} are assigned to the hydroxyl group (OH) of an alcohol, whilst bands occurring between 2900 – 2800 cm^{-1} are due to methylene (-CH_2-) groups. The presence of the C–O functional group of an alcohol is known by the band occurring around 1057 cm^{-1}.[19] These bands were observed in the IR spectra of Cu/Al_2O_3 and Cu/Cr_2O_3 used for the reaction with fresh and water-spiked feed. This indicates that primary alcohols most likely remain on the catalyst. The band around 1547 – 1557 cm^{-1} is indicative of the carboxylate group and may be due to unreacted carboxylic acid groups.[20] Of the bands mentioned above, the band indicative of methylene groups is present in the IR spectra of Cu/SiO_2 after the reaction with the fresh feed and the water-spiked feed. This provides little information to determine the type of organic species that remains on this catalyst. The bands below 1000 cm^{-1} are due to the supported catalyst (as determined in Section 5.9).

Table 6.5: A list of the wavenumbers observed in the IR spectrum of each catalyst

Catalyst	Wavenumber/cm^{-1}
Cu/Al_2O_3 fresh feed	3380; 2918; 1563; 1452; 1086; 802; 487
Cu/Al_2O_3 water-spiked feed	3335; 2924; 1557; 1460; 1065; 725; 476
Cu/Cr_2O_3 fresh feed	3411; 2925; 1549; 1409; 908; 776; 552; 452
Cu/Cr_2O_3 water-spiked feed	3401; 2923; 2854; 1547; 1431; 4058; 912; 766; 553; 479
Cu/SiO_2 fresh feed	2927; 1053; 798; 451
Cu/SiO_2 water-spiked feed	2927; 1049; 800; 451

Table 6.6: The weight losses seen for each catalyst in the TGA-DSC curve under N_2 and static air environments

Catalyst	N_2 atmosphere		Static air atmosphere	
	Weight loss 1 (RT – 200 °C)/%	Weight loss 2 (200 – 1000 °C)/%	Weight loss 1(RT – 200 °C)/%	Weight loss 2 (200 – 1000 °C)/%
Cu/Al_2O_3 fresh feed	4.4	11.4	4.7	6.0
Cu/Al_2O_3 water-spiked feed	8.3	13.8	6.4	7.0
Cu/Cr_2O_3 fresh feed	1.7	9.8	1.4	4.5
Cu/Cr_2O_3 water-spiked feed	6.5	9.3	6.3	5.7
Cu/SiO_2 fresh feed	2.1	5.5	2.2	2.6
Cu/SiO_2 water-spiked feed	2.1	5.1	1.9	1.6

6.4. A Brief Summary of the Results

The catalytic testing shows that both CuO/Al_2O_3 and CuO/Cr_2O_3 are effective for the hydrogenation of octanal at 160 °C and a hydrogen/aldehdye ratio of 2, whilst CuO/SiO_2 did not maintain its activity during the course of the reactions. The presence of water in the reaction has been shown to be beneficial to the hydrogenation of octanal and does not negatively alter the make-up of the catalyst.

6.4. References

1. P. Gallezot and D. Richard, *Catal. Rev.-Sci. Eng.*, 1998, **40**, 81.
2. K. K. Yeong, A. Gavriilidis, R. Zapf and V. Hessel, *Catal. Today*, 2003, **81**, 641.
3. J. M. Bonello, R. M. Lambert, N. Künzle and A. Baiker, *J. Am. Chem. Soc.*, 2000, **122**, 9864.
4. X. Wang, R. Y. Saleh and U. Ozkan, *J. Catal.*, 2005, **231**, 20.
5. X. Wang, G. Li and U. S. Ozkan, *J. Mol. Catal. A: Chem.*, 2004, **217**, 219.
6. C. G. Armistead, A. J. Tyler, F. H. Hambleton, S. A. Mitchell and J. A. Hockey, *J. Phys. Chem.*, 1969, **73**, 3947.
7. C. Arrouvel, M. Digne, M. Breysse, H. Toulhoat and P. Raybaud, *J. Catal.*, 2004, **222**, 152.
8. C. M. Koretsky, D. A. Sverjensky, J. W. Salisbury and D. M. D'Aria, *Geo. et Cosmochimica Acta*, 1997, **61**, 2193.
9. J.-F. Lambert and M. Che, *J. Mol. Catal. A: Chem.*, 2000, **162**, 5.
10. X. Liu and R. E. Truitt, *J. Am. Chem. Soc.*, 1997, **119**, 9856.
11. J. K. Thomas, *Chem. Rev.*, 1993, **93**, 301.
12. U. Pillai, E. Sahle-Demessie and D. Young, *Appl. Catal. B: Environ.*, 2003, **43**, 131.
13. R. Rao, A. Dandekar, R. T. K. Baker and M. A. Vannice, *J. Catal.*, 1997, **171**, 406.
14. F. Pinna, *Catal. Today*, 1998, **41**, 129.
15. D. R. Kinney, I. Chuang and G. E. Maciel, *J. Am. Chem. Soc.*, 1993, **115**, 6786.
16. E. J. Fernández, J. M. López-de-Luzuriaga, M. Morge, M. Elena, R. C. Puelles, A. Laguna, A. A. Mohamed and J. J. P Fackler, *Inorg. Chem.*, 2008, **47**, 8069.
17. D. J. Moodley, C. v. Schalkwyk, A. Spamer, J. M. Botha and A. K. Datye, *Appl. Catal. A: Gen.*, 2007, **318**, 155.
18. P. H. Matter, D. J. Braden and U. S. Ozkan, *J. Catal.*, 2004, **223**, 340.
19. P. Y. Bruice, *Organic Chemistry*, Fourth edn., Pearson Education International, Upper Saddle River New Jersey, 2004.
20. A. D. Roddick-Lanzilotta, P. A. Connor and A. J. McQuillan, *Langmuir*, 1998, **14**, 6479.

Chapter 7

Summary and Conclusion

Three supported copper oxide catalysts were synthesized for this project. Using the wet impregnation method, copper oxide supported on alumina (CuO/Al_2O_3) and silica (CuO/SiO_2) were prepared, whilst copper oxide supported on chromia (CuO/Cr_2O_3) was synthesized using the method of co-precipitation. The catalysts contained between 23 – 26 wt % of copper. These catalysts were characterized and used for the hydrogenation of octanal in a high pressure fixed bed reactor. However, the primary focus of the project was the influence of water on the reaction and the catalysts.

An initial study using CuO/Al_2O_3 was carried out to investigate the effect of temperature and hydrogen/aldehyde ratio on the steady state, catalytic activity and selectivity to octanol. It was found that the ideal operating conditions for the reaction were 160 °C and a hydrogen to aldehyde ratio of two. At the optimum conditions, a 99 % conversion of octanal was achieved with 97 % selectivity to octanol. The major by-product formed during the reaction was the C16 diol at a selectivity of around 2 %. Other by-products included alkanes, other alcohols, ethers, octyl octanoate and the C24 acetal.

Using the optimum conditions, a water-impact study was carried out using all three catalysts. A water-spiked feed with approximately 1.8 wt % water in the octanal fresh feed was used for the investigation. For the reactions using CuO/Al_2O_3 and CuO/Cr_2O_3 as the catalysts, the water-spiked feed was introduced into the system after steady state conditions were reached using the fresh feed. For the reaction using CuO/Al_2O_3, the conversion remained unchanged (at 99 %) indicating that the presence of water in the feed did not influence the activity of the catalyst. However, an increase in the selectivity to octanol (1.5 %) was observed. The increase in the octanol selectivity was attributed to the interaction of the water molecules with the surface hydroxyls on alumina. These selectivity trends indicated that the presence of water in the reactant stream could suppress the by-product formation and improve the selectivity to the octanol. In addition,

the excellent catalytic results obtained with CuO/Al_2O_3 indicate that this catalyst could be a suitable alternative to the commercially used copper chromite catalyst.

For the reaction using CuO/Cr_2O_3, the conversion of octanal remained unchanged (at 99 %), whilst the selectivity to octanol showed a minor increase of 0.5 % after the introduction of the water-spiked feed. The selectivity trends obtained in the presence of water indicated that the catalyst most probably had of a small quantity of surface hydroxyls. Furthermore, since the selectivity to the C16 diol and the C24 acetal decreased negligibly in the presence of water, it implied that the acid and base sites promoting their production were partially passivated or did not contain functional groups that could interact with water. The unaltered conversion and slight increase in octanol selectivity indicated that the presence of water in the reactant stream did not significantly influence the hydrogenation of octanal. The conversion of octanal obtained when using CuO/Cr_2O_3 is similar to the conversion obtained when using CuO/Al_2O_3 and may be due to the similar degree of reducibility, as shown in the TPR experiments (86 and 84 % respectively). Furthermore, the similar conversions indicate that the surface area of the catalyst does not influence catalytic activity, since the BET surface area for CuO/Cr_2O_3 is low (25.3 $m^2 g^{-1}$) compared to the much higher surface area for CuO/Al_2O_3 (128.8 $m^2 g^{-1}$).

The conversion of octanal and the selectivity to octanol obtained when using CuO/SiO_2 and fresh feed, steadily decreased over time. The conversion of octanal decreased from 95 % to 22 %, whilst the selectivity to octanol decreased to 89 % after 55 hours on stream. This indicated that the catalyst underwent catalyst deactivation. With the drop in octanol selectivity, the selectivity to the C24 acetal gradually increased to 7.5 % by the end of the reaction, whilst the selectivity to other by-products decreased. These selectivity trends may possibly be due to the low isoelectric point of silica, which allows for changes in the surface charge as the reaction proceeds and favors the adsorption of cations. This hydrogenation of octanal over CuO/SiO_2 was then carried out using water-spiked feed, since deactivation set-in and steady state was not reached when using the fresh feed. In the presence of water, the conversion gradually decreased to 73 % after 55 hours on stream, whilst the selectivity remained unchanged at 98 %. Hence, the presence of water in the feed slows down the catalyst deactivation process. Furthermore, in the presence of water the CuO/SiO_2 catalyst is able to maintain a selectivity to octanol that is similar to that obtained with the more stable and active catalysts. The improved

selectivity to octanol in the presence of water, compared to the selectivity drop when using fresh feed only, may be due to the interaction of the water with the surface hydroxyls on silica. It is possible that this interaction will prevent any changes in the surface charge, allowing for the adsorption of octanal to occur so that the conversion to octanol is promoted. The decline in the conversion of octanal when using the fresh feed and water-spiked feed indicated that a deactivation mechanism plays a significant role in the loss of catalytic activity. The decrease in the BET surface area and the presence of smaller particles in the SEM image, confirmed that mechanical failure occurred.

The characterization of used catalysts were carried out using XRD, SEM, EDS composition scanning, TEM, BET surface area and pore volume, TGA-DSC and IR. In comparing the information from the characterization of the catalysts used for the reaction with the water-spiked feed to that obtained for the catalysts used for the reaction with the fresh feed, it was determined that the presence of water did not negatively impact the make-up of the catalyst. Except for changes due to mechanical failure seen for CuO/SiO_2, the changes seen in the used catalysts (*versus* the fresh catalysts) were mainly due to the reduction process.

The catalytic results show that CuO/Al_2O_3 and CuO/Cr_2O_3 were effective for the hydrogenation of octanal at 160 °C and a hydrogen to aldehyde ratio of two using fresh feed and water-spiked feed, whilst CuO/SiO_2 underwent catalyst deactivation under these conditions. In addition, the presence of water in the reactant stream proved to be beneficial to the hydrogenation of octanal.

Appendix A

Additional Figures and Information

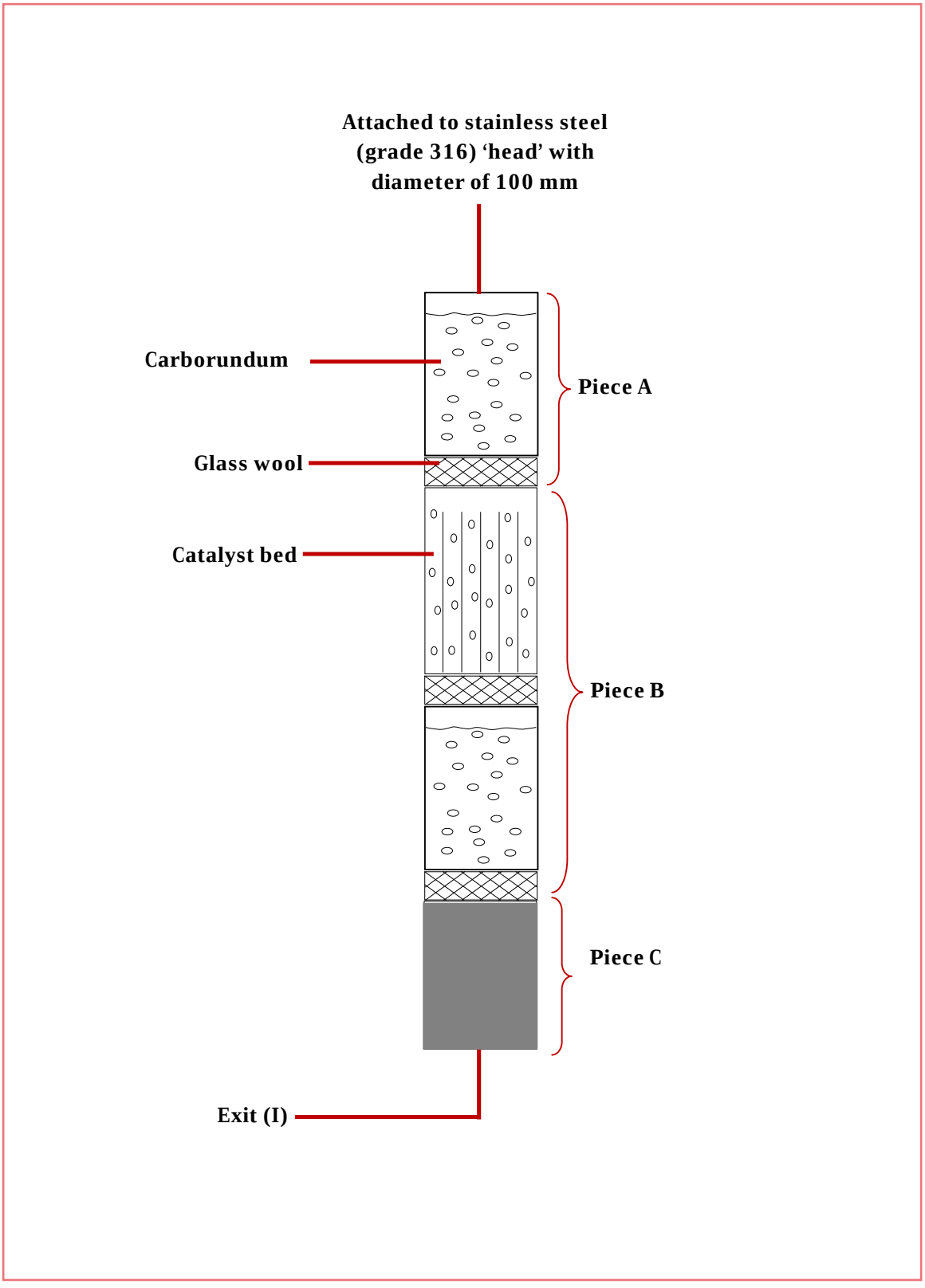

Figure A 1: A simplified diagram showing a packed reactor tube

A 1. Packing of reactor tube

The reactor tube utilized for the reaction was comprised of three pieces (A, B and C). Each piece fitted into the preceding piece of the reactor by being screwed on to it and was protected from leaks by means of copper seals. The length of piece A was 100 mm, piece B was 175 mm and piece C was 50 mm. Glass wool was placed into piece A and the required amount of carborundum was added. This carborundum was kept in place using glass wool. This exact position was measured and noted to allow for temperature profiling during the reaction. Piece B was then screwed onto piece A and the required amount of catalyst diluted with the required amount of carborundum was then added. The position of this catalyst bed was also measured and recorded. Glass wool was placed at the end of the catalyst bed to keep it in position. Carborundum was added until the end of piece B and glass wool was placed at this point. Piece C (a stainless steel block with a 1 mm diameter hole through its centre) was then screwed onto piece B. Each of these pieces was then tightened by means of a water-pump spanner to prevent any leaks.

A 2. Torque process

The reactor was torqued to 100 Nm and left for 1 hour when new copper seals were used. After this time, the torque was increased to 110 Nm and the pressure testing was started. For each new reaction, the torque was increased by 10 Nm from the previous reaction. Once the torque used reached 230 Nm, the copper seals were changed.

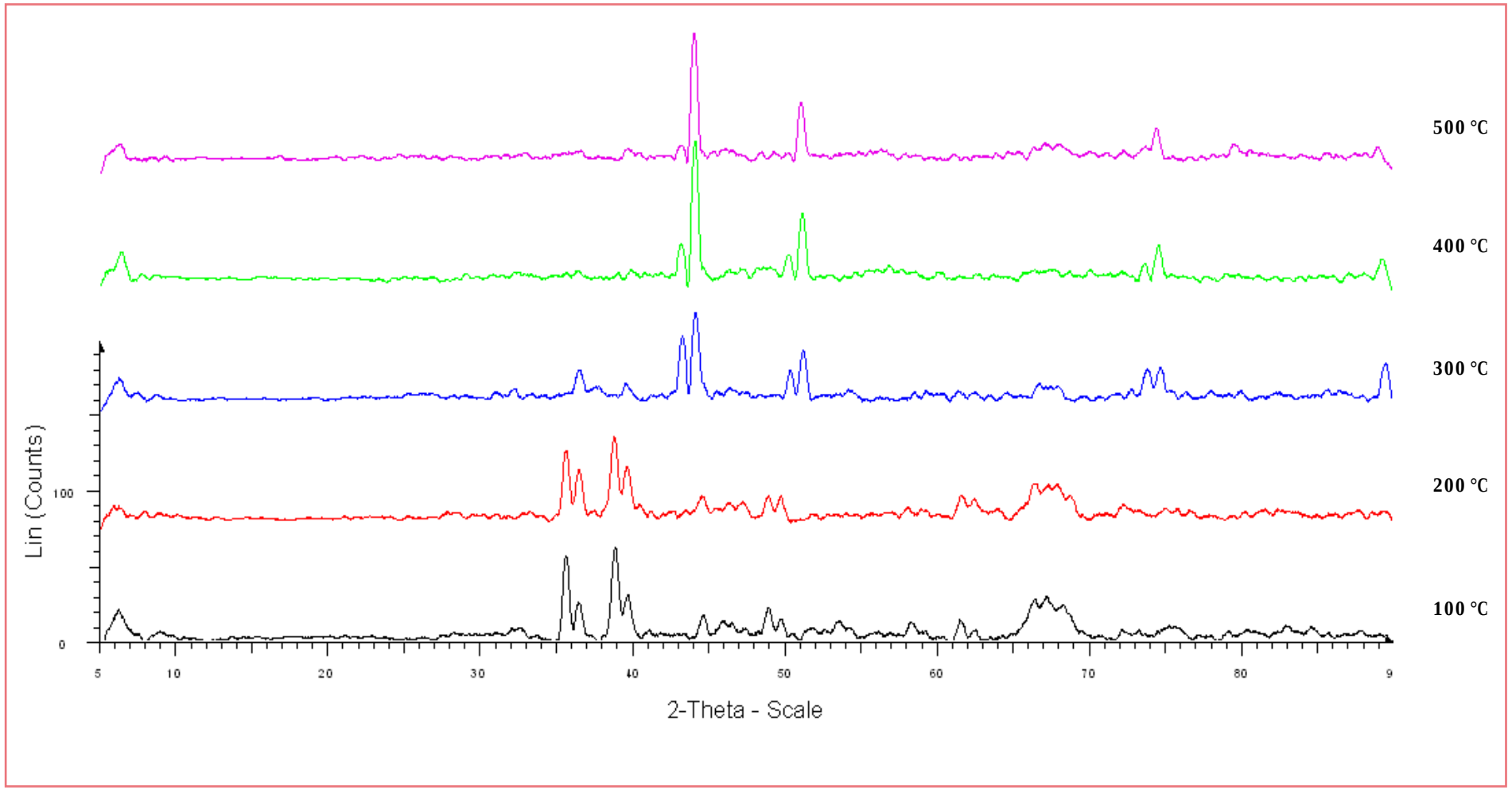

Figure A 2: H_2 *in situ* diffractograms of CuO/Al_2O_3

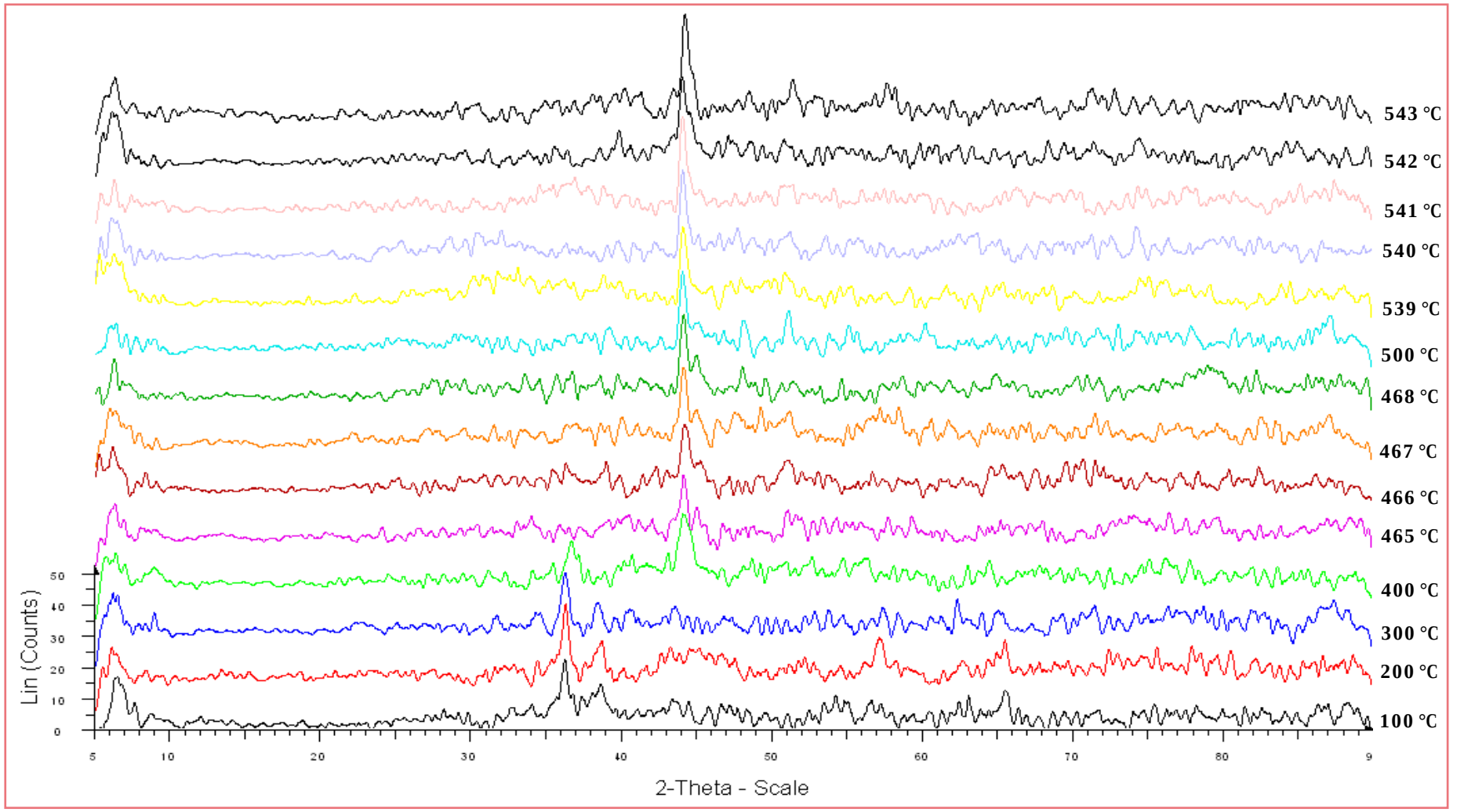

Figure A 3: H_2 *in situ* diffractograms of CuO/Cr_2O_3

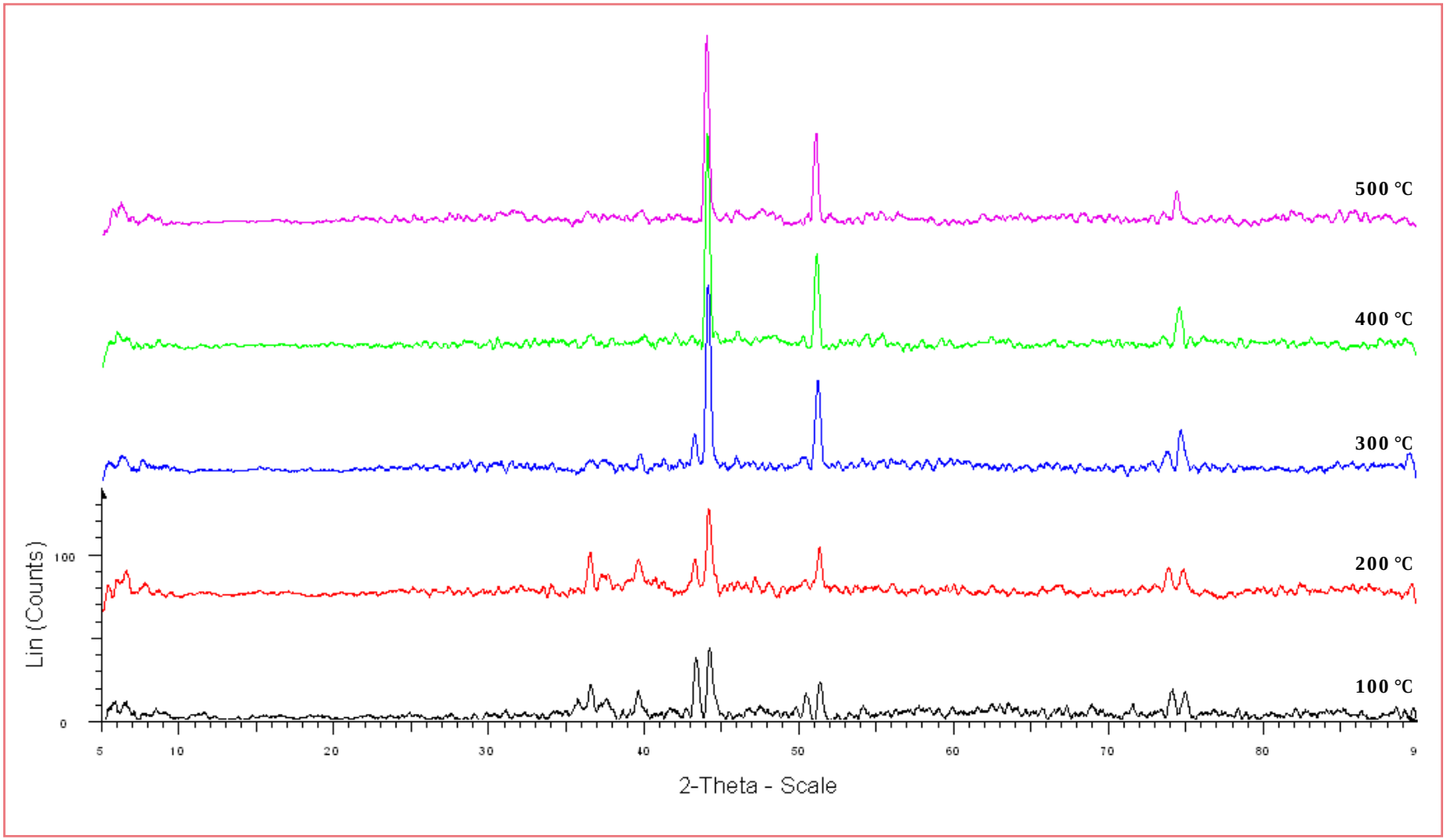

Figure A 4: H_2 *in situ* diffractograms of CuO/SiO_2

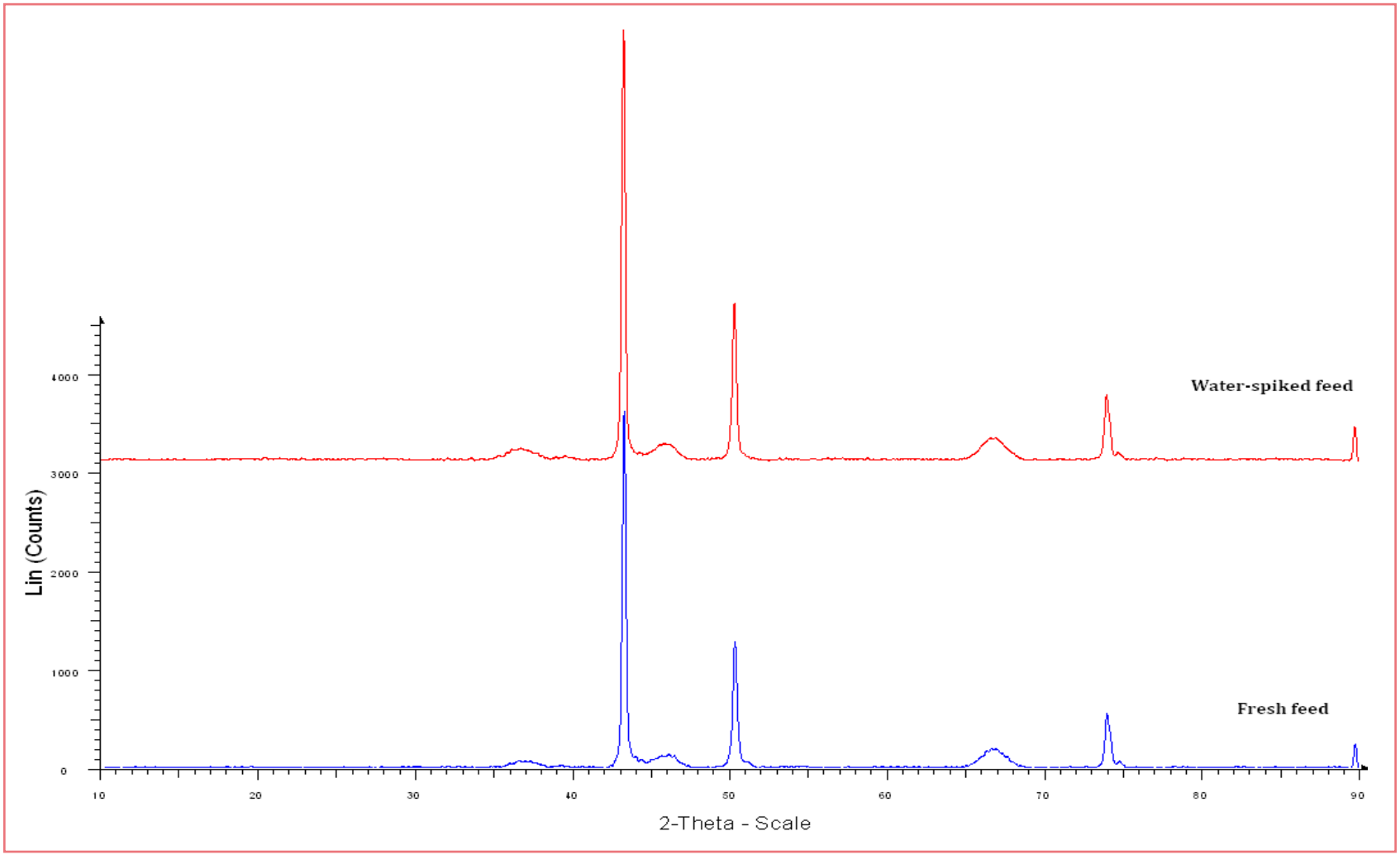

Figure A 5: Diffractograms of used Cu/Al_2O_3 after the reaction with fresh feed only and water-spiked feed

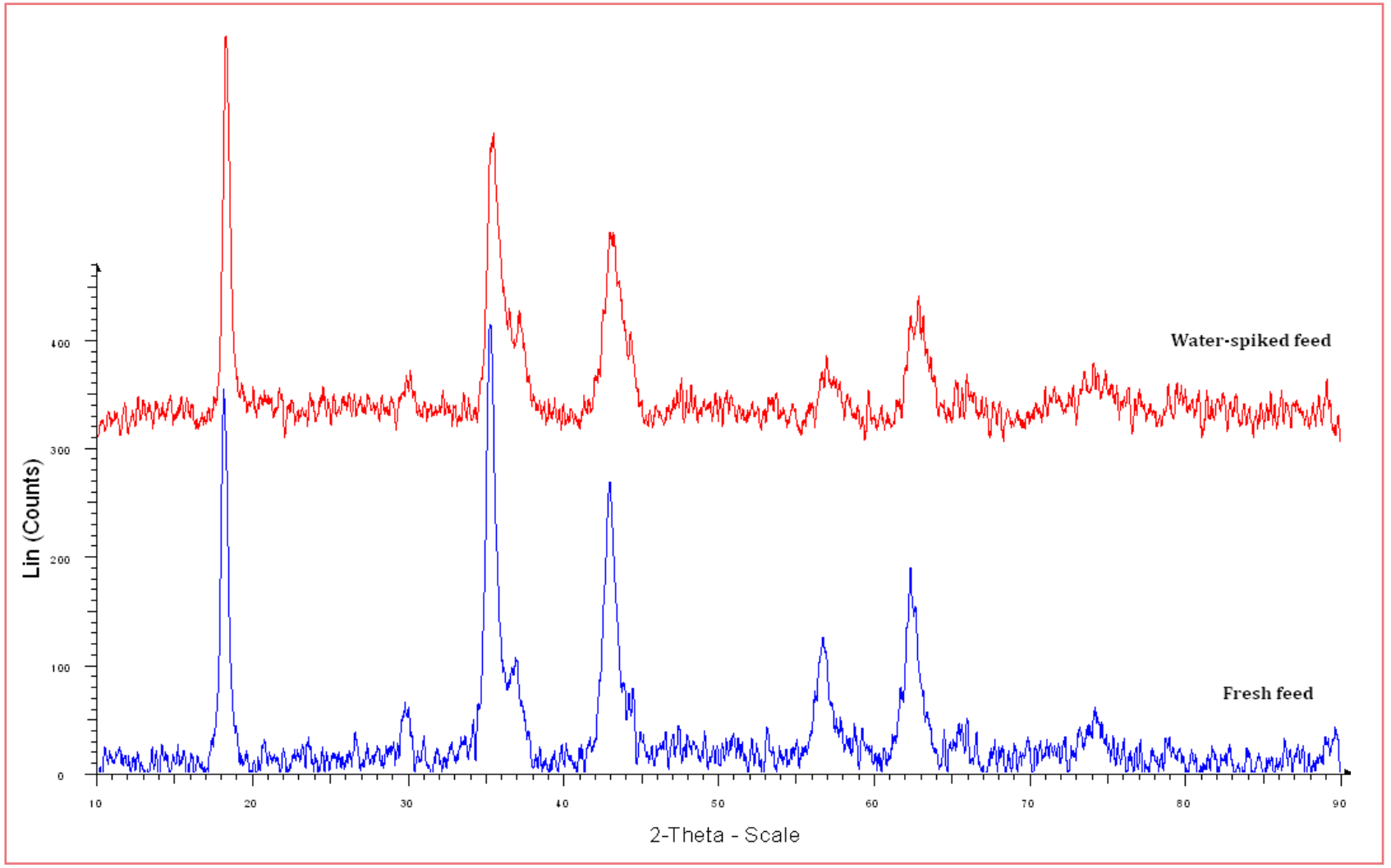

Figure A 6: Diffractograms of used Cu/Cr_2O_3 after the reaction with fresh feed only and water-spiked feed

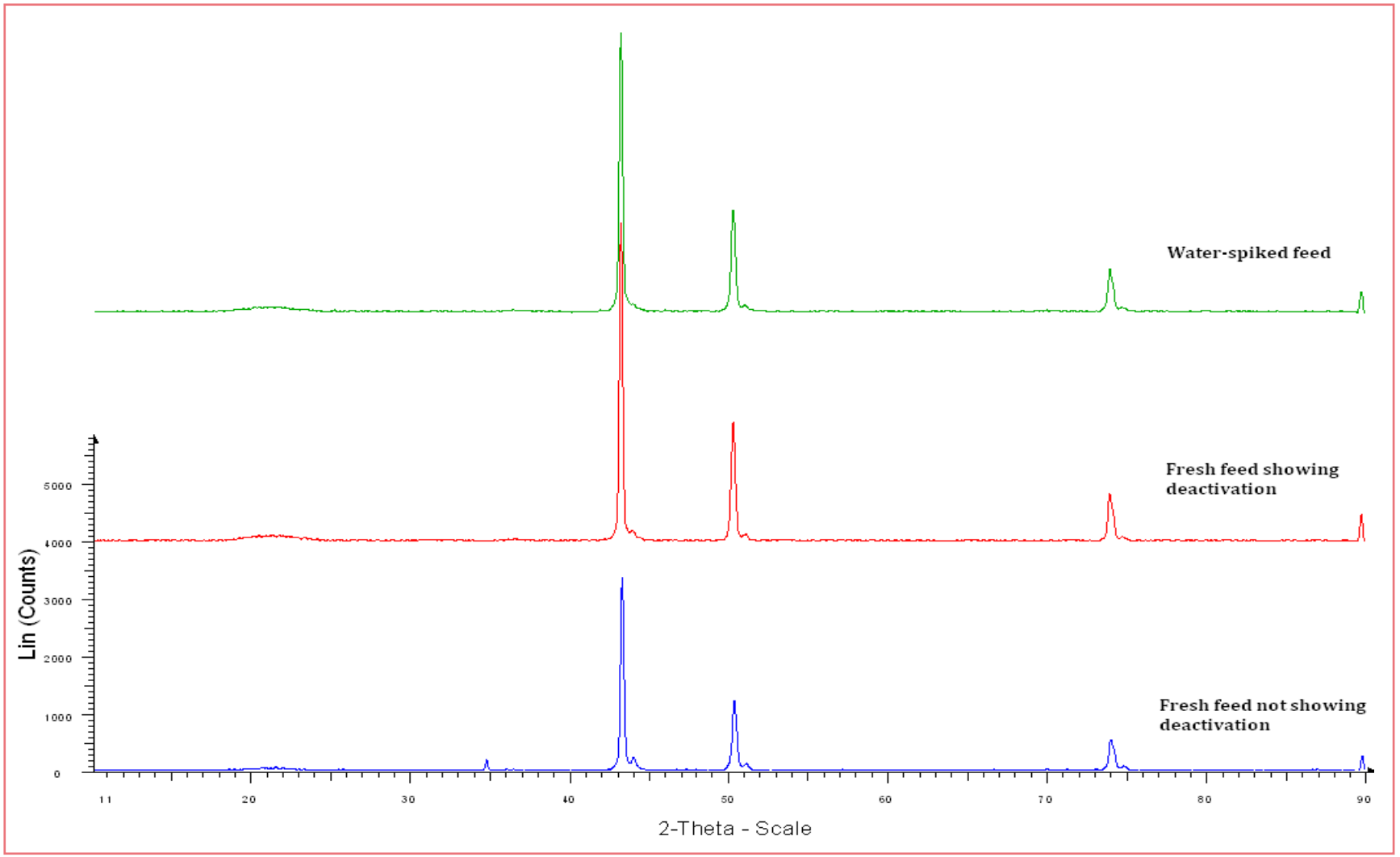

Figure A 7: Diffractograms of used Cu/SiO_2 after the reaction with fresh feed only and water-spiked feed

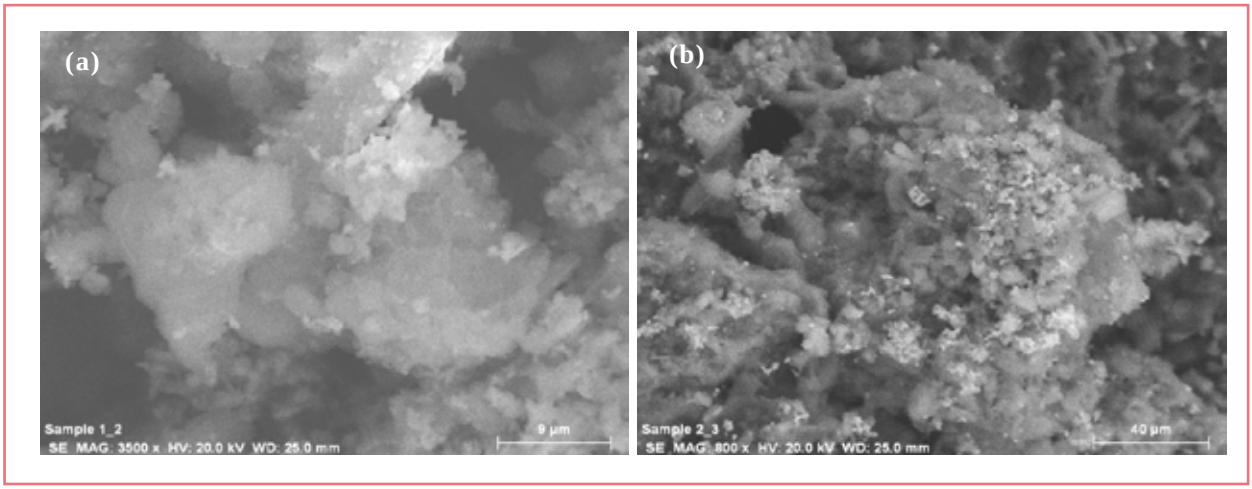

Figure A 8: SEM images of Cu/Al_2O_3 after (a) the reaction with fresh feed and (b) reaction with the water-spiked feed

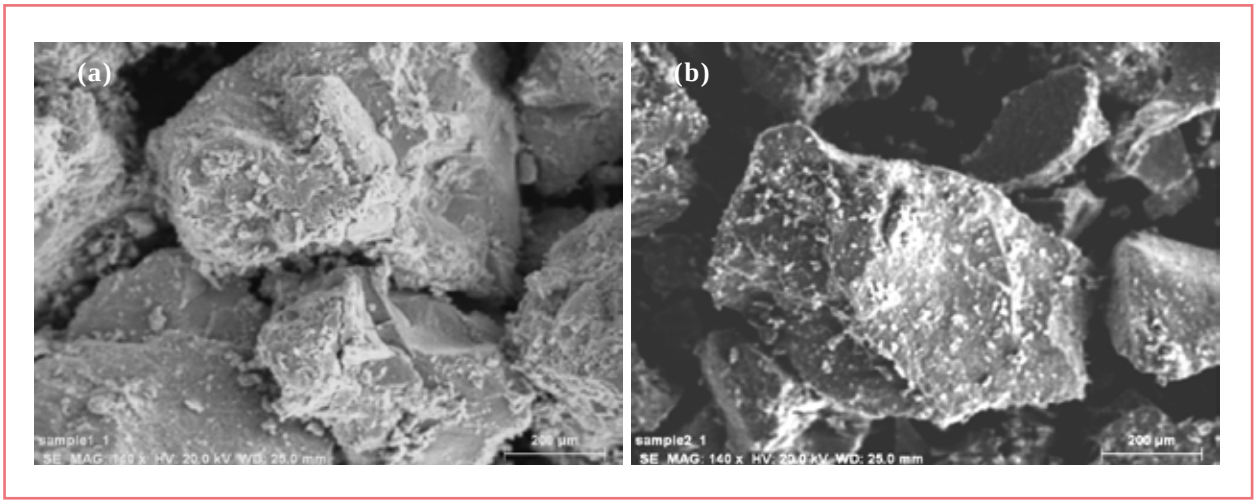

Figure A 9: SEM images of Cu/Cr_2O_3 after (a) the reaction with fresh feed and (b) reaction with the water-spiked feed

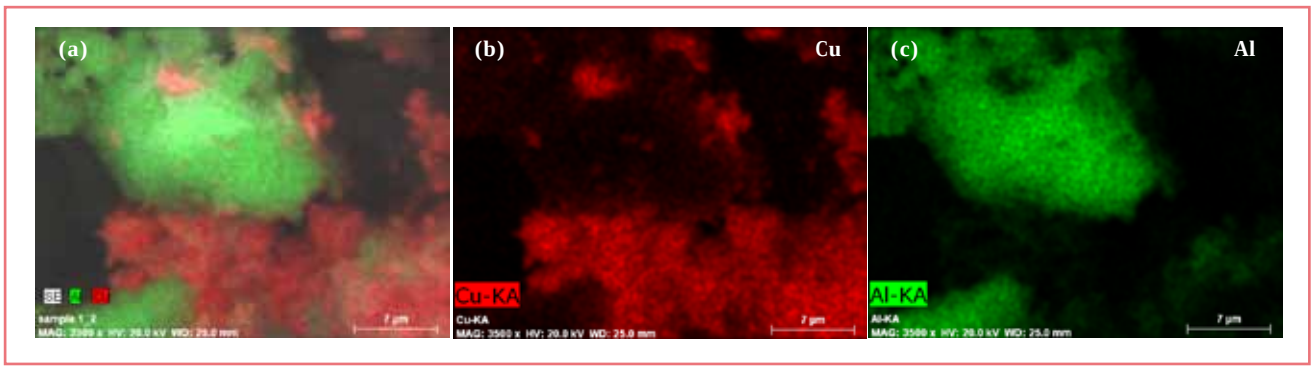

Figure A 10: (a) – (c) EDS composition map data for Cu/Al_2O_3 used for the reaction with fresh feed

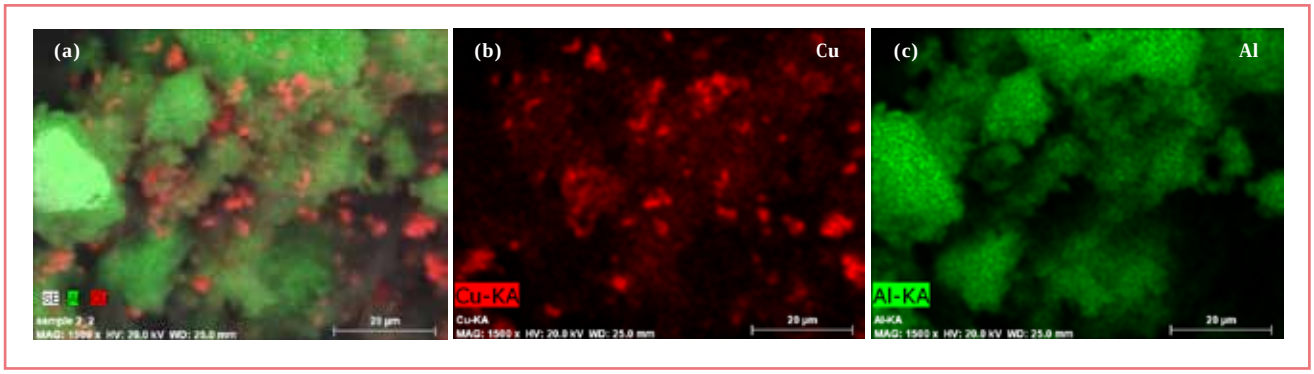

Figure A 11: (a) – (c) EDS composition map data for Cu/Al_2O_3 used for the reaction with water-spiked feed

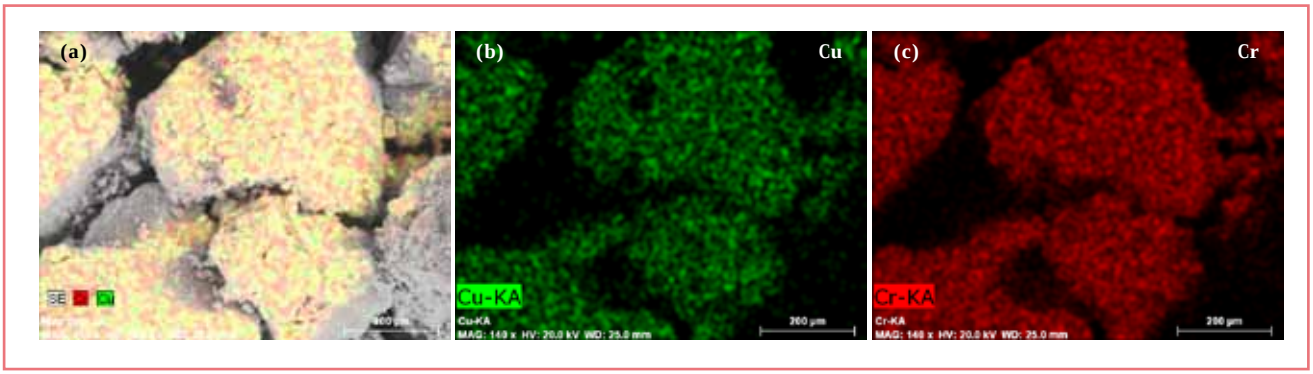

Figure A 12: (a) – (c) EDS composition map data for Cu/Cr_2O_3 used for the reaction with fresh feed

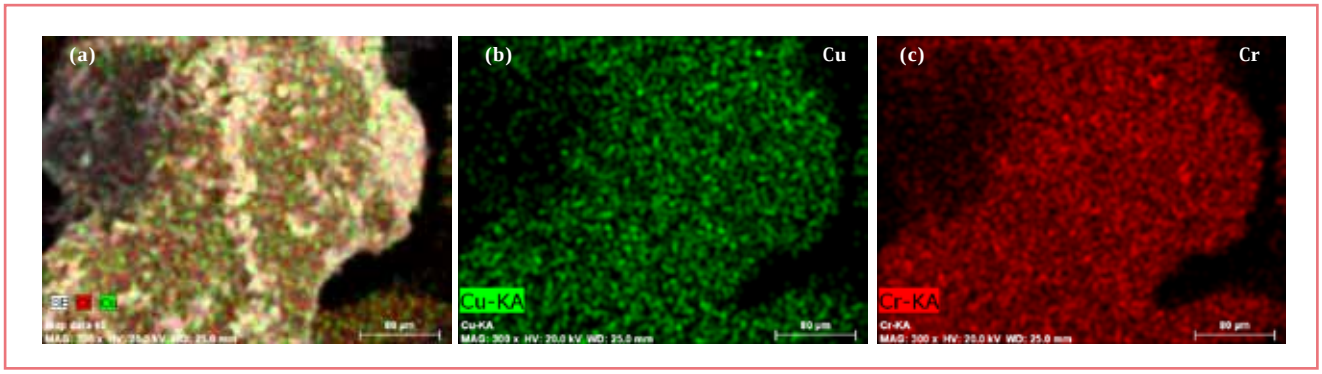

Figure A 13: (a) – (c) EDS composition map data for Cu/Cr_2O_3 used for the reaction with water-spiked feed

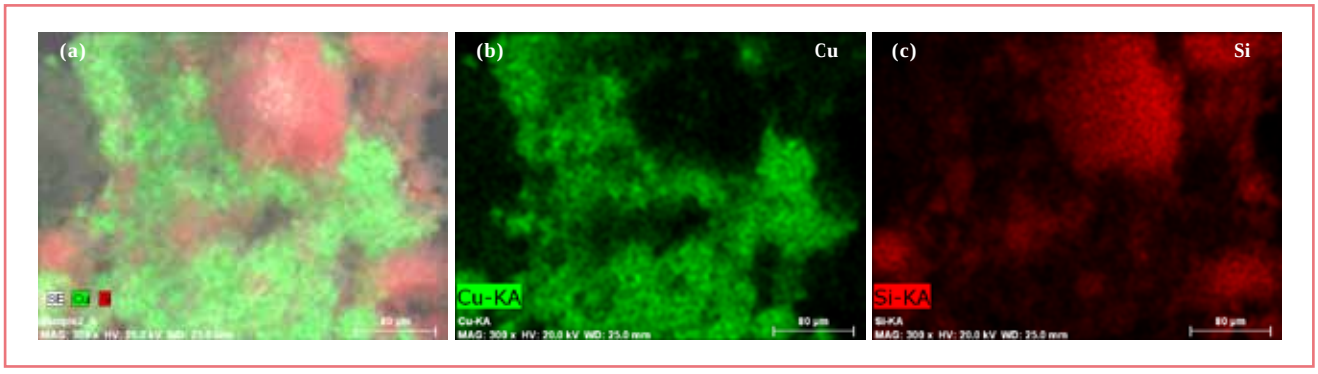

Figure A 14: (a) – (c) EDS composition map data for Cu/SiO_2 used for the reaction with fresh feed

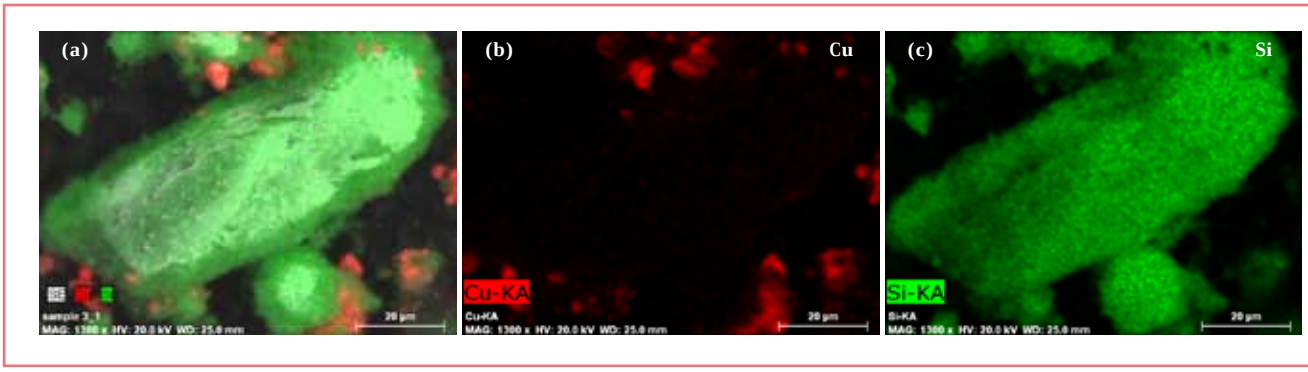

Figure A 15: (a) – (c) EDS composition map data for Cu/SiO_2 used for the reaction with water-spiked feed

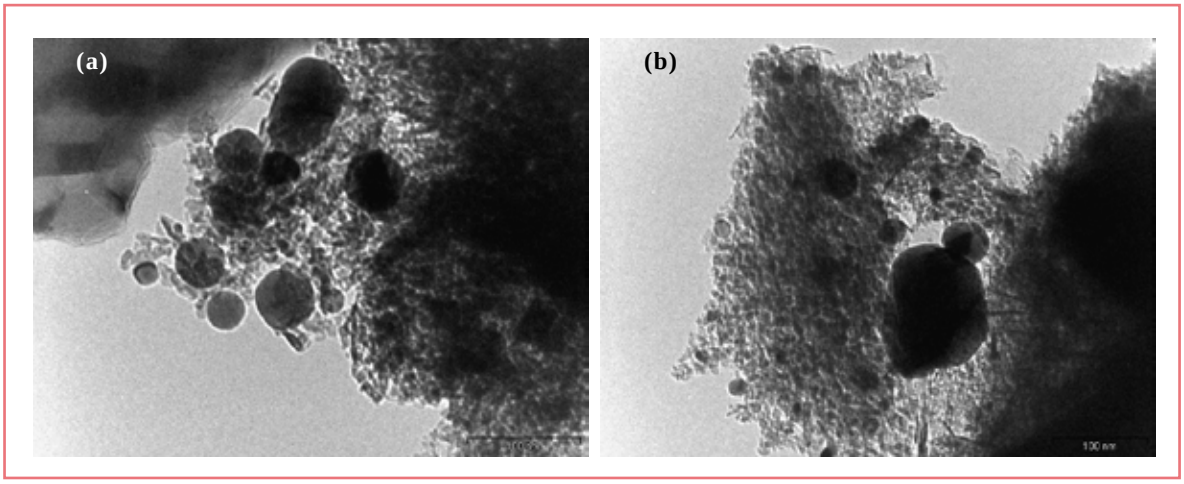

Figure A 16: TEM images of Cu/Al_2O_3 after (a) the reaction with fresh feed and (b) reaction with the water-spiked feed

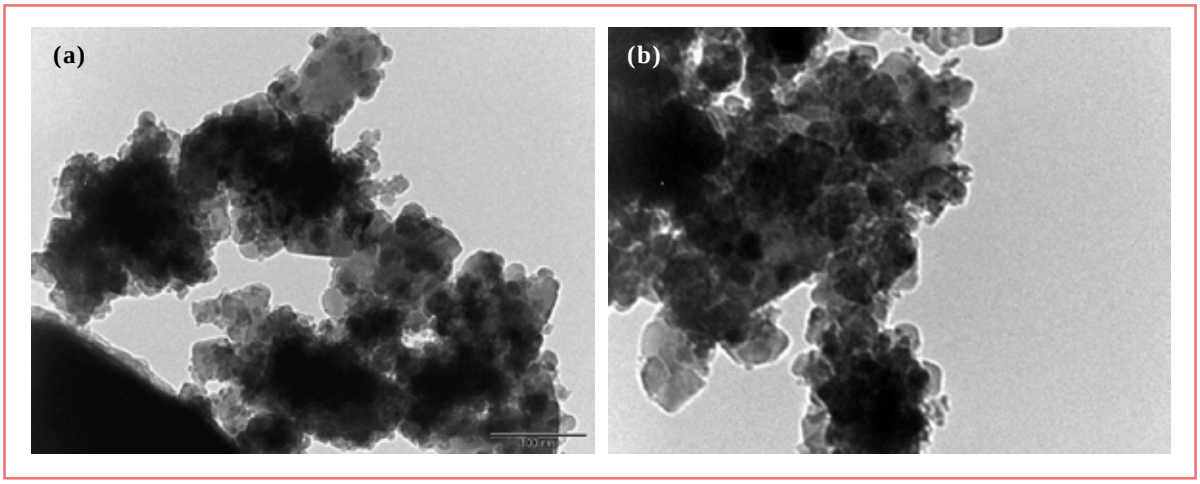

Figure A 17: TEM images of Cu/Cr_2O_3 after (a) the reaction with fresh feed and (b) reaction with the water-spiked feed

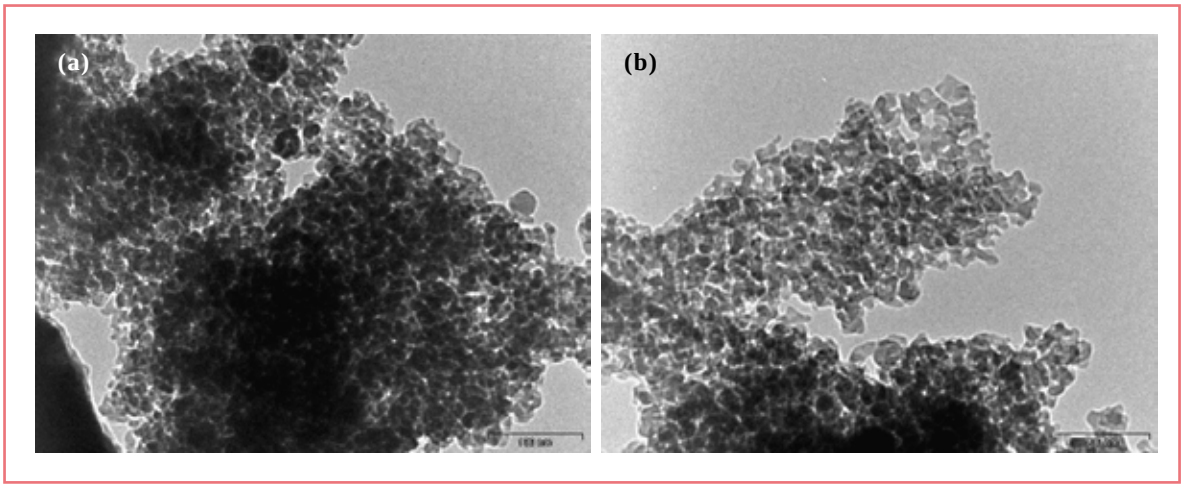

Figure A 18: TEM images of Cu/SiO_2 after (a) the reaction with fresh feed and (b) reaction with the water-spiked feed

Table A 1: A summary of the range and average particle sizes determined for each catalyst

Catalyst	Average Particle Size/nm	Range of Particle sizes/nm
Cu/Al_2O_3 fresh feed	23	3 – 50
Cu/Al_2O_3 water-spiked feed	15	4 – 54
Cu/Cr_2O_3 fresh feed	33	11 – 73
Cu/Cr_2O_3 water-spiked feed	24	7 – 70
Cu/SiO_2 fresh feed	20	7 – 43
Cu/SiO_2 water-spiked feed	17	6 – 44

Table A 2: A list of the copper loadings in the used Cu/SiO_2

Catalyst	Cu loading/wt %
Cu/SiO_2 fresh feed	24.4
Cu/SiO_2 water-spiked feed	25.2

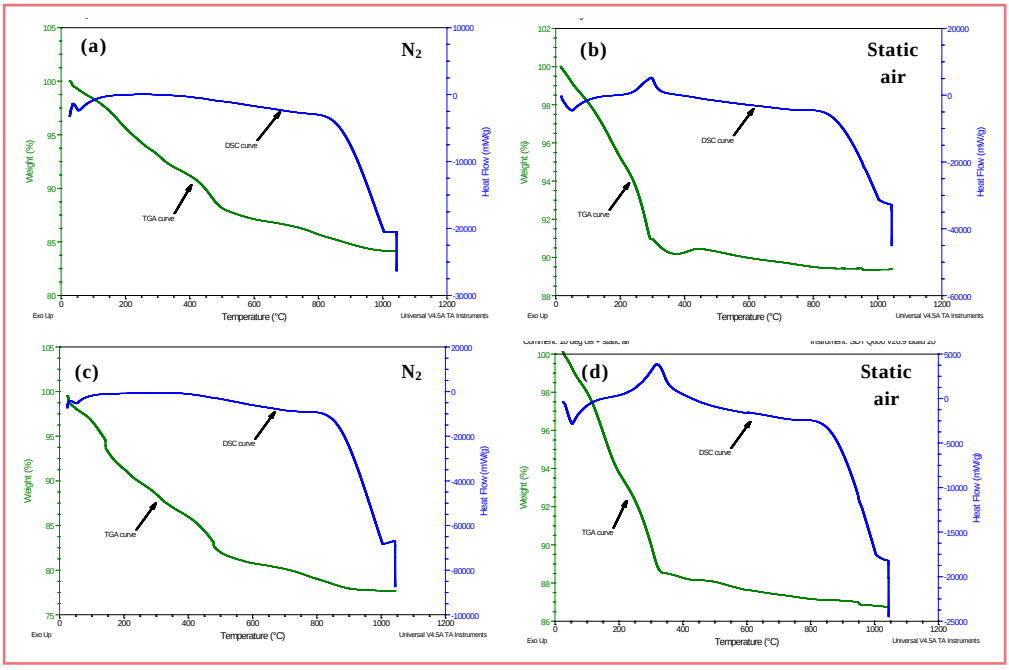

Figure A 19: TGA-DSC curves of Cu/Al_2O_3 after (a) and (b) the reaction with fresh feed and (c) and (d) reaction with the water-spiked feed

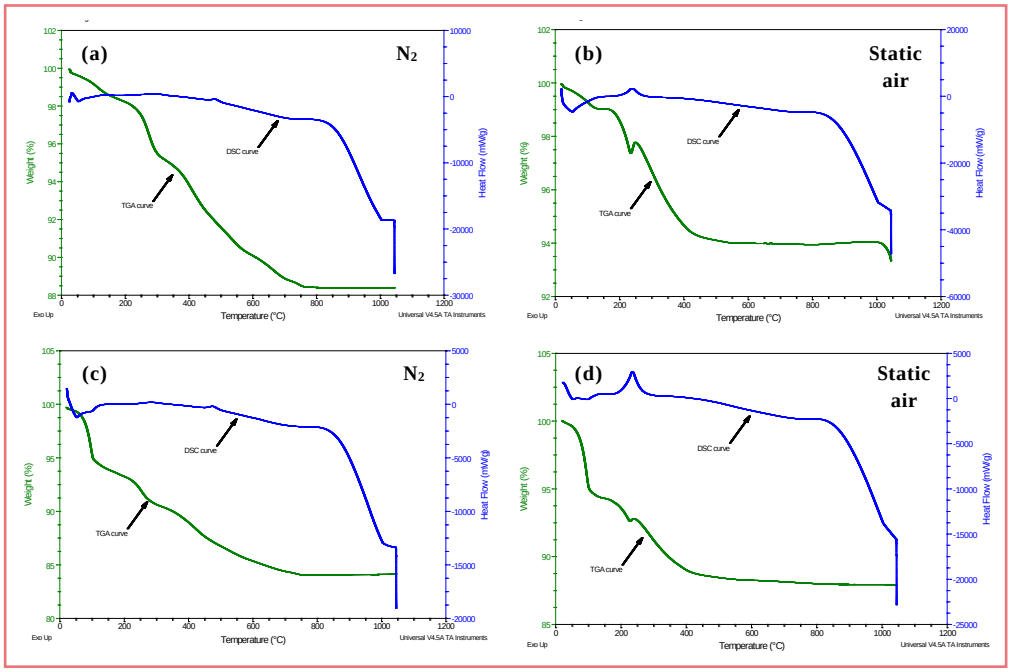

Figure A 20: TGA-DSC curves of Cu/Cr_2O_3 after (a) and (b) the reaction with fresh feed and (c) and (d) reaction with the water-spiked feed

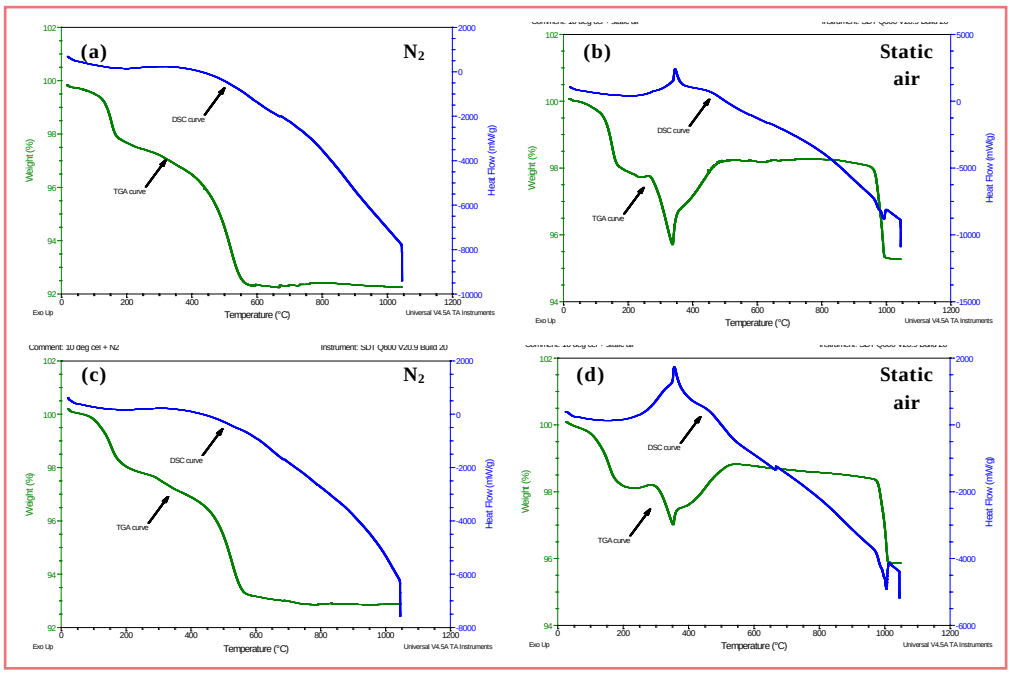

Figure A 21: TGA-DSC curves of Cu/SiO_2 after (a) and (b) the reaction with fresh feed and (c) and (d) reaction with the water-spiked feed

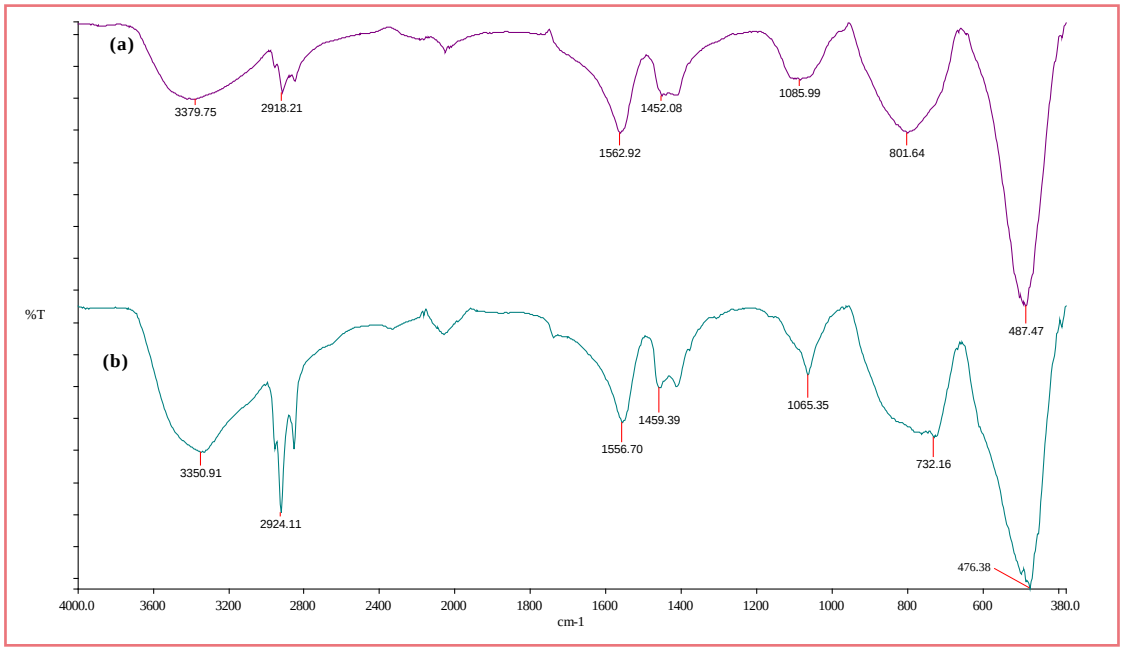

Figure A 22: IR spectra of Cu/Al_2O_3 after (a) the reaction with fresh feed and (b) reaction with the water-spiked feed

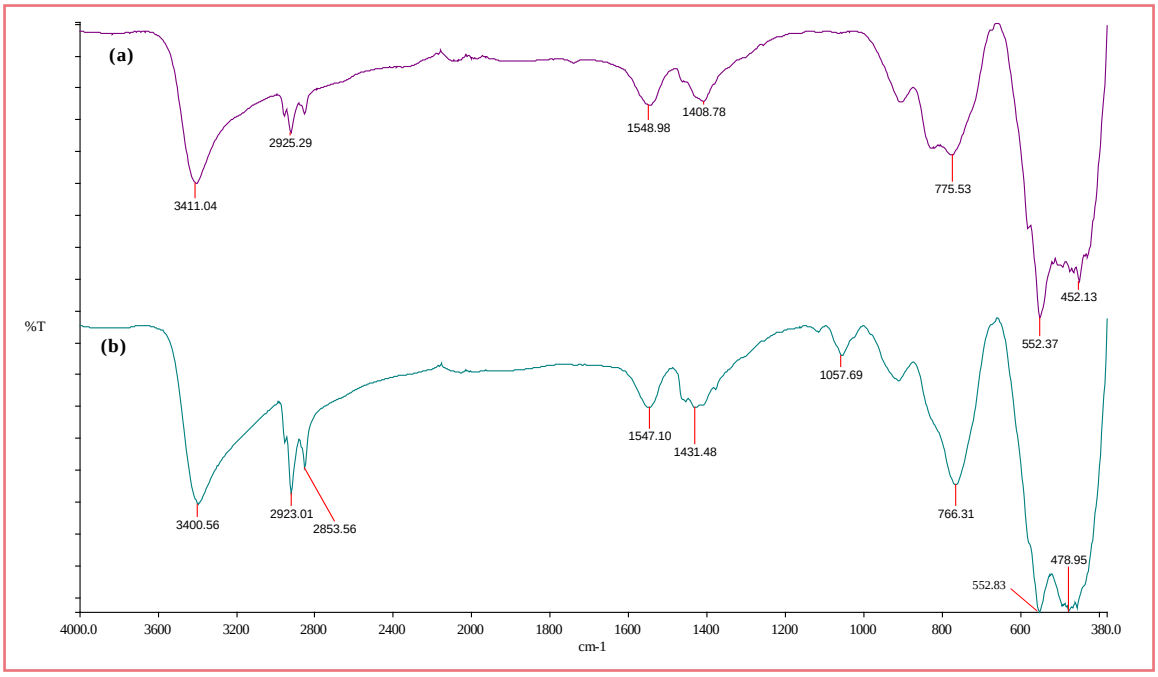

Figure A 23: IR spectra of Cu/Cr_2O_3 after (a) the reaction with fresh feed and (b) reaction with the water-spiked feed

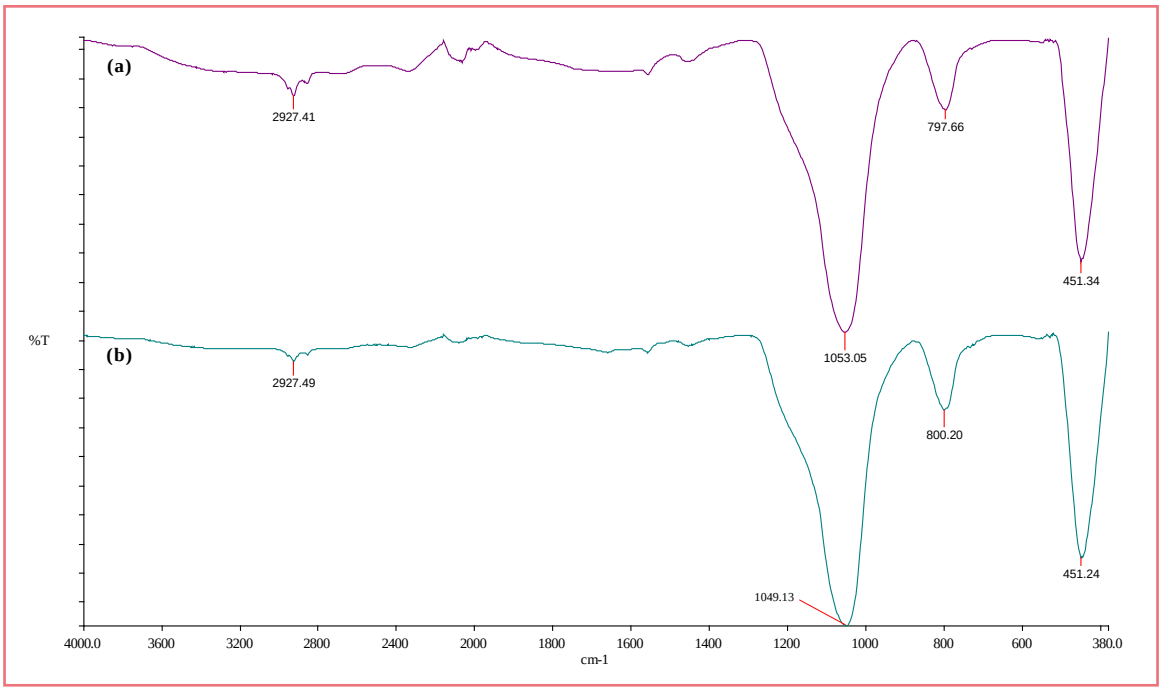

Figure A 24: IR spectra of Cu/SiO_2 after (a) the reaction with fresh feed and (b) reaction with the water-spiked feed